Intermediate-Temperature Fuel Cells Using a Proton-Conducting $Sn_{0.9}In_{0.1}P_2O_7$ Electrolyte

HEO, Pilwon

Intermediate-Temperature Fuel Cells Using a Proton-Conducting $Sn_{0.9}In_{0.1}P_2O_7$ Electrolyte

（プロトン導電体 $Sn_{0.9}In_{0.1}P_2O_7$ を電解質に用いた中温作動燃料電池）

HEO, Pilwon

（許　弼源）

Doctor of Engineering

Graduate School of Environmental Studies,

Nagoya University

（名古屋大学大学院環境学研究科　博士（工学））

2008

Contents

Summary

Proton exchange membrane fuel cells (PEMFCs) have received increasing attention for transportation and residential applications because of their high efficiencies and environmentally-friendly characteristics. However, there still remain several challenges regarding technology and materials costs for their widespread commercialization. In the PEMFCs, the electrolyte (usually Nafion) requires highly humidified conditions to achieve its sufficient proton conductivity and then gas humidifiers required increase the complexity and the cost of the fuel cell system. Current PEMFCs typically run at ~80ºC because of the working temperature limitation of the electrolyte, which causes serious CO poisoning of the anode catalyst and needs to use the expensive Pt catalysts. Such challenges can obviously be overcome by using a proton conductor functioning as the electrolyte above 100ºC under unhumidified conditions. Thus, considerable efforts have been devoted to developing such proton conductors worldwide. Recently, Hibino et al. found an anhydrous proton conductor, 10 mol% In^{3+}-doped SnP_2O_7 ($Sn_{0.9}In_{0.1}P_2O_7$), showing high proton conductivities at intermediate temperatures between 150 and 350ºC under unhumidified conditions. This study aimed to demonstrate the feasibility of intermediate-temperature fuel cells using $Sn_{0.9}In_{0.1}P_2O_7$ as an electrolyte and to prove desirable advantages in the intermediate-temperature fuel cells over current PEMFCs.

The proton conductivity of $Sn_{0.9}In_{0.1}P_2O_7$ and the proton conduction mechanism in the $Sn_{0.9}In_{0.1}P_2O_7$ were reported in Chapter 2. The proton conductivity of $Sn_{0.9}In_{0.1}P_2O_7$ was more than 10^{-1} S cm^{-1} between 125 and 350ºC in unhumidified conditions, where a conductivity value of 1.95 x 10^{-1} S cm^{-1} was achieved at 250ºC. $Sn_{0.9}In_{0.1}P_2O_7$ had proton transport numbers of ~ 1 and exhibited a large H/D isotope effect on conductivity. These results indicate that the charge carriers of $Sn_{0.9}In_{0.1}P_2O_7$ were not H_3O^+ ions, but protons which migrated between the lattice oxide ions according to a hopping mechanism.

Performance of a fuel cell using $Sn_{0.9}In_{0.1}P_2O_7$ as an electrolyte was investigated in the temperature range of 150-300ºC under unhumidified conditions in Chapter 3. In a H_2/air fuel cell with Pt/C anode and cathodes, open circuit voltages (OCVs) were about 920 mV and the peak power density reached 152 mW cm^{-2} and 264 mW cm^{-2} at 250ºC using the electrolytes with 1.00 and 0.35 mm thickness, respectively. Furthermore, the fuel cells showed excellent tolerance toward 10% CO and good thermal stability under unhumidified conditions.

One of the additional advantages in the intermediate-temperature fuel cell is the use of Pt-free electrodes. The development of alternative catalysts to replace Pt is attempted for anode and cathodes in the intermediate-temperature fuel cell in Chapter 4. Carbon-supported molybdenum carbide - zirconia (Mo_2C-ZrO_2/C) showed a high anode performance toward the hydrogen oxidation reduction. The performance of a fuel cell using Mo_2C-ZrO_2/C as an anode was almost comparable to that using a Pt/C as an anode at 250ºC or higher. Carbon-supported zirconia (ZrO_2/C) showed a high cathode performance. The performance of a fuel cell using

the ZrO_2/C cathode was about one-third of that using the Pt/C cathode at 250ºC or higher.

The other additional advantage in the intermediate-temperature fuel cell is the direct use of alternative fuels to replace hydrogen. Direct DME fuel cells (DDMFCs) and direct hydrocarbon fuel cells at the intermediate temperatures between 150 and 300ºC are investigated in Chapter 5. In these fuel cells, all the DME and hydrocarbons were electrochemically converted into CO_2 along with their direct oxidation at the intermediate temperatures and reasonable cell performances were achieved.

$Sn_{0.9}In_{0.1}P_2O_7$ electrolytes may be required to be a thin, dense, and flexible electrolyte membrane for their practical applications. $Sn_{0.9}In_{0.1}P_2O_7$ - based organic/inorganic composite membranes were developed in Chapter 6. The composition of the composite membrane was determined to be 90 wt.% $Sn_{0.9}In_{0.1}P_2O_7$ for achieving both the high proton conductivity and flexibility of the composite membranes. Fuel cell tests verified that the OCV was maintained at a constant value of approximately 970 mV regardless of the electrolyte thickness (60-200 μm) and the peak power densities achieved with unhumidified H_2 and air were 197 mW cm^{-2} at 150ºC, and 226 mW cm^{-2} at 200ºC. Furthermore, a membrane electrode assembly (MEA) fabrication technique offered the potential for enhancing the fuel cell performance.

The intermediate-temperature fuel cell using the $Sn_{0.9}In_{0.1}P_2O_7$ electrolyte exhibited a more stable performance at low relative humidities and high CO concentrations compared to current PEMFCs. Furthermore, it was demonstrated that the present fuel cells have additional advantages such as the use of non-Pt electrodes and the direct use of alternative fuels. The preferred advantages in the intermediate-temperature fuel cell would improve the overall fuel cell efficiency and make fuel cell systems significantly simpler and more economic.

要旨

固体高分子形燃料電池（PEMFC）は自動車・家庭用エネルギー変換機として注目されているが、その実用化のためには未だ様々な課題が残っている。通常使用されている電解質である Nafion は含水状態でのみ高いプロトン導電率を示すために過度な加湿が必要であり、それによって必要とされる加湿装置は燃料電池システムをより複雑にさせ、そのコストを高める。また、作動温度が 80℃以下であるためアノード触媒が燃料中の CO によって被毒され、更に高価の Pt 電極触媒を使用しなければいけない。これらの課題は 100℃以上、無加湿条件下で作動できるプロトン導電体を使用することで解決されるはずである。それ故、そのようなプロトン導電体材料の開発は世界中で活発に行われている。最近、150℃～350℃の中温域、無加湿条件下で高いプロトン導電率を示す非含水系プロトン導電体 10 mol% In^{3+}ドープ SnP_2O_7 ($Sn_{0.9}In_{0.1}P_2O_7$)が日比野らによって見出された。本研究ではこの材料を電解質として使用した中温作動燃料電池の実現と、PEMFC に対する中温作動燃料電池の利点の実証を目的とした。

第 2 章においては $Sn_{0.9}In_{0.1}P_2O_7$ のプロトン導電率とプロトン伝導機構を報告した。$Sn_{0.9}In_{0.1}P_2O_7$ は 125℃～350℃、無加湿条件下で 10^{-1} S cm^{-1} 以上のプロトン導電率を示し、250℃では 1.95×10^{-1} S cm^{-1} であった。また、$Sn_{0.9}In_{0.1}P_2O_7$ はほぼ 1 に近いプロトン輸率を持ち、導電率において高い H/D 同位体効果を示した。この結果は、$Sn_{0.9}In_{0.1}P_2O_7$ の電荷担体が H_3O^+イオンではなくプロトン(H^+)であり、そのプロトンは格子酸素イオン間をホッピング機構によって移動することを示している。

第 3 章では $Sn_{0.9}In_{0.1}P_2O_7$ を電解質として使用し、150-300ºC の温度範囲・無加湿条件下で燃料電池の性能を評価した。Pt/C を電極に使用した水素/空気燃料電池において、電解質の膜厚を 1.00 mm と 0.35 mm にした場合、250ºC で、それぞれ 152 mW cm^{-2} と 264 mW cm^{-2} の最大出力密度が得られた。更に、この燃料電池は 10%CO 含有燃料に対しても優れた耐性を示し、無加湿条件下でも熱的に安定であった。

中温作動燃料電池において、その他の利点として Pt フリー電極の使用がある。第 4 章では中温作動燃料電池のアノードとカソードにおける Pt 代替触媒の開発を試みた。水素酸化反応においてはモリブデンカーバイドージルコニア担持カーボン(Mo_2C-ZrO_2/C)が高いアノード性能を示した。作動温度 250℃以上において、Mo_2C-ZrO_2/C をアノードに使用した燃料電池の性能は Pt/C をアノードに使用した場合の性能に匹敵した。また、ジルコニア担持カーボン(ZrO_2/C)は高いカソード性能を示した。作動温度 250℃以上において、ZrO_2/C をカソードに使用した燃料電池の性能は Pt/C をカソードに使用した場合の性能の約 1/3 程度であった。

中温作動燃料電池の利点としてもう一つは水素の代替燃料の使用である。第 5 章では 150～300℃の中温域におけるダイレクトジメチルエーテル燃料電池(DDMEFC)とダイレクト炭化水素燃料電池を調べた。これらの燃料電池において DME と炭化水素燃料は、電気化学的直接酸化反応によって CO_2 に変換され、妥当な電池性能が得られた。

$Sn_{0.9}In_{0.1}P_2O_7$ 電解質はその実用化のために、薄くて緻密性、柔軟性ある電解質膜にする必要がある。第 6 章では $Sn_{0.9}In_{0.1}P_2O_7$ を含む有機/無機コンポジット膜の開発を行った。コンポジット膜の高いプロトン導電率と柔軟性の両方を考慮して、膜中の $Sn_{0.9}In_{0.1}P_2O_7$ 量は 90wt%とした。燃料電池を構成したところ、OCV は電解質の膜厚（60~200 μ m）に依存せず約 970 mV で維持され、最大出力密度は 150℃で 197 mW cm^{-2}、200℃で 226 mW cm^{-2} であった。更に、電解質膜電極複合(MEA)の作製により燃料電池性能は向上した。

以上のように $Sn_{0.9}In_{0.1}P_2O_7$ 電解質を使用した中温作動燃料電池は PEMFC に比べ、低い相対湿度と高い CO 濃度での安定した性能を示した。また、本燃料電池は Pt フリー電極の使用や代替燃料の直接使用などの更なる利点を持つことが実証された。これらの利点により中温作動燃料電池は燃料電池総合効率の向上とそのシステムの大幅な簡略化・低コスト化が期待できる。

1 Introduction

1.1 Generality of fuel cells

1.1.1 Advantages of fuel cells

Fuel cells are electrochemical devices that convert chemical energy of fuel directly into electrical energy. This energy conversion attracts great attention in our society today because of its high efficiency and low emission of pollutants.

It is the greatest advantage that the theoretical efficiency of an energy conversion for fuel cells is higher than that for a thermal engines such as internal-combustion engines and thermal power generators (by about a factor of 2) [1]. Typically, in the thermal engines, an electricity generation from fuel involves several energy conversion steps, as shown in Fig. 1-1(a). A combustion of fuel converts chemical energy of fuel into heat, and this heat is then used to boil water and generate steam. The steam is used to run a turbine in a process that converts thermal energy into mechanical energy, and finally mechanical energy is used to run a generator that generates electricity. A fuel cell circumvents all these processes and generates electricity in a single step (direct conversion), as shown in Fig. 1-1(b).

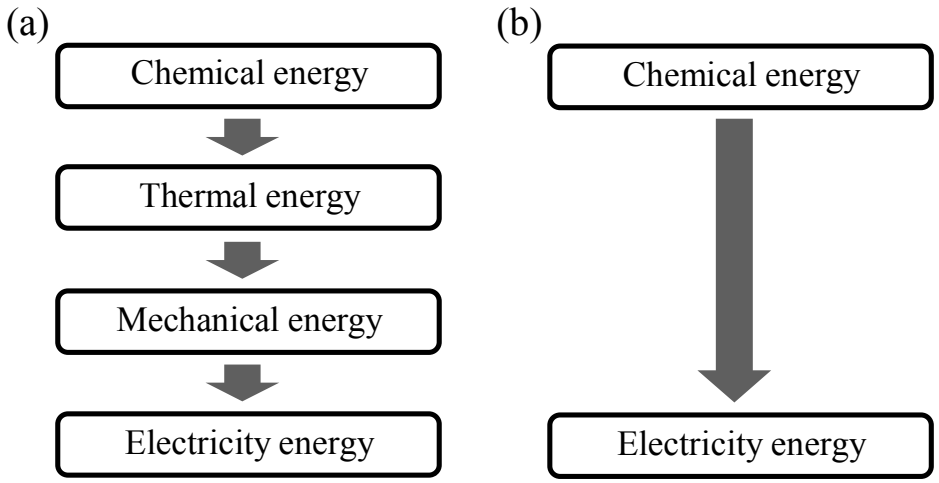

Figure 1-1. Electricity generations for (a) a thermal engine and (b) a fuel cell.

Another important advantage of fuel cells is environmental friendliness. The process of electricity generation in fuel cells does not involve any moving parts so that its system can be operated without ambient noise and machinery vibrations. If hydrogen is used as a fuel for fuel cells, it has no emission of greenhouse gas such as CO_2. In particular, as related today's urban environment issue, a fuel cell electric vehicle has received increasing attention because its exhaust gas does not involve hazardous air pollutants such as NOx, CO, and SPM (suspended particulate matter) [2].

1.1.2 Theory of fuel cells

1.1.2.1 A basic principle of fuel cells

Fuel cells, unlike batteries, do not require to be periodically recharged. It can produce electricity continuously as long as supplied with fuel and oxidants into fuel cells. Typical reactants for fuel cells are hydrogen and oxygen. Fuel cells that composed of an electrolyte, an anode, and a cathode generates DC electricity through electrochemical reactions, the oxidation of a fuel at the anode and the reduction of an oxidant at the cathode, as shown in Fig. 1-2. The basic fuel cell reactions are:

At the anode: $H_2 \rightarrow 2H^+ + 2e^-$ (1-1)

At the cathode: $1/2O_2 + 2H^+ + 2e^- \rightarrow H_2O$ (1-2)

Overall: $H_2 + 1/2O_2 \rightarrow H_2O$ (1-3)

The protons released during the oxidation of hydrogen are conducted through an electrolyte to the cathode. Since the electrolyte is not an electron conductor, the electrons released from the hydrogen travel along the electrical detour provided and an electrical current is generated.

Another difference between fuel cells and batteries is that fuel cells generate by-products; waste heat and water. Fuel cell systems are required to manage the by-products. The waste heat can be used as a continuous heat source to keep the operating temperature of fuel cells. In addition, the waste heat from fuel cells is helpful for where use boil water and steams–for

example, distributed CHP (combined heat and power) systems for stationary applications.

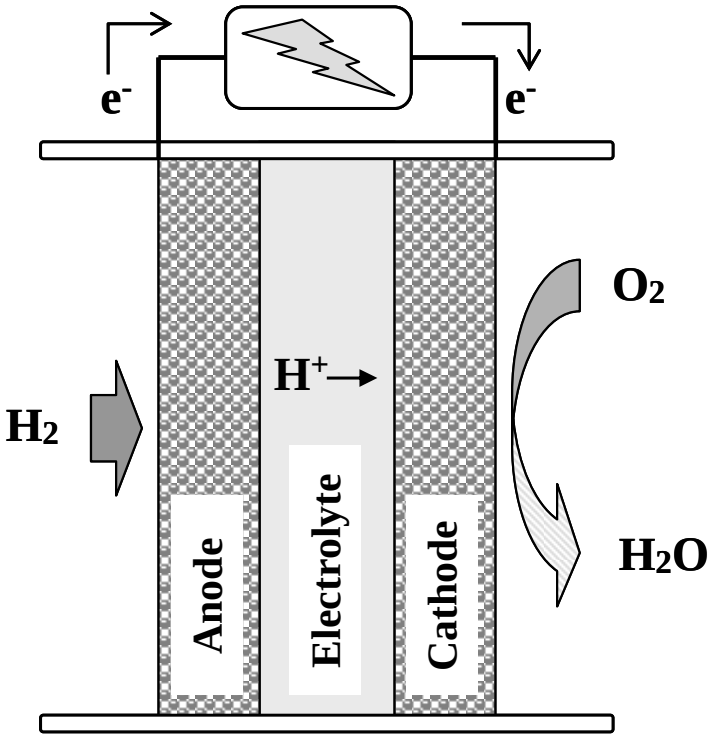

Figure 1-2. Schematic of a fuel cell, comprise of an electrolyte, an anode, and a cathode.

1.1.2.2 Fuel cell thermodynamics

The energy conversion of fuel cells must obey the laws of thermodynamics [3]. The overall reaction in Eq. 1-3 is the same as the reaction of hydrogen combustion. Combustion is an exothermic process, which means that there is energy released in the process:

$$H_2 + 1/2O_2 \rightarrow H_2O + \text{heat} \qquad (1\text{-}4)$$

At 25ºC, heat of formation of liquid water is -286 $kJmol^{-1}$. Therefore,

$$H_2 + 1/2O_2 \rightarrow H_2O(l) + 286\ kJ\ mol^{-1} \qquad (1\text{-}5)$$

The enthalpy of hydrogen combustion reaction in Eq. 1-5 (i.e., 286 kJ mol^{-1}) is also called the hydrogen's heating value (higher heating value, HHV). However, if the product water is in the form of vapor, less heat will be released, exactly 241kJ. This is known as hydrogen's lower heating value (LHV). Because there is no combustion in fuel cells the relevance of hydrogen's

heating value should be considered. In every chemical reaction some entropy is produced, and because of that, a portion of the hydrogen's heating value cannot be converted into useful work–electricity. The hydrogen's heating value converting to electricity in fuel cells corresponds to Gibbs free energy and is given by the following equation:

$$\Delta G = \Delta H - T\Delta S \quad (1\text{-}6)$$

In other words, there are some irreversible losses in energy conversion due to creation of entropy, ΔS. Therefore, at 25 ºC, out of 286 kJ mol^{-1} of available energy, 237 kJ mol^{-1} can be converted into electrical energy and the remaining 49 kJ mol^{-1} is converted into heat.

1.1.2.3 Fuel cell electrochemistry

The electrical energy generated in fuel cells corresponds to Gibbs free energy (ΔG), which is also a product of charge (q) and potential (E). Therefore,

$$-\Delta G = qE = nFE \quad (1\text{-}7)$$

here, q = charge (Coulombs mol^{-1}), E = potential (Volts), n = number of electros per molecule of H_2 =2 electrons per molecule, and F = 96485 Coulombs/electron-mol.

The theoretical potential of fuel cells is then:

$$E = \frac{-\Delta G}{nF} \quad (1\text{-}8)$$

At 25 ºC, the theoretical hydrogen/oxygen fuel cell potential is 1.23 Volts.

Actual cell potentials are always smaller than the theoretical ones due to irreversible losses. Voltage losses in operational fuel cells are caused by ohmic losses and polarization losses (overpotentilas). Figure 1-3 shows current-voltage characteristics of fuel cells, which is formed by subtracting the losses from the open circuit voltage (E_{OCV}). Therefore, the cell voltages (E_{cell}) are presented to be:

$$E_{cell} = E_{OCV} - iR - \eta_a - \eta_c - \eta_m \quad (1\text{-}11)$$

where, iR is Ohmic losse due to ionic resistance in the electrolyte, η_a and η_c are anodic and

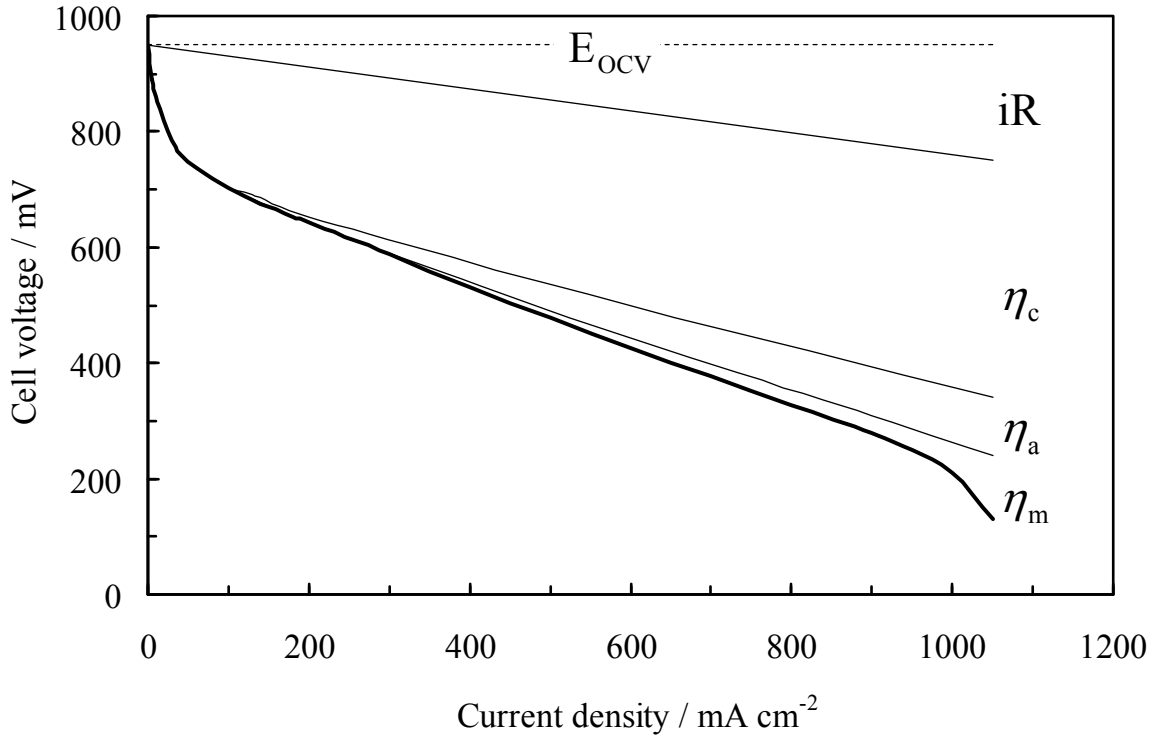

Figure 1-3. Current-voltage characteristics of a fuel cell.

cathodic overpotentials, respectively, due to kinetics of the electrochemical reaction, and η_m is a concentration overpotential due to difficulties in getting the reactants to reaction sites.

The current-voltage curve is the most important characteristic of fuel cells. It may be used for diagnostic purpose, as well as for sizing and control of fuel cells. Power density (in W/cm^2) is a product of potential and current density:

$$w = V \cdot i \tag{1-12}$$

Power density vs current density may be plotted together with the current-voltage curve on the same diagram. Such a plot shows that there is a maximum power density a fuel cell may reach.

The efficiency of any energy conversion device is defined as the ratio between useful energy output and energy input. In case of fuel cells, the useful energy output is the electrical energy produced, and energy input is the enthalpy of hydrogen. Assuming that all of the Gibbs free energy can be converted into electrical energy, the theoretical efficiency of fuel cells is:

$$\varepsilon_{\text{the}} = \frac{\Delta G}{\Delta H} = \frac{237.34}{286.02} = 83\% \tag{1-13}$$

However, in practice, fuel cells will be operated under the voltage losses and will consider the fuel utilization supplied. The fuel cell efficiency is then:

$$\varepsilon = \varepsilon_{\text{the}} \varepsilon_{\text{v}} \alpha \tag{1-14}$$

where, ε_{the} is the theoretical efficiency, ε_v is the voltage efficiency (E_{cell}/E_{OCV}), and α is the fuel utilization (used fuel/ applied fuel).

1.1.3 Types of fuel cells

The types of fuel cells are usually classified by the type of electrolyte they used, which are summarized in Fig. 1-4.

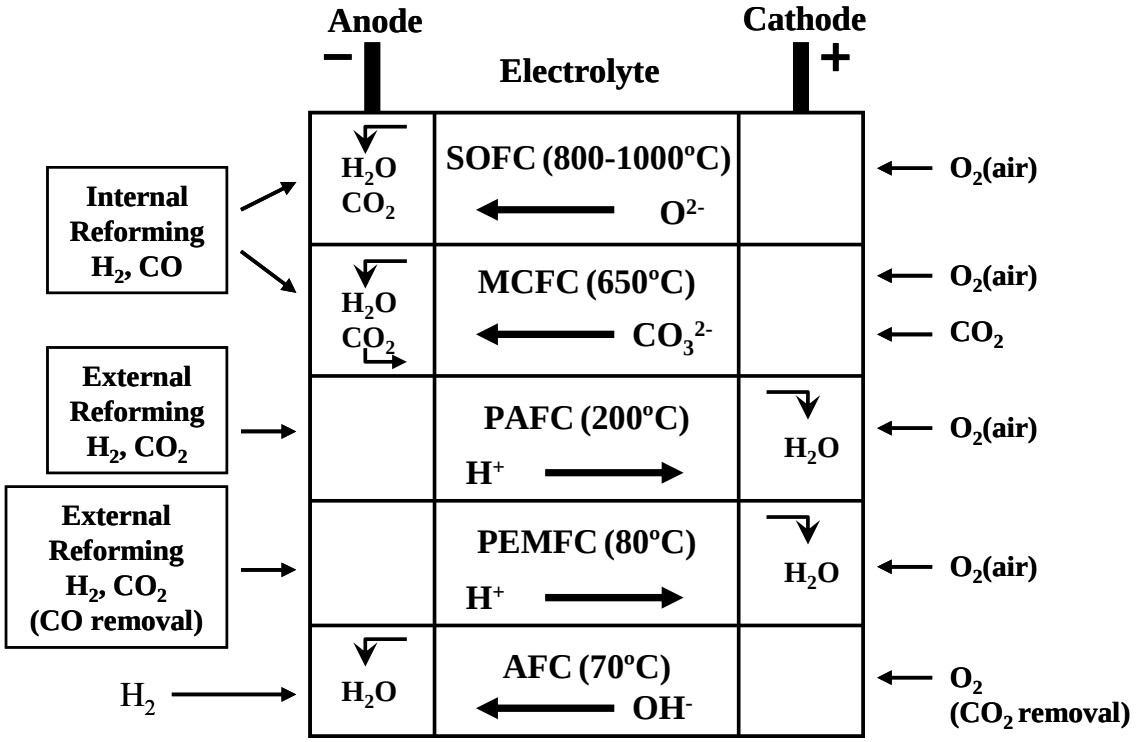

Figure 1-4. Summery of fuel cell types.

Alkaline fuel cells (AFCs) use KOH as the electrolyte and operate between 60 and 220ºC. The electrolyte is retained in a matrix (usually asbestos), and a wide range of electrocatalysts

can be used (such Ni, Ag, metal oxides and noble metals). Because the alkaline electrolyte reacts with carbon oxide gases, AFCs have to use pure hydrogen and pure oxygen where must not involve CO_2. Therefore, AFCs have been limited to an application of space flight.

Proton exchange membrane (or Polymer electrolyte membrane) fuel cells (PEMFCs) use a thin proton conductive polymer membrane (such as perfluorosulfonated acid polymer) as the electrolyte. Operating temperature is typically between 60 and 80ºC. The catalyst is platinum supported on carbon (Pt/C). PEFCs require relatively pure hydrogen (<100ppm CO) to be supplied to the anode. Accordingly, the use of hydrocarbon or alcohol fuels requires an external fuel processor to be incorporated into the system. PEMFCs operated with a high power density and a rapid start-up are a considerable candidate for automotive application, but also for small-scale distributed stationary power generation, and for portable power application as well.

Phosphoric acid fuel cells (PAFCs) use concentrated phosphoric acid (~100%) as the electrolyte. The matrix used to retain the acid is usually SiC, and the electrocatalyst is platinum. Operating temperature is typically between 150 and 200ºC. Most component materials in PAFCs are relatively expensive carbonaceous system and noble metals, since normal metals are corroded by phosphoric acid, causing a high cost of the fuel cell system. PAFCs are already semicommercially available in container packages (200kW) for stationary electricity generations.

Molten carbonate fuel cells (MCFCs) have the electrolyte composed of a combination of alkali (Li, Na, K) carbonates, which is retained in a ceramic matrix of $KiAlO_2$. Operating temperature is between 600 and 700ºC where the carbonates form a highly conductive molten salt, with carbonate ions providing ionic conduction. At such high operating temperatures, noble metal catalysts are typically not required. These fuel cells are in the precommercial/demonstration stage for stationary power generations.

Solid oxide fuel cells (SOFC) use a solid, nonporous metal oxide, usually Y_2O_3-stablilized

ZrO_2 (YSZ) as the electrolyte. These cells operate at 800 to1000ºC where ionic conduction by oxygen ions takes place. Corrosion problems are less severe than the other types of fuel cells. Lower operating temperature is preferred and solid oxide ion conductors are now under investigation for this purpose. Similar to MCFC, these fuel cells are in the precommercial/demonstration stage for stationary power generations, although smaller units are being developed for portable power and auxiliary power in automobiles.

1.2 Proton exchange membrane fuel cells (PEMFCs)

Among the various types of fuel cells, PEMFCs have the advantage of high power densities at relatively low operating temperature; they can be fast start-up and immediate response to change in the demand for power. For these reasons, PEMFCs are considered to be the most suitable for fuel cells in vehicular and residential applications. Many efforts have been devoted into the research and development (R&D) of PEMFCs for transportation. In the past decades, great advances have been achieved for PEMFCs. However, some challenges on technology and material cost are yet to be made for its widespread commercialization. In this section, general properties of cell components used in PEMFCs are presented, and then attention is focused on material requirements and challenges in present PEMFCs.

1.2.2 Fuel cell components

The heart of a fuel cell is a proton conducting membrane, which is commonly fluoropolymers such as Nafion. There is an electrode on both sides of the membrane. The electrodes must be porous because the reactant gases are fed from the back and must reach the interface between the electrodes and the membrane. The electrode consists of a catalyst layer on a gas diffusion layer (GDL). Typically, platinum supported on carbon (Pt/C) is used as a catalyst. The multilayer assembly of the membrane sandwiched between the two electrodes is

commonly called the membrane electrode assembly (MEA). The MEA is then sandwiched between the collector/separator plates, i.e., bipolar plates. The bipolar plate provides the pathways for flow of reactant gases, and the cell structural rigidity.

1.2.2.1 Membrane

Typically, the membranes for PEMFCs are made of perfluorocarbon-sulfonic acid ionomer (PFSA). The best-known and commonly used membrane material is Nafion made by Dupont. Similar materials have been developed and sold as either a commercial or development product by other manufacturers such as Asahi Glass (Flemion), Asahi Chemical (Aciplex), and Chlorine Engineer (C membrane).

Figure 1-5 shows the chemical structure of PFSA such as Nafion. The SO_3H group is ionically bonded, and so the end of the side chain is actually an SO_3^- ion with H^+ ion. Because the sulphonic acid at the end of the side chain is highly hydrophyllic, this kind of material absorbs relatively large amounts of water (in some cases up to 50% by weight). As such, the membrane contains liquid-like regions of water between the polymer chains. The protons (H^+) attach themselves to water and diffuse as H_3O^+ ions through the membrane (vehicular mechanism) [4]. Therefore, PEMFCs require an external humidification subsystem in a fuel

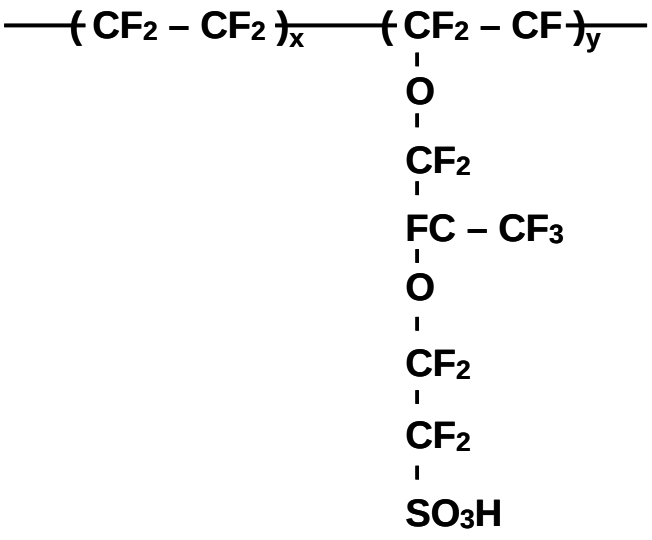

Figure 1-5. Structure of PFSA polymer (Nafion).

cell system and their operating temperature is limited to the dehydration temperature of ~100ºC (typically at 80ºC). The proton conductivity of PFSA membranes significantly increases with increasing water content and temperatures. As a result, the proton conductivity of fully hydrated membrane (i.e., 100% humidification) is about 0.1 S cm^{-1} at 80ºC.

1.2.2.2 Electrode

The electrochemical electrode reaction takes place on the catalyst layer where three phases, namely gases, electrons, and protons, have access for the reaction. The catalyst layer which is commonly Pt/C is in direct contact with the membrane and the GDL as shown in Fig. 1-6 [5].

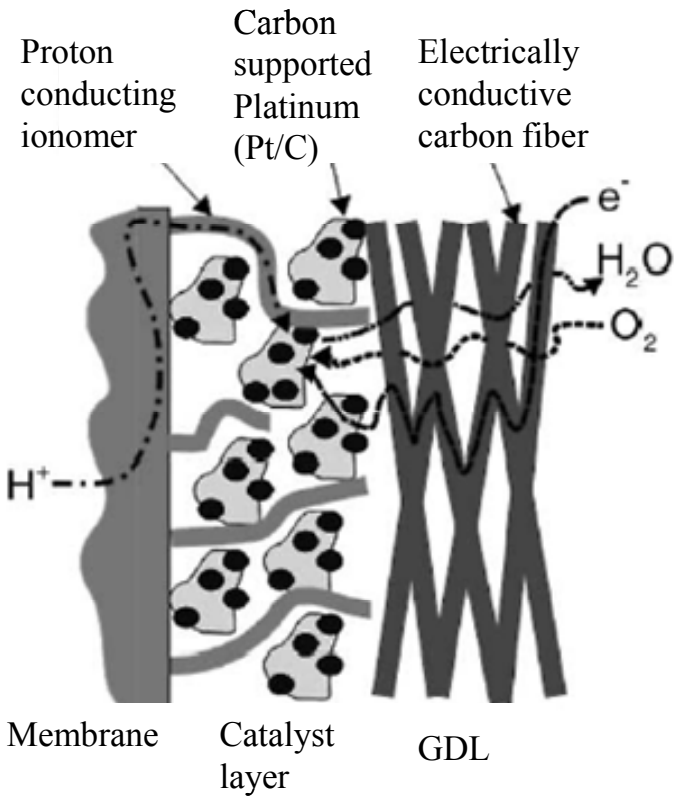

Figure 1-6. Transport of gases, protons, and electrons in a PEMFC electrode.

The three transport processes required are those of proton from the membrane to the catalyst, electrons from the current collector to the catalyst through the GDL, and reactant gases from gas channels to the catalyst layer through the GDL.

There are two methods of preparation of catalyst layer and its attachment to the membrane. Such a combination of membrane and catalyst layers is called MEA. The first method of preparing an MEA is to form the catalyst layer to the GDL, and then hot-press it to the membrane. In this case, the catalyst particles are bound by a hydrophobic polytetrafluoroethylene (PTFE) binder on the gas diffusion layer. In order to provide ionic transport to the catalyst site, the catalyst layer is typically impregnated with Nafion by brushing or spraying before the hot pressing [6]. The second method of preparing an MEA is to apply the catalyst layer directly to the membrane. The catalyst layers are formed by coating the catalyst particles with an ionomer solution (Nafion) on the both sides of the membrane and followed by placing the GDL and pressing the membrane-catalyst layer [7]. Because of high materials cost and supply limitations, the reduction of the amount of platinum is required. Platinum loading of 0.4 mg cm^{-2} is currently applied in PEMFCs [8]. It is important to have small platinum particles (~4 nm) with large surface area finely dispersed on the surface of catalyst support, typically carbon powders (ca. 40 nm). The cell performance is improved by optimizing ionomer content in the catalyst layer. This may be the effect of increased catalyst surface active area. The optimum amount of Nafion in the catalyst layer is about 30% as literatures reported [9,10].

The GDL consists of carbon paper or carbon cloths, which is usually hydrophobic treated with PTFE.

1.2.2.3 Bipolar plate

The bipolar plates perform as the current conductors between cells, provide conduits for reactant gases flow, and constitute the backbone of a fuel cell stack. Early bipolar plates are graphite materials which are preferred for a corrosion resistance. However the fabrication costs of graphite plates incorporating gas-distribution channels are very high. With the result that other materials are under development, graphite-composite plate (composite of polymer

and graphite powder [11]) and metallic materials (stainless steels [12]) have been applied. The graphite composites are produced by the hot molding of a carbon or graphite filler in a thermoplastic matrix, which have a trade-off between mechanical strength and electrical conductivity, i.e, brittle/high electric conduct or flexible/low electric conduct. On the other hand, the metals have higher electrical conductivity, higher mechanical strength, and better manufacturability compared with the graphite composite. However, the metallic plates have problems of a metallic corrosion and a passive layer causing a high surface contact resistance. Thus recent researches are conducted on the metallic bipolar plates to prevent corrosion while maintaining a low contact resistance [13].

1.2.3 Challenges of PEMFCs

PEMFCs in the operation with pure hydrogen and oxygen (or air) achieved the high power density and low degradation. Currently, the most important challenge in PEMFCs for its widespread commercialization is the reduction in the cost. The challenges also include some technical problems; adequate water and heat management, and the tolerance to impurities such as carbon monoxide (CO). Current PEMFCs typically run at ~80ºC because of the working temperature limitation of the membrane (usually Nafion) as mentioned above. As this membrane requires highly humidified conditions to achieve sufficient proton conductivity, humidifying units required increase the complexity and the cost of the fuel cell system [14,15]. Furthermore, the cost of perfluorinated polymer such as Nafion remains high, around US$56 m^{-2} in large volumes [16].

PEMFCs essentially require relatively pure hydrogen to be supplied to the anode. For the use of hydrogen from hydrocarbons such as natural gas, external reformer equipment is incorporated into the system. The reformate fuel contains small amount CO which poisons the Pt anode catalyst and so depresses the performance of PEMFCs [16]. This also causes the complexity and high cost of the fuel cell system. To overcome the CO poisoning problem in

PEMFCs, the reduction of CO concentration in the reformate fuel is additionally performed by the CO selective oxidation process (bleeding very low levels of oxidant into fuel), while some fuel loss and increased system cost [17]. Considerable efforts have been devoted to the development of CO-tolerant electrocatalyst such as a PtRu catalyst [18,19]. Nevertheless, CO tolerance is ~100 ppm at 80ºC.

At low operating temperatures in PEMFCs, Pt or Pt-based catalysts are essential for the reasonable cell performance. To reduce the cost, the reduction in the Pt catalyst content without a significant degradation of the cell performance has been, and continues to be an important R&D activity [20].

High temperature operation of PEMFCs above 100ºC may be a key to solve such problems. At the high temperature above 100ºC, at least, two important benefits are expected. One is that water management can be simplified because only a single phase of water needs to be considered [21]. Another is that CO tolerance is dramatically increased thereby allowing fuel cells to use lower quality reformed hydrogen [16]. These will bring out the simplicity and the low cost in the present PEMFC system. Therefore, considerable efforts have recently been devoted to the development of PEMFCs that operate above 100ºC. Such fuel cells operating at higher temperatures are called “High Temperature PEMFCs” or “Intermediate-Temperature Fuel Cells”. I will describe the fuel cells as “Intermediate-Temperature Fuel Cells” in the following sections.

1.3 Intermediate-Temperature Fuel Cells

PEMFCs have shown great promise for transportation and residential applications. However, there remain several technical obstacles hinder their widespread commercialization. These mainly include water and heat management, CO tolerance, and their cost issues. Such obstacles can obviously be overcome by using a proton conductor functioning as the

electrolyte above 100ºC under low humidity or dry atmosphere. The introduction of alternative materials/processes enable to operate at the higher temperatures would have a major impact on the successful commercialization of fuel cell technology.

1.3.1 Advantages of intermediate-temperature fuel cells

At the high temperature above 100ºC, many desirable advantages are expected as follows:

Simplicity of water management – it can be simplified because only a single phase of water needs to be considered, i.e., water vapor phase [22]. Operation of PEMFCs at around 80ºC close to the boiling point of water involves a dual-phase water system, i.e., liquid water/water vapor. When the humidification is too high, water condenses and the gas diffusion electrodes are flooded, which makes water management difficult. However, at the high temperature above 100ºC, it only requires the control of only a water vapor pressure in feed-gases. Moreover, the use of anhydrous proton conductors, which do not require its hydration, as an electrolyte in the fuel cell makes it possible to remove the humidifying units in the fuel cell systems.

High CO tolerance – Such an operating temperature of PEMFCs at around 80ºC causes serious CO poisoning of the anode electrocatalyst, which has been one of the key issues for the system design and operation. The CO tolerance will be enhanced as the adsorption of CO on Pt catalysts is weakened with increasing temperatures [16], for example, the CO tolerance is 10-20ppm at 80ºC, 1000ppm at 130ºC, and up to 30,000ppm at 200ºC [23]. The high CO tolerance will provide fuel cells to use lower quality reformed hydrogen.

Clearly, the simpler water management and higher CO tolerance may be the greatest advantages in the intermediate-temperature fuel cells, which make the fuel cell systems possible to be significantly simpler and more economic.

Simplicity of heat management – Increase of the operating temperature will make a simpler cooling system in the fuel cell-powered vehicles [24]. The heat from a working fuel

cell stack must be quickly removed otherwise the fuel cell system will overheat. It is well known that the rate of heat transport is proportional to the temperature difference between the fuel cell and the environment. For PEMFC operating at the low temperature of 80ºC, the heat rejection rate of the automotive radiators is insufficient to reject continuous full power waste heat, which requires a complex cooling system with a large dimension and weight. For example, the cooling system in the fuel cell cars accounts for about 50 wt.% of the total fuel cell system. However, if the operating temperature is elevated, the volume and weight of the radiators will be smaller and lighter with increasing its heat rejection rate.

Utilization of waste heat (Heat recovery) – The waste heat from the intermediate-temperature fuel cells can be efficiently used. The heat energy from a PEMFC stack at around 80ºC is of little value to recover for stationary applications. If the operating temperature is elevated to, for example, 200ºC, water steam of up to 15 atm can be produced from a fuel cell stack [22]. This heat can be directly used for heating so that the overall efficiency will be improved for the stationary purposes. For example, it will be efficiently applied for residential heating and boiled water. In can be also be used to operate the system at high pressures or to produce steam for fuel reforming. For steam reforming of both natural gas at 800ºC and methanol at 300ºC, preheating fuels and water up to 200ºC will significantly improve the overall system energy efficiency.

Direct use of alternative fuels – Hydrogen, which is commonly used as fuel in PEMFCs, presents several problems, such as low storage density, high cost, and lack of distribution infrastructure [25]. An external fuel processor such as reforming and shift reaction (CO removal) is commonly incorporated into the system to produce the hydrogen. However, if alternative fuels such as alcohol, ether, and hydrocarbons can be used as a direct fuel for the fuel cell, it not only decreases the cost and complexity of the fuel cell systems, but also increases the overall efficiency. For the use of the alternative fuels, high operating temperatures above 100ºC may be required due to low electrode kinetics for oxidation of the

fuels.

Non-platinum catalysts – With the increase of operating temperature, the electrode reaction kinetics will be greatly enhanced, thus make it possible to use non-platinum catalysts, reducing the total cost of PEMFCs [26].

1.3.2 Progress in intermediate-temperature fuel cells

In order to operate PEMFCs above 100ºC with a low humidified condition, many current research efforts have been devoted to the development of alternative electrolytes. The researches can be classified into three groups: (1) modified PFSA membranes, (2) sulfonated or acid doped hydrocarbon polymers, and (3) anhydrous proton conductors.

1.3.2.1 Modified PFSA membranes

PFSA membranes such as Nafion were modified by incorporating hygroscopic oxides such as SiO_2 and TiO_2. Watanabe et. al reported the first the Nafion/SiO_2 (or TiO_2) composite membrane which showed an improved water retention and a cell operation using a lower humidity, while no elevated H_2/O_2 PEMFC experiments above 100°C [27]. Such modified PFSA membranes were also tasted at higher temperatures above 100°C while in humidified conditions. They have higher water content and almost comparable proton conductivities up to around 120°C compared the unmodified Nafion membrane [28]. A fuel cell using the Nafion/TiO_2 composite as an electrolyte showed relatively high cell performance at 110°C in fully humidified conditions, comparable to that of PEMFCs at the normal operating temperature, although above temperature reduced the cell performance [29].

1.3.2.2 Sulfonated or acid doped hydrocarbon polymers

Another approach to the high temperature operation is the development of alternative polymer electrolytes to PFSA membranes. Considerable investigations have focused on

sulfonated hydrocarbon polymers such as polyetheretherketone (PEEK), polyimides (PI), poly(4-phenoxybenzoyl-1,4-phenylene) (PPBP), and polybenzimidazoles (PBI) due to their good thermal stability and mechanical properties [22,30]. High conductivity of sulfonated hydrocarbon polymers can be obtained at high sulfonation degree, but high sulfonation results in poor mechanical properties, especially at higher operating temperatures. Such a progressive mechanical deterioration leads to a downfall of the conductivity [31]. As their proton conductivities, for example, the conductivity of S-PEEK with a sulfonation level of 60 mol% was 5×10^{-2} S cm^{-1} at 100 °C and 100% relative humidity [32]. However, it was further claimed that the S-PEEK loses water up to 150°C, leading to a decrease in the conductivity, and degradation of the sulphonic groups take place up to 240°C. They are not very good proton conductors at the intermediate temperatures, even in a water-saturated environment and the performance of most has not been reported in operating fuel cells. More evaluation is needed for their application in the intermediate-temperature fuel cells.

On the other hand, acid-doped polymer represents an effective approach to development of proton-conducting membranes. A basic polymer such as polybenzimidazole (PBI) can be complexed with acids. In particular, it has been shown that H_3PO_4-doped PBI membranes present relatively high proton conductivities up to 5×10^{-2} S cm^{-1}, depending on the acid-doping level, at elevated temperatures and low humidified conditions [33,34]. Thus 'acid management' may pose long-term challenges for these materials. The conductivity increases significantly with RH as the rate of proton transfer involving H_2O is faster. However, under dry condition and high temperature, doped H_3PO_4 is dimerized or condensed to form higher polyphosphoric acid, causing low conductivity. As reported by Ma et al.[35], the proton conductivity of the H_3PO_4-doped PBI membranes decreases above 130-140°C under dry condition due to the formation of pyrophosphoric acid ($H_4P_2O_7$). Hggins and Baldwin studied the species equilibrium of pure H_3PO_4 at 176°C and obtained 40% pyrophosphoric acid [36]. As a result, its operating temperatures can be up to 150°C without any humidification [35,37],

and up to 200°C with some humidified conditions while its RH is relatively low, 5~30% [38,39]. More recently, it has been reported that its cell performance at 160°C is comparable to that of the normal PEMFCs at a low operating temperature [40].

1.3.2.3 Anhydrous proton conductors

The third approach to the high temperature operation is the development of anhydrous proton conductors which do not require water for its proton transport. As an electrolyte for the intermediate-temperature fuel cells, the proton conductors are desirable to be solid state and to show conductivities $>10^{-2}$ S cm^{-1} above 150°C and unhumidified conditions. Such proton conductors usually consist of oxyanions (SO_4^{2-} or PO_4^{3-}), wherein an oxide ion joined with a proton by a hydrogen bond. However, there is a temperature limitation on the use of sulfonate-based proton conductors due to thermal decomposition of the SO_4^{2-} ions above 200ºC [41]. Accordingly, a recent attention has focused on phosphate-based proton conductors, which are stable up to 200ºC or higher. Although various types of phosphate-based proton conductors have been investigated thus far including inorganic crystals [42-44], glasses (or gels) [45,46], and inorganic/organic composites [47,48], most of them cannot meet the criterion, i.e., conductivities $>10^{-2}$ S cm^{-1} in unhumidified conditions. Therefore, my attention has focused on the development of phosphate-based anhydrous proton conductor with higher proton conductivity and its intermediate-temperature fuel cells, as described in the next section entitled “Aim of the thesis”.

1.4 Aim of the thesis

1.4.1 Background

PEMFCs have received increasing interest in recent years because of their high efficiency and environmentally-friendly characteristics. Proton-conducting PFSA such as Nafion are

commonly used as the electrolytes. However, these electrolytes present some challenges regarding technology and materials costs for the commercialization of PEMFCs as described above sections. Since protons attach themselves to water and diffuse as H_3O^+ ions through the electrolyte, the operating temperature of PEMFCs is limited to the dehydration temperature of ~100ºC, causing serious CO poisoning of the anode elctrocatalysts and requiring the use of the expensive Pt catalyst to catalyze the electrode reactions. These electrolytes also require highly humidified conditions to achieve sufficient proton conductivity, and the use of the large water control unit required complicates fuel cell systems. These challenges would be overcome by using a proton conductor capable of operating above 100ºC under unhumidified conditions.

Recently, Hibino et al. found that an anhydrous proton conductor, In^{3+}-doped SnP_2O_7 ($Sn_{0.9}In_{0.1}P_2O_7$), shows high proton conductivities between 150 and 300°C under unhumidified conditions [49]. $Sn_{0.9}In_{0.1}P_2O_7$ shows a cubic structure with SnO_6 octahedra and P_2O_7 units at the corners and the edges, respectively (Fig. 1-7). Such closely packed P_2O_7 units could provide many proton bonding sites and associated transport pathways in the bulk, resulting in high proton conductivities above 0.1 S cm^{-1} between 150 and 350°C under

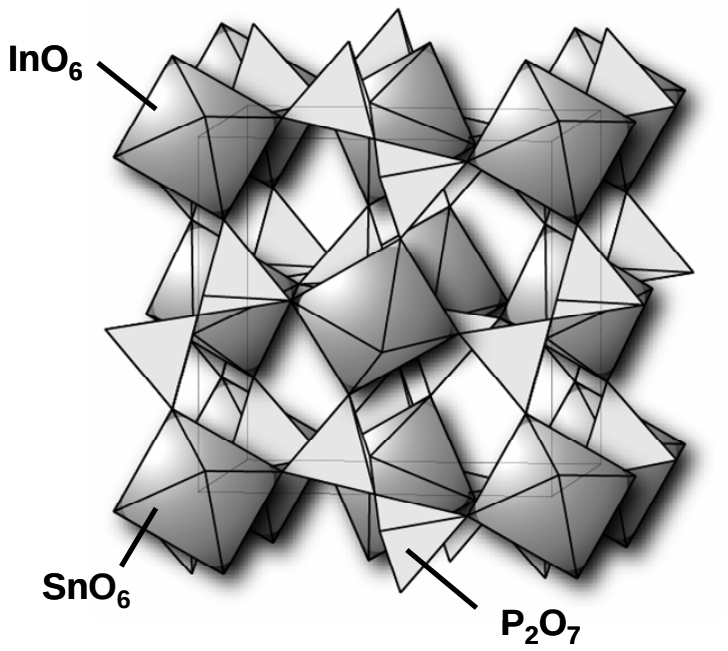

Figure 1-7. Structure of $Sn_{0.9}In_{0.1}P_2O_7$.

unhumidified conditions.

1.4.2 Aim of this thesis

The aim of this study is to demonstrate the feasibility of intermediate-temperature fuel cells using $Sn_{0.9}In_{0.1}P_2O_7$ as an electrolyte and to prove desirable attributes in the intermediate-temperature fuel cells over current PEMFCs. The desirable attributes include operation in unhumidified condition, high CO tolerance, use of alternative catalysts to expensive Pt catalyst and use of alternative fuels to pure hydrogen as well.

1.4.3 Scope

In Chapter 2, the proton conductivity of $Sn_{0.9}In_{0.1}P_2O_7$ and the proton conduction in the $Sn_{0.9}In_{0.1}P_2O_7$ are presented. Especially, the In^{3+} doping effect on the proton conductivity of SnP_2O_7 and the incorporation of protons in In^{3+}-doped SnP_2O_7 are discussed in this study. In Chapter 3, performance of the intermediate-temperature fuel cell is investigated between 150 and 300°C under unhumidified condition. In particular, this study is centered on fuel cell performance under unhumidified conditions and on tolerance of the electrocatalyst to CO. There are additional advantages expected in the intermediate-temperature fuel cell. The development of alternative catalysts to replace Pt is attempted for anode and cathodes in the intermediate-temperature fuel cell in Chapter 4. Furthermore, alternative fuels to replace hydrogen are directly used in the intermediate-temperature fuel cell in Chapter 5. Especially, the anode reactions of the fuels used are investigated in this study. However, $Sn_{0.9}In_{0.1}P_2O_7$ electrolytes may be required to be a thin, dense, and flexible electrolyte membrane for its practical applications. In Chapter 6, thus, organic/inorganic composite membranes based on $Sn_{0.9}In_{0.1}P_2O_7$ are investigated for the intermediate-temperature fuel cell.

1.5 References

[1] S. Srinivasan, "Fuel Cells: From Fundamentals to Applications", *Springer Science* (2006).

[2] T. Kudo, O. Yamamoto, and H. Iwahara, "Fuel cells: Fundamentals from Thermodynamics and Development of Actual Technology", *Uchida Rokakuho* (2005).

[3] F. Barbir, "PEM Fuel Cells: Theory and Practice", *Elsevier Academic Press* (2005).

[4] T. Norby, *Nature*, **410**, 877 (2001).

[5] S. Lister and G. McLean, *J. Power Sources*, **130**, 61 (2004).

[6] E.A. Ticianelli, C.R. Derouin, A. Redondo and S. Srinivasan, *J. Electrochem. Soc.* **135** (1988).

[7] J. Xie, F. Garzon, T. Zawodzinsk and W. Smith, *J. Electrochem. Soc.*, **151**, A1084 (2004).

[8] H. A. Gasteiger, S. S. Kocha, B. Sompalli, and F. T. Wagner, *Appl. Catal. B: Environ.*, **46**, 9 (2005)

[9] Z. Qi and A. Kaufman, *J. Power Sources*, **113**, 37 (2003).

[10] E. Passalacqua, F. Lufrano, G. Squadrito, A. Patti and L. Giorgi, *Electrochim. Acta*, **46**, 799(2001).

[11] J. Scholta, B. Rohaland, V. Trapp, and U. Focken, *J. Power Sources*, **84**, 231 (1999).

[12] D. P. Davies, P. L. Adcock, M. Turpin, and S. J. Rowen, *J. Power Sources*, **86**, 237 (2000).

[13] H. Tawfik, Y. Hung, and D. Mahajan, *J. Power Sources*, **163**, 755 (2007).

[14] A. Karthikeyan, C. Martindale, and S. W. Martin, *J. Non-Cryst. Solids*, **349**, 215 (2004).

[15] P. Berg, K. Promislow, J. S. Pierre, J. Stumper, and B. Wetton, *J. Electrochem. Soc.*, **151**, A341 (2004).

[16] C. Yang, P. Costamagna, S. Srinivasan, J. Benziger, A. B. Bocarsly, *J. Power Sources*, **103**, 1 (2001).

[17] N. P. Brandon, S. Skinner and B. C. H. Steele, *Ann. Rev. Mater. Res.* **33**, 183 (2003).

[18] M. Watanabe, M. Uchida, and S. Motoo, *J. Electroanal. Chem.*, **229**, 395 (1987).

[19] D. C. Papageorgopoulos, M. P. de Heer, M. Keijzer, J. A. Z. Pieterse, and F. A. de Bruijn, *J. Electrochem. Soc.*, **151,** A763 (2004).

[20] H. A. Gasteiger, J. E. Panels and S. G. Yan, *J. Power Sources*, **127** 162 (2004).

[21] J. Zhang, Z. Xie, J. Zhang, Y. Tang, C. Song, T. Navessin, Z. Shi, D. Song, H. Wang, D. P. Wilkinson, Z. Liu, and Steven Holdcroft, *J. Power Sources*, **160**, 872 (2006).

[22] Q. Li, R. He, J. O. Jensen, and N. J. Bjerrum, *Chem. Mater.*, **15**, 4896 (2003).

[23] Q. Li, R. He, J. Gao, J. O. Jensen, and N. J. Bjerrum, *J. Electrochem. Soc.*, **150**, A1599 (2003).

[24] Y. Shao, G. Yin, Z. Wang, and Y. Gao, *J. Power Sources*, **167**, 235 (2007).

[25] M. M. Mench, H. M. Chance, and C. Y. Wang, *J. Electrochem. Soc.*, **151**, A144 (2004).

[26] B. Wang, *J. Power Sources*, **152**, 1 (2005).

[27] M. Watanabe, H. Uchida, Y. Seki and M. Emori, *J. Electrochem. Soc.*, **143**, 3827 (1996).

[28] N. Miyake, J. Wainright and R. Savinell *J. Electrochem. Soc.*, **148**, A898 (2001).
[29] A. Saccà, A. Carbone, E. Passalacqua, A. D'Epifanio, S. Licoccia, E. Traversa, E. Sala, F. Traini and R. Ornelas, *J. Power Sources*, **152**, 16 (2005).
[30] B. Smitha, S. Sridhar and A. A. Khan, *J. Membr. Sci.*, **259**, 10 (2005).
[31] M.L. Di Vona, D. Marani, A. D'Epifanio, S. Licoccia, I. Beurroies, R. Denoyel and P. Knauth, *J. Membr. Sci.*, **304**, 76 (2007).
[32] O. Savadogo, *J. Power Sources*, **127**, 135 (2004).
[33] J. S. Wainright, J. T. Wang, R. F. Savinell, and M. H. Litt, *J. Electrochem. Soc.*, **142**, L121 (2004).
[34] B. Xing and O. Savadogo, *J. New Mater. Electrochem. Syst.*, **2**, 95 (1999).
[35] Y.-L. Ma, J. S. Wainright, M. H. Litt, and R. F. Savinell, *J. Electrochem. Soc.*, **151**, A8 (2004).
[36] C. E. Higgins and W. H. Baldwin, *Anal. Chem.*, 27, 1780 (1955).
[37] J. Lobato, P. Canizares, M. A. Rodrigo, and J. J. Kinares, *Electrochim. Acta.*, **52***,* 3910 (2007).
[38] J. T. Wang, R. F. Savinell, J. Wainright, M. Litt, and H. Yu, *Electrochim. Acta.*, **41***,* 193 (1996).
[39] R. He, Q. Li, A. Bach, J. O. Jensen, and N. J. Bjerrum, *J. Membr. Sci.*, **227**, 38 (2006).
[40] L. Xiao, H. Zhang, E. Scanlon, L. S. Ramanathan, E.-W. Choe, D. Rogers, T. Apple and B. C. Benicewicz, *Chem. Mater.*, **17**, 5328 (2005).
[41] S. M. Haile, D. A. Boysen, C. R. I. Chisholm, R. B. Merle, *Nature*, **410**, 910 (2001).
[42] T. Kenjo, Y. Ogawa, *Solid State Ionics*, **76**, 29 (1995).
[43] T. Matsui, S. Takeshita, Y. Iriyama, T. Abe, M. Inaba, Z. Ogumi, *Electrochem Commun.*, **6**, 180 (2004).
[44] D. A. Boysen, T. Uda, C. R. I. Chisholm, S. M. Haile, *Science*, **303**, 68 (2004).
[45] W. Wieczorek, G. Zukowska, R. Borkowska, S. H. Chung, S. Greenbaum, *Electrochim. Acta*, **46**, 1427 (2001).
[46] A. Matsuda, T. Kanzaki, K. Tadanaga, M. Tatsumisago, T. Minami, *Solid State Ionics*, **154-155**, 687 (2002).
[47] J. D. Kim, I. Honma, *Electrochim. Acta.*, **49***,* 3179 (2004).
[48] C. Yang, S. Srinivasan, A. B. Bocarsly, S. Tulyani, J. B. Benziger, *J. Memb. Sci.*, **237**, 145 (2004).
[49] M. Nagao, A. Takeuchi, P. Heo, T. Hibino, M. Sano, A. Tomita, *Electrochem. Solid-State Lett.*, **9**, A105 (2006).

2 A Proton-Conducting In^{3+}-doped SnP_2O_7 Electrolyte

2.1 Introduction

Considerable efforts have recently been devoted towards the development of solid-state proton conductors with conductivities $>10^{-2}$ S cm^{-1} between 150 and 400ºC. Although many hydrous proton conductors have been reported, most of them cannot meet this criterion. This is because protons attach themselves to water and diffuse as H_3O^+ ions through the solid (vehicular mechanism) [1], which limits the operating temperature to the dehydration temperature of ~100ºC. On the other hand, anhydrous proton conductors can, in principle, avoid this problem, since protons migrate via jumps between adjacent oxide ions by a series of "making and breaking" hydrogen bonds (Grotthuss mechanism) [1]. Such proton conductors usually consist of oxyanions (SO_4^{2-} or PO_4^{3-}), wherein an oxide ion joined with a proton by a hydrogen bond. However, there is a temperature limitation on the use of sulfonate-based proton conductors due to thermal decomposition of the SO_4^{2-} ions above 200ºC [2]. Thus, recently, attention has increasingly focused on phosphate-based proton conductors, which are stable up to 200ºC or higher. Various types of phosphate-based proton conductors have been investigated thus far including inorganic crystals [3-5], glasses (or gels) [6,7], and inorganic/organic composites [8,9]. CsH_2PO_4 is a very promising material for intermediate-temperature proton conductors, showing a conductivity of 2.0×10^{-2} S cm^{-1} at a temperature of 235ºC and a water partial pressure (P_{H2O}) of 0.3 atm [5]. A further increase in the proton conductivity and further reduction in the relative humidity would enhance the position of intermediate-temperature fuel cells as preferred electric power generation devices.

Recently, Hibino et al. found that an anhydrous proton conductor, SnP_2O_7, shows high proton conductivities $> 10^{-2}$ S cm^{-1} between 150 and 300°C under unhumidified conditions

[10]. This material has a cubic or pseudo-cubic structure over a wide temperature range, which is characterized by SnO_6 octahedra at the corners and P_2O_7 units at the edges [11]. There are nominally no structural protons in SnP_2O_7, suggesting that protons dissolve as defects in the presence of hydrogen-containing gases. A similar proton incorporation mechanism has been proposed for Ca^{2+}- or Sr^{2+}-doped $LaPO_4$ in phosphate-based proton conductors [12,13]. However, the proton conductivities of the $LaPO_4$-based proton conductors were much lower than those of SnP_2O_7 in the temperature range from 150 to 300°C, probably due to the difference in their constituent oxyanions ($P_2O_7^{4+}$ and PO_4^{3+}). Indeed, the previous study showed that the conductivity of $SnHPO_4$ was about three orders of magnitude lower than that of SnP_2O_7 [10].

The goal of this study is to improve the proton conductivity of SnP_2O_7 by the substitution of In^{3+} cations for a part of Sn^{4+} cations and to investigate proton conduction in In^{3+}-doped SnP_2O_7 by various techniques.

2.2 Experimental

2.2.1 Synthesis of In^{3+}-doped SnP_2O_7

In^{3+}-doped SnP_2O_7 was prepared as follows. SnO_2 and In_2O_3 powders were mixed with 85% H_3PO_4 and ion-exchanged water. The mixture was held with stirring at 300°C (plate temperature) until they formed a high viscosity paste. In this case, the H_3PO_4/MO_x (M=Sn and In) molar ratio was controlled to be 2.8, since a fraction of H_3PO_4 was lost by the subsequent heating treatment (for example, 6.782 g SnO_2, 0.6941 g In_2O_3, 16.141 g H_3PO_4, and 100 mL ion-exchanged water were used at once time). The pastes were calcined in an alumina pot with an alumina cap at 650°C for 2.5 hours and then ground with a mortar and pestle.

$Sn_{1-x}In_x(P_2O_7)_{1-y}$ was also synthesized in a similar manner. In this case, the x and y values were changed by varying the molar ratio of the raw materials, i.e., SnO_2, In_2O_3, and H_3PO_4.

2.2.2 Material characteristics

The final P/(Sn+In) molar ratio of the compounds was confirmed to be 2.0 (±0.02) from X-ray fluorescence (XRF). The crystalline structure of the compounds was analyzed by X-ray diffraction (XRD). FT-IR spectra of the compounds were measured in the transmission mode by KBr pellets technique. Data points were obtained in 60 scans with a resolution of 4 cm^{-1}. Temperature programmed desorption (TPD) spectra of the compounds were measured on a conventional TPD apparatus with an on-line mass spectrometer [22]. The sample powders were heated in a stream of humidified argon at 200°C for 2 hours. After the purging with dry argon (99.999%) for 12 hours, the sample powders were heated at a rate of 5°C min^{-1} until the evolution of gases was completed.

2.2.3 Electrochemical measurements

For electrochemical measurements, the compound powders were pressed into pellets under a pressure of 2 x 10^3 kg cm^{-2}. Impedance spectra measurements (i.e., ac conductivity measurement) were carried out by the standard four probe method. The frequency range was 0.1 - 10^6 Hz, and the AC amplitude was 10 mV. The H/D isotope effect on the conductivity was also investigated by replacing argon with P_{H2O} = 0.03 atm and P_{D2O} = 0.03 atm. Two types of galvanic cells, H_2 and steam concentration cells, were fabricated using the pellet (thickness: 1.0-1.2 mm, diameter: 12 mm) as the electrolyte membrane. Both anode and cathode (area: 0.5 cm^2) were made from catalyst (10 wt.% Pt/C, E-TEK) and carbon paper (Toray TGPH-090), wherein the Pt loading was 0.6 mg cm^{-2}.

2.3 Results and Discussion

2.3.1 Conductivity of In^{3+}-doped SnP_2O_7

Figure 2-1 shows typical XRD patterns of non- and In^{3+}-doped SnP_2O_7 measured at room temperature. The peaks observed for SnP_2O_7 were almost identical to those reported in the literature [11]. $Sn_{1-x}In_xP_2O_7$ with In^{3+} content of not more than 10 mol% showed the same patterns as those of SnP_2O_7 and an increasing lattice constant with increasing In^{3+} content; 7.945 Å for SnP_2O_7 and 7.950 Å for $Sn_{0.9}In_{0.1}P_2O_7$. However, $Sn_{1-x}In_xP_2O_7$ with In^{3+} contents of 20 and 30 mol% contained some other unidentified peaks. It seems that the In^{3+} content of 10 mol% is a substitutable limit of In^{3+} for Sn^{4+}.

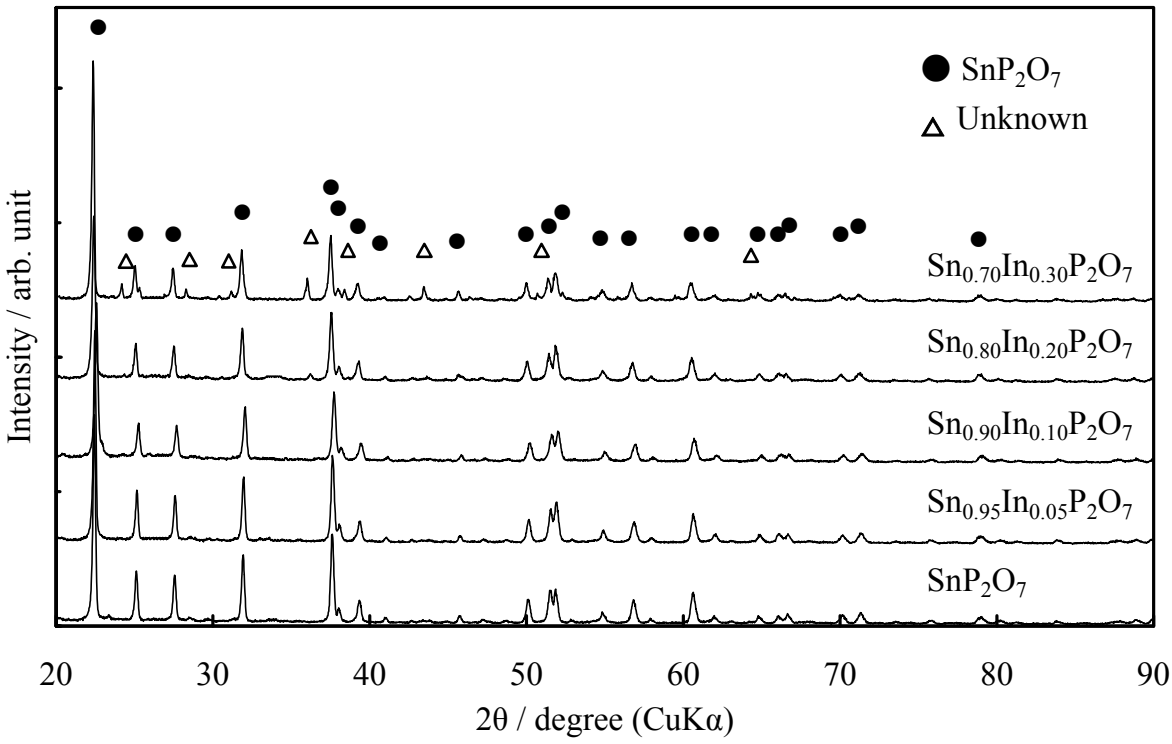

Figure 2-1. XRD patterns of non- and In^{3+}-doped SnP_2O_7.

The conductivities of non- and In^{3+}-doped SnP_2O_7 at different temperatures in an unhumidified air (P_{H_2O} = ~0.0075 atm) are shown in Fig. 2-2. The substitution of In^{3+} for Sn^{4+} enhanced the conductivity, and an impurity phase formed at the In^{3+} contents of more than 10 mol% deteriorated the conductivity. It should be noted that the conductivities of non- and In^{3+}-doped SnP_2O_7 increased monotonously with increasing temperature, which was different from "superprotonic" behavior [1,2,5] that shows a sharp increase in the conductivity of some

orders of magnitude by a structural transition from low- to high-temperature phase. This is because SnP_2O_7 shows no structural transition in the temperature range of interest, as described above. 10 mol% In^{3+}-doped SnP_2O_7 ($Sn_{0.9}In_{0.1}P_2O_7$) with the highest conductivity of 1.95 x 10^{-1} S cm^{-1} at 250°C was used in subsequent experiments.

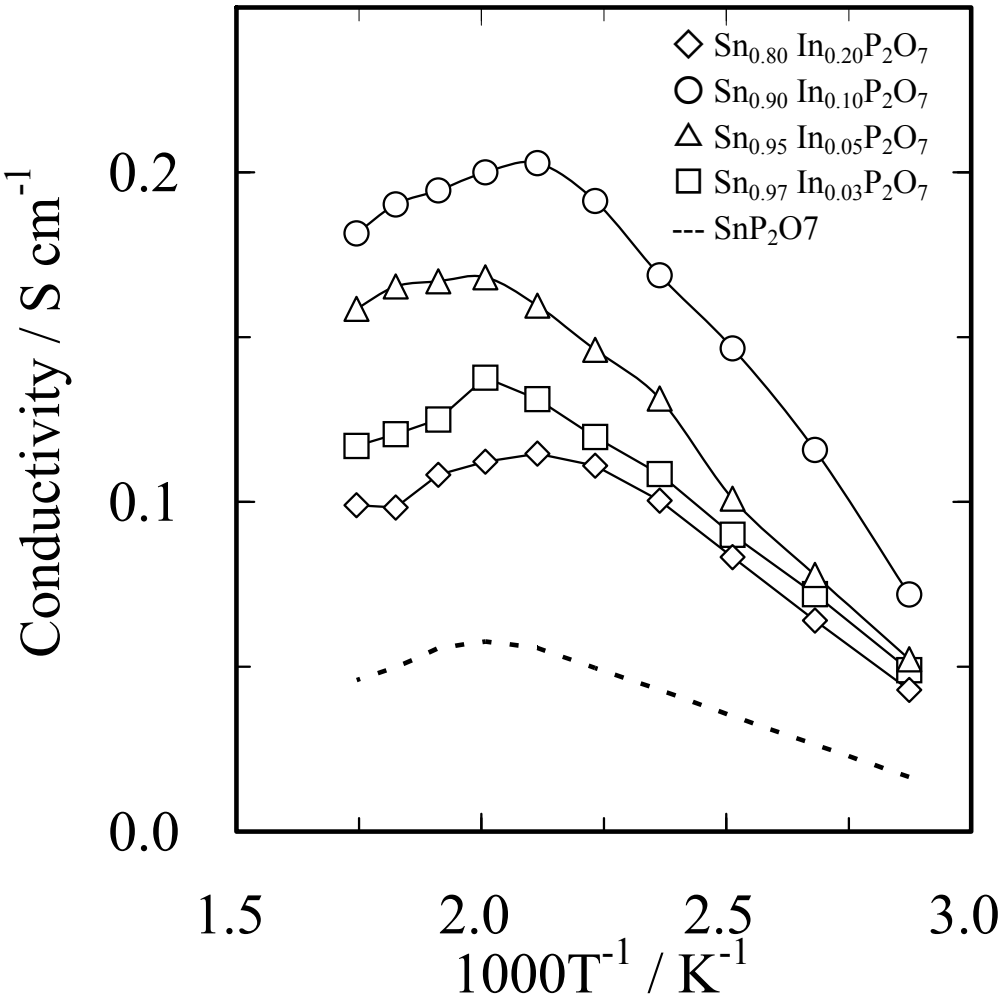

Figure 2-2. Temperature dependence of conductivity of non- and In^{3+}-doped SnP_2O_7. The samples were maintained in unhumidified air (P_{H2O} = ~0.0075 atm).

2.3.1 Proton conduction in $Sn_{0.9}In_{0.1}P_2O_7$

2.3.1.1 Proton transport number of $Sn_{0.9}In_{0.1}P_2O_7$

Comparison of the electromotive force (EMF) value of the following galvanic cells with the theoretical value calculated from Nernstian's equation was performed to estimate the ionic

transport number of $Sn_{0.9}In_{0.1}P_2O_7$ under various conditions:

$$H_2\ (1\ atm),\ Pt/C\,|\,Sn_{0.9}In_{0.1}P_2O_7\,|\,Pt/C,\ H_2{+}Ar\ (0.1\ atm) \quad (2\text{-}1)$$

$$H_2,\ Pt/C\,|\,Sn_{0.9}In_{0.1}P_2O_7\,|\,Pt/C,\ air \quad (2\text{-}2)$$

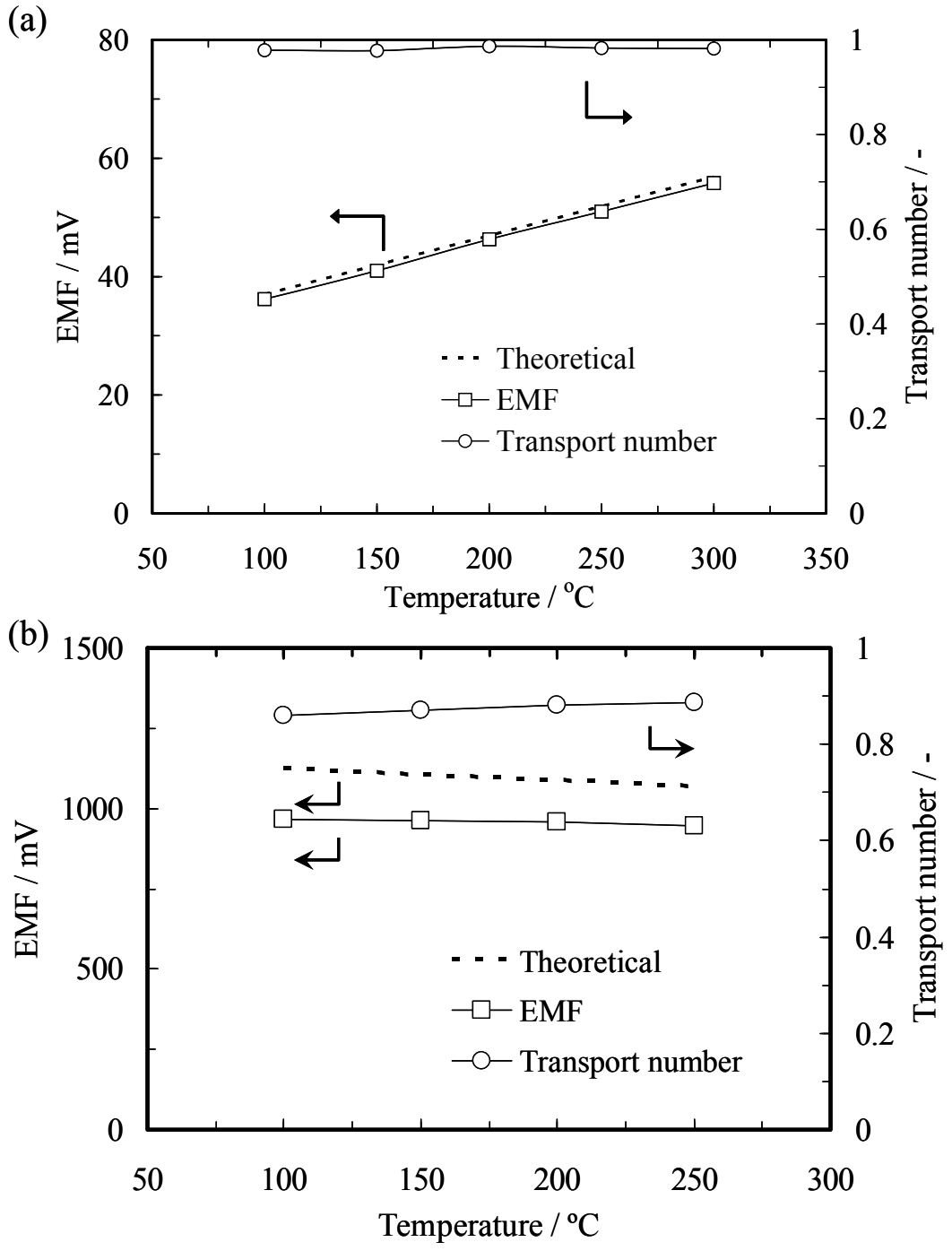

Figure 2-3. EMF values of various galvanic cells using $Sn_{0.9}In_{0.1}P_2O_7$ as an electrolyte membrane. (a) anode gas = H_2 (1 atm); cathode gas = H_2 + Ar (0.1 atm); (b) anode gas = H_2; cathode gas = air.

It can be seen from Fig. 2-3 (a) that the EMF values observed for the H_2 concentration cell (Eq. 2-1) were very near the theoretical values. I note that the cell (Eq. 2-1) is a H_2 concentration cell and also a sort of O_2 concentration cell, since the following equilibrium is established between O_2, H_2, and H_2O at each electrode;

$$H_2 + 1/2O_2 \leftrightarrows H_2O \qquad (2\text{-}3)$$

Thus, the ratio of the EMF value to the theoretical value shows the ionic (proton or oxide ion) transport number, which was calculated to be about 0.98. This means that $Sn_{0.9}In_{0.1}P_2O_7$ is substantially a pure proton conductor in H_2 atmosphere. On the other hand, it is found in Fig. 2-3 (b) that the EMF values observed for the H_2/air fuel cell (Eq. 2-2) were as high as ~0.92 V, which lower than the theoretical values of ~1.1 V. The proton transport number of $Sn_{0.9}In_{0.1}P_2O_7$ was 0.89-0.92 in H_2/air fuel cell conditions. At least two factors are responsible for the lower EMF: (1) Physical leakage of gas through the electrolyte because the EMF increased with increasing electrolyte thickness, for example, the EMF value increased from 922 to 934 mV with increasing electrolyte thickness from 1.2 to 2.6 mm;

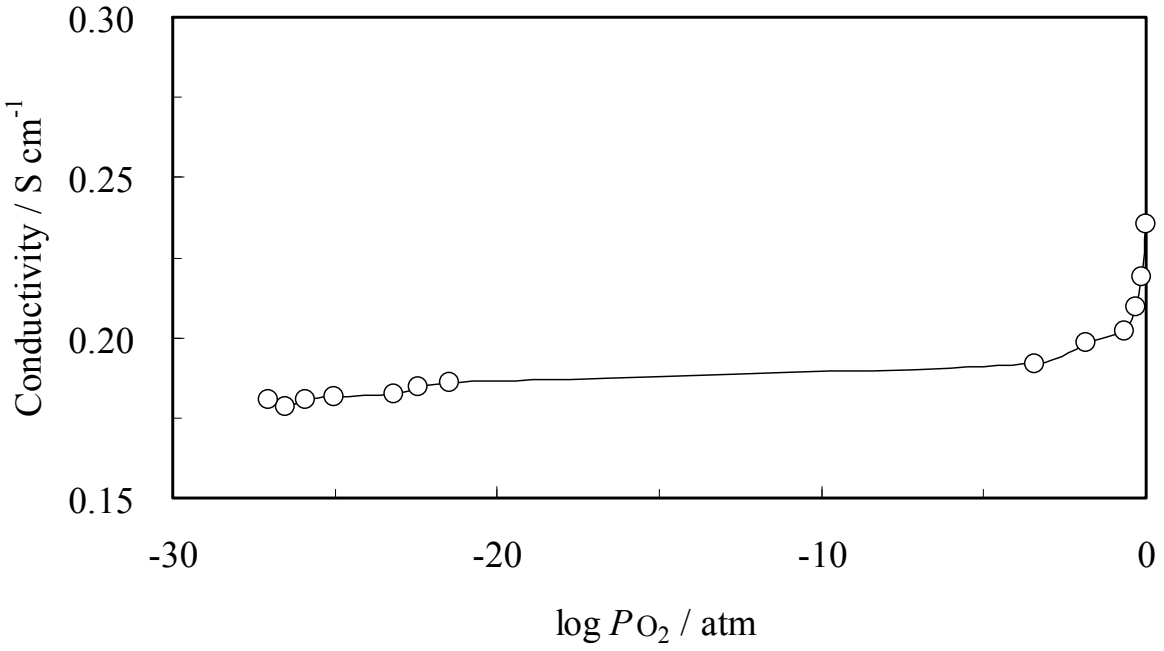

Figure 2-4. P_{O2} dependence of conductivity of $Sn_{0.9}In_{0.1}P_2O_7$ at 250°C. P_{H2O} = 0.0062, which controlled by passing O_2 gas through iced water (0°C).

(2) partial electron-hole conduction in the electrolyte causing an internal short circuit. This consideration can be supported by the dependence of the total conductivity of $Sn_{0.9}In_{0.1}P_2O_7$ on P_{O2}. The conductivity at 250°C was almost independent of P_{O2} from 10^{-22} to 10^{-3} atm, while it increased gradually with increasing P_{O2} from 10^{-3} to 1 atm, as shown in Fig. 2-4.

2.3.1.2 Proton incorporation into $Sn_{0.9}In_{0.1}P_2O_7$

$Sn_{0.9}In_{0.1}P_2O_7$ nominally does not contain protons in the bulk. I attempted to clarify the presence of protons in $Sn_{0.9}In_{0.1}P_2O_7$ by FT-IR measurements. IR spectrum of $Sn_{0.9}In_{0.1}P_2O_7$ was represented in Fig. 2-5, including the result for SnP_2O_7 for comparison. In both IR spectra, some absorption bands appeared from 1560 to 3720 cm^{-1}, with large differences in the absorbance between the two materials. The wide absorption bands centered at 1655 and 3410

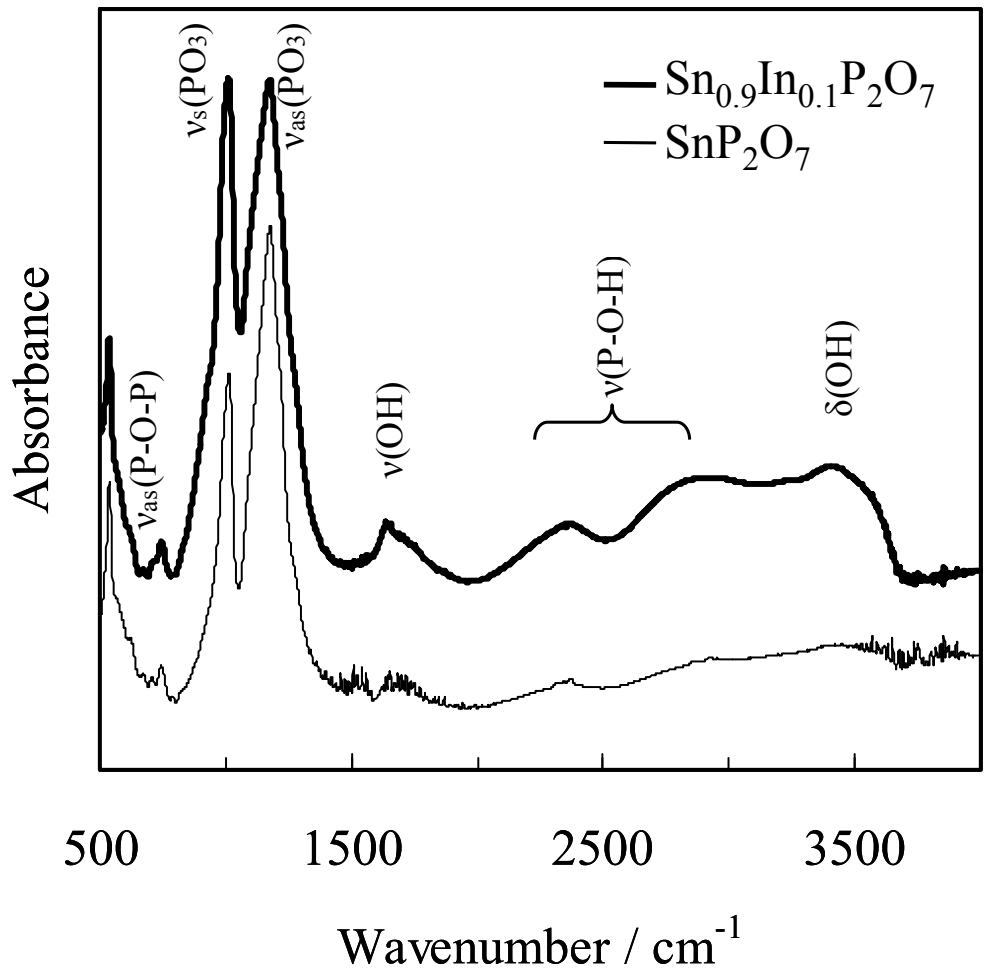

Figure 2-5. IR spectra of $Sn_{0.9}In_{0.1}P_2O_7$ and SnP_2O_7.

cm^{-1} are the evidence of υ(OH) and δ(OH), respectively, although I cannot assign perfectly all the bands to specific vibration modes. The absorbance ratios of $Sn_{0.9}In_{0.1}P_2O_7$ to SnP_2O_7 were 5.2 and 5.7 for υ(OH) and δ(OH), respectively, which are comparable to their conductivity ratio of 4.6 at 50°C (Fig. 2-2). While care should be taken for water adsorbed on the sample surface, these results at least suggest that the absorption bands are mainly attributable to protons incorporated in the bulk. It is also suggested the protons interact with the lattice oxide ions to form hydrogen bonds.

A more quantitative measurement of the proton concentration in $Sn_{0.9}In_{0.1}P_2O_7$ and SnP_2O_7 was made by TPD of hydrogen species, and their spectra are shown in Fig. 2-6. Water vapor and a small amount of H_2 were evolved from 260 to 1050°C. The evolution of water vapor from water adsorbed on the surface of the samples cannot be neglected, especially for data at relatively low temperatures. However, I determined the proton concentrations in $Sn_{0.9}In_{0.1}P_2O_7$ and SnP_2O_7 by assuming that all the evolved water vapors and H_2 are attributable to the incorporated protons. The resulting proton concentration values were 10.4 and 2.5 mol% for $Sn_{0.9}In_{0.1}P_2O_7$ and SnP_2O_7, respectively. Note that the former value was in well agreement with the proton concentration predicted from the In^{3+} content of 10 mol%. It thus appears that the protons were fully introduced as the point defects yielded by the substitution of In^{3+} to Sn^{4+}. Protons are said to dissolve in perovskite oxides such as $SrCe_{0.95}Yb_{0.05}O_{3-\alpha}$ according to Eqs. (2-4) and (2-5) [17]:

$$H_2O(g) + V_{\ddot{O}} \rightarrow 2H_i^{\cdot} + Oo^{x} \qquad (2\text{-}4)$$

$$H_2O(g) + 2h^{\cdot} \rightarrow 2H_i^{\cdot} + \frac{1}{2}O_2(g) \qquad (2\text{-}5)$$

where, $V_{\ddot{O}}$, $H_i^{\cdot}$, $h^{\cdot}$, and Oo^{x} are an oxygen vacancy, a proton, an electron hole, and a lattice oxide ion, respectively.

Eq. 2-5 may be a more appropriate equilibrium for non-doped SnP_2O_7 than Eq. 2-4, because this material has essentially electron holes rather than oxygen vacancies as the point defects.

However, when the proton conductivity of $Sn_{0.9}In_{0.1}P_2O_7$ was measured at different P_{H2O} values at 250°C, it slightly increased with increasing P_{H2O}. This result suggests that protons are incorporated into $Sn_{0.9}In_{0.1}P_2O_7$ through the reaction of Eq. 2-4 rather than the reaction of Eq. 2-5, because the order of mobility is oxygen vacancy < proton < electron hole. Therefore, the reaction of Eq. 2-4 as well as the reaction of Eq. 2-5 are possible mechanisms of proton incorporation.

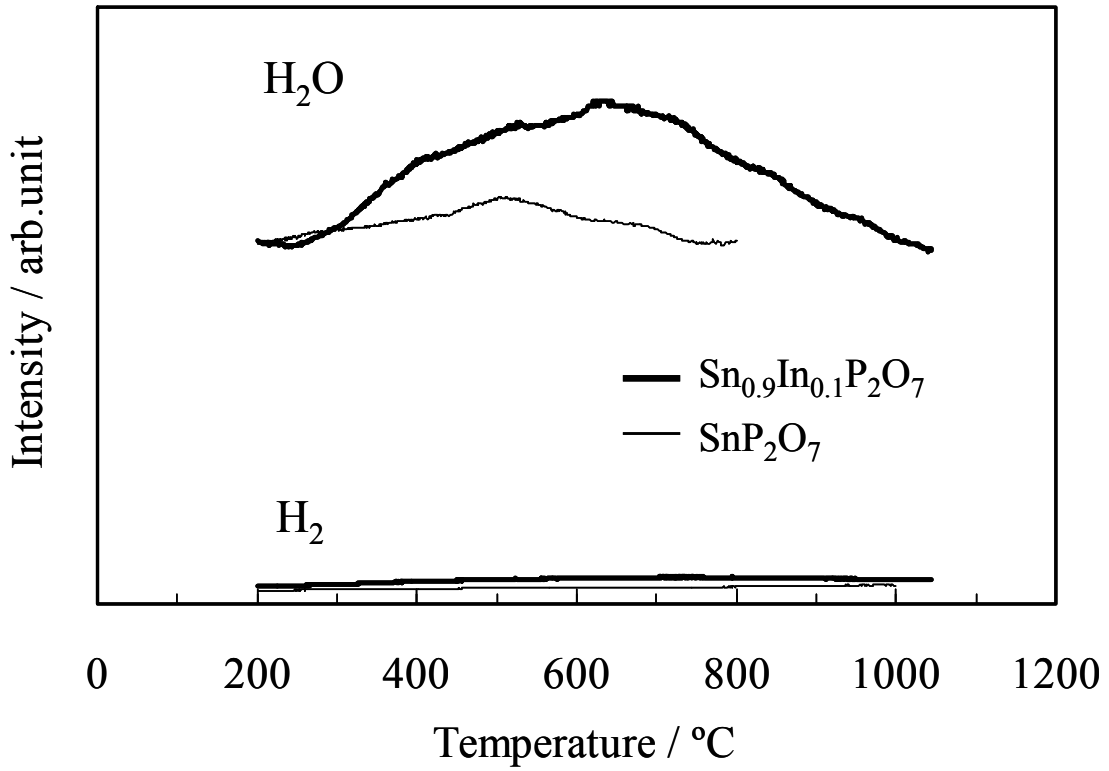

Figure 2-6. TPD spectra of $Sn_{0.9}In_{0.1}P_2O_7$ and SnP_2O_7.

2.3.1.3 Proton migration in $Sn_{0.9}In_{0.1}P_2O_7$

The H/D isotope effect on the proton conductivity provides useful information on proton conduction from different points of view. As can be seen in Fig. 2-7, $Sn_{0.9}In_{0.1}P_2O_7$ yielded a 1.06 – 1.32 times higher conductivity and lower activation energy of 0.03 eV for H_2O- than for D_2O-containing atmospheres. According to non-classical [18] or semi-classical H/D isotope effect [19], when the dissociation of the O-H bond is a rate-determining step for

proton conduction, the activation energy for D^+ is higher than that for H^+ by a difference in zero-point energy of 0.05 eV, which is near the difference in activation energy shown above. It is thus proposed that protons migrate via dissociation of hydrogen bonds with oxide ions in the P_2O_7 units. As described earlier, the protons migrated in $Sn_{0.9}In_{0.1}P_2O_7$ in a different way with respect to Grotthuss mechanism. Thus, a hopping mechanism is proper to interpret proton conduction in the present case.

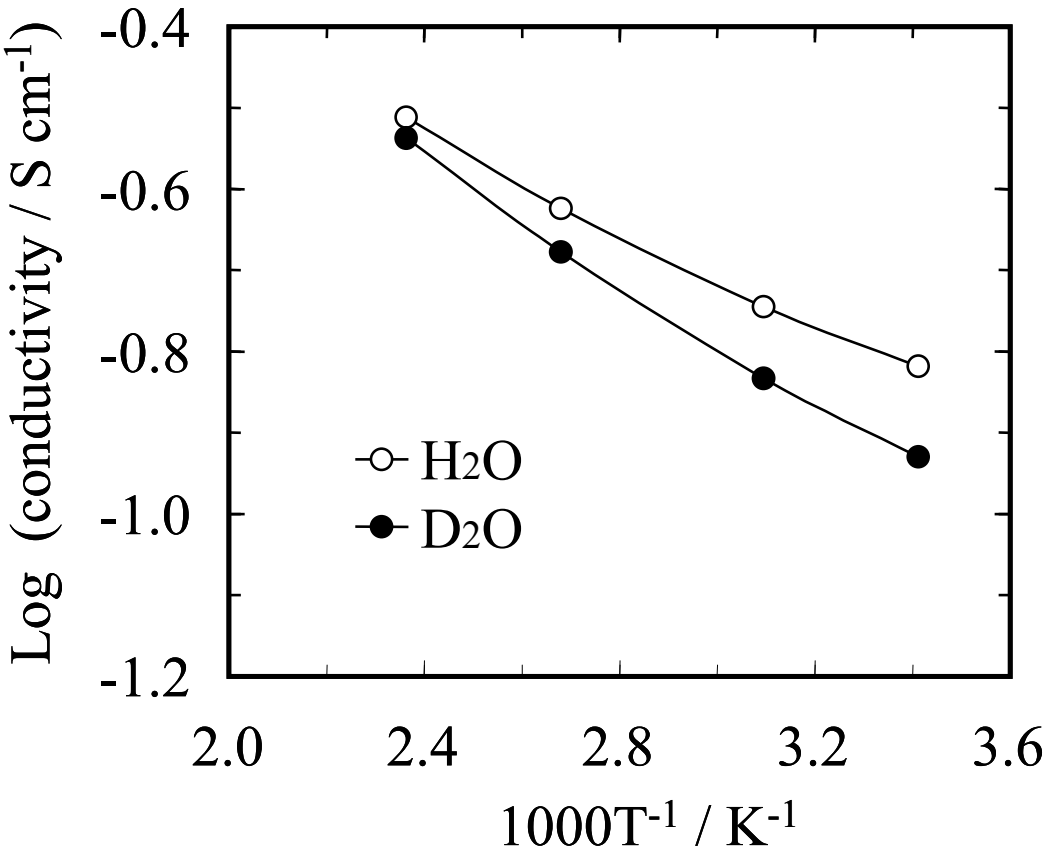

Figure 2-7. Isotope effect on conductivity of $Sn_{0.9}In_{0.1}P_2O_7$. The data were obtained in Ar saturated with H_2O or D_2O vapor at 20ºC.

2.3.1.3 Effects of P_2O_7 deficiency in $Sn_{0.9}In_{0.1}P_2O_7$ on proton conduction

P_2O_7-deficient $Sn_{0.9}In_{0.1}(P_2O_7)_{1-y}$ with y values of 0-0.15 were synthesized. Figure 2-8 shows the results of XRD measurements for $Sn_{0.9}In_{0.1}(P_2O_7)_{1-y}$. The XRD data showed

similarities in the peak position and intensity among the various $Sn_{0.9}In_{0.1}(P_2O_7)_{1-y}$ samples and an increase in the full width at half maximum (FWHM) with the amount of P_2O_7 deficiency. For example, the FWHMs for the (200) reflection of $Sn_{0.9}In_{0.1}P_2O_7$ and $Sn_{0.9}In_{0.1}(P_2O_7)_{0.85}$ were 0.192 to 0.200˚, respectively. These results suggest substantial distortion and disorder of the crystalline structure of $Sn_{0.9}In_{0.1}(P_2O_7)_{1-y}$. On the other hand, a significant decrease in the conductivity with P_2O_7 deficiency can be seen in Fig. 2-9. The proton conductivity of $Sn_{0.9}In_{0.1}(P_2O_7)_{0.85}$ was about two orders of magnitude lower than that of $Sn_{0.9}In_{0.1}P_2O_7$, indicating that the conductivity is strongly affected by the number of $P_2O_7^{4-}$ ions in the lattice.

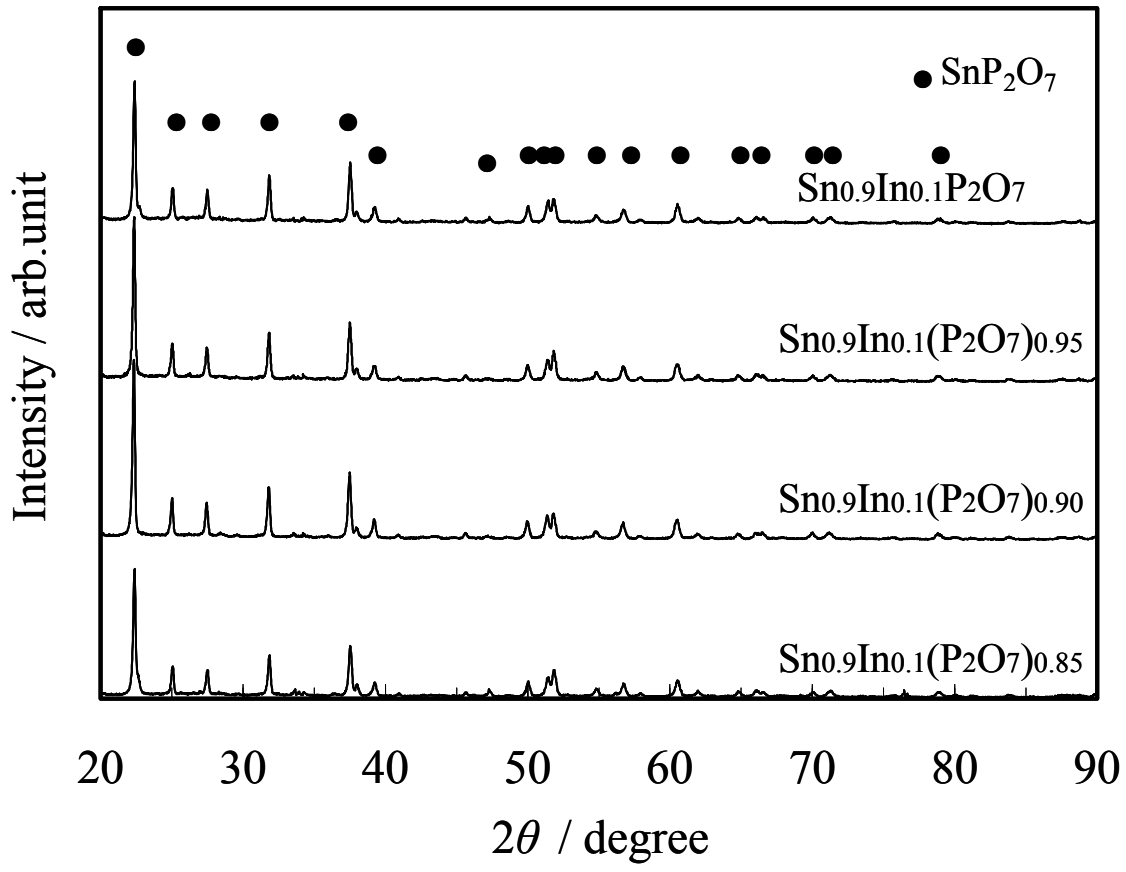

Figure 2-8. XRD patterns of $Sn_{0.9}In_{0.1}(P_2O_7)_{1-y}$.

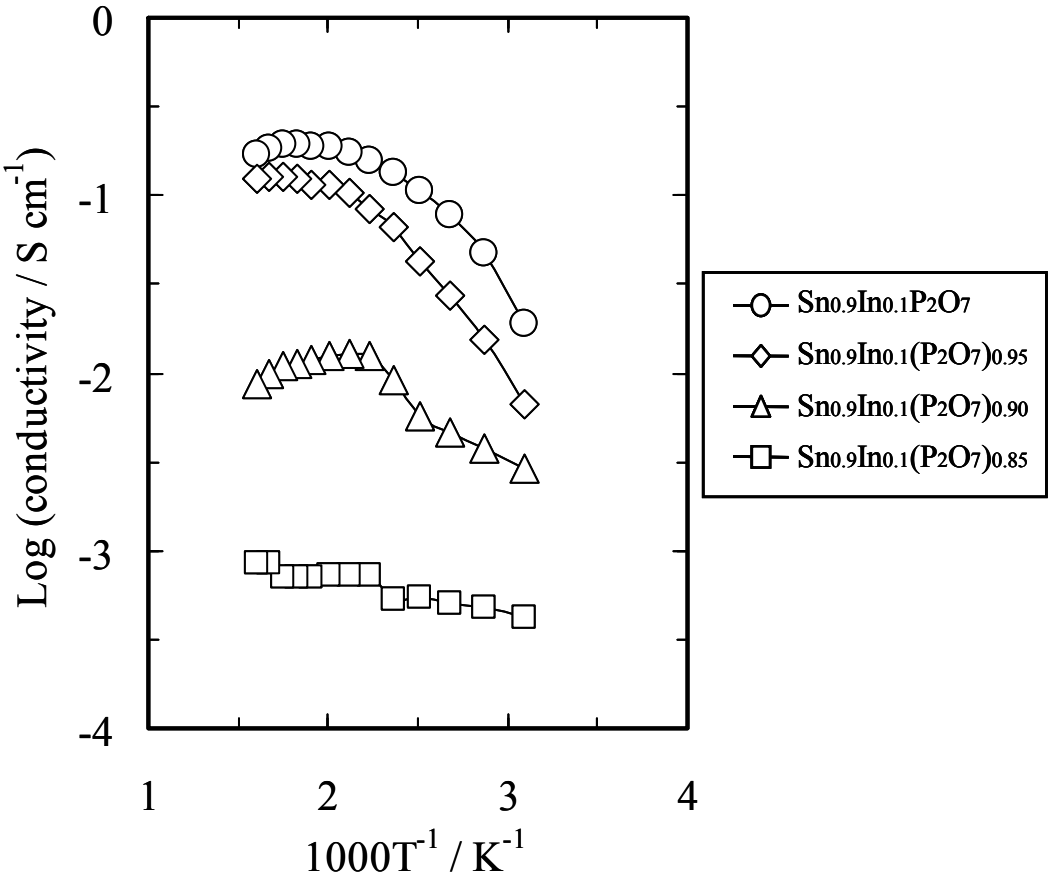

Figure 2-9. Temperature dependence of conductivity of $Sn_{0.9}In_{0.1}(P_2O_7)_{1-y}$. The samples were maintained in unhumidified air (P_{H2O} = ~ 0.0075 atm).

FT-IR measurements of $Sn_{0.9}In_{0.1}(P_2O_7)_{0.85}$ were conducted to clarify the effect of P_2O_7 deficiency on the proton conductivity. As shown in Fig. 2-10, the IR spectrum showed large peaks at almost the same wavenumbers as those observed for $Sn_{0.9}In_{0.1}P_2O_7$. The absorbance ratios of $Sn_{0.9}In_{0.1}P_2O_7$ to $Sn_{0.9}In_{0.1}(P_2O_7)_{0.85}$ were 1.4 and 1.5 for υ(OH) and δ(OH), respectively, which are much smaller than their conductivity ratio shown in Fig. 2-9. A similar behavior was obtained for the TPD spectra, as shown in Fig. 2-11. The proton concentration in $Sn_{0.9}In_{0.1}(P_2O_7)_{0.85}$ was estimated to be about 8.1 mol% per unit, which is not significantly different from the value of 10.4 mol% observed for $Sn_{0.9}In_{0.1}P_2O_7$. Therefore, it is suggested that the large difference in proton conductivity between $Sn_{0.9}In_{0.1}P_2O_7$ and $Sn_{0.9}In_{0.1}(P_2O_7)_{0.85}$ can be attributed to the difference in proton mobilities rather than proton concentrations between them. The proton conductivity, σ_H, is generally defined as follow [23];

$$\sigma_H = F\ \mu_H\ [H\cdot]\ /\ v \qquad (2\text{-}6)$$

where, σ_H, F, μ_H, $[H\cdot]$, and v are a proton conductivity, Faraday's constant, a proton mobility, a proton concentration, and a molar volume of $Sn_{0.9}In_{0.1}P_2O_7$, respectively.

The proton mobilities in $Sn_{0.9}In_{0.1}P_2O_7$ and $Sn_{0.9}In_{0.1}(P_2O_7)_{0.85}$ were calculated to be 1.49 x 10^{-3} and 6.3 x 10^{-6} $cm^2\ s^{-1}\ V^{-1}$, respectively. Considering the results from the XRD and FT-IR measurements, it is assumed that the extremely low proton mobility in $Sn_{0.9}In_{0.1}(P_2O_7)_{0.85}$ is not associated with the local environmental of the protons in the crystalline lattice, but is correlated with the long-range nature for the proton transfer between the crystalline lattices. This assumption is supported by the strong dependence of the proton conductivity on the crystalline structure of the P_2O_7-based tin phosphates with different types of P_2O_7 networks shown in Fig. 2-12. Thus, a possible speculation on the proton mobility of $Sn_{0.9}In_{0.1}(P_2O_7)_{0.85}$ is that the P_2O_7 deficiency causes a partial disconnection of the P_2O_7 network for proton conduction, resulting in a large energy barrier for proton jumps between sites.

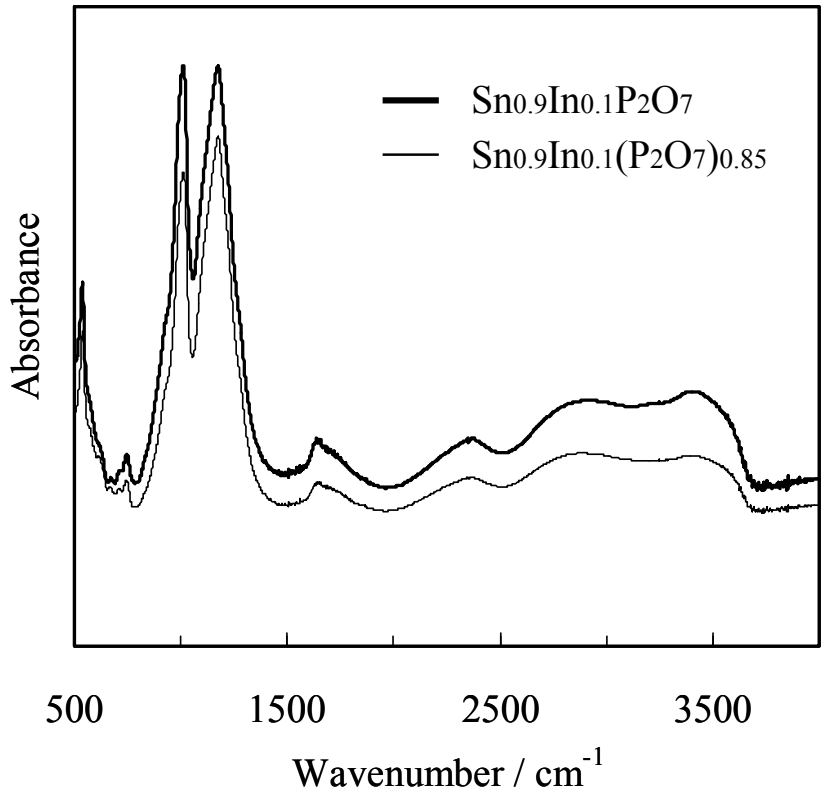

Figure 2-10. IR spectra of $Sn_{0.9}In_{0.1}P_2O_7$ and $Sn_{0.9}In_{0.1}(P_2O_7)_{0.85}$.

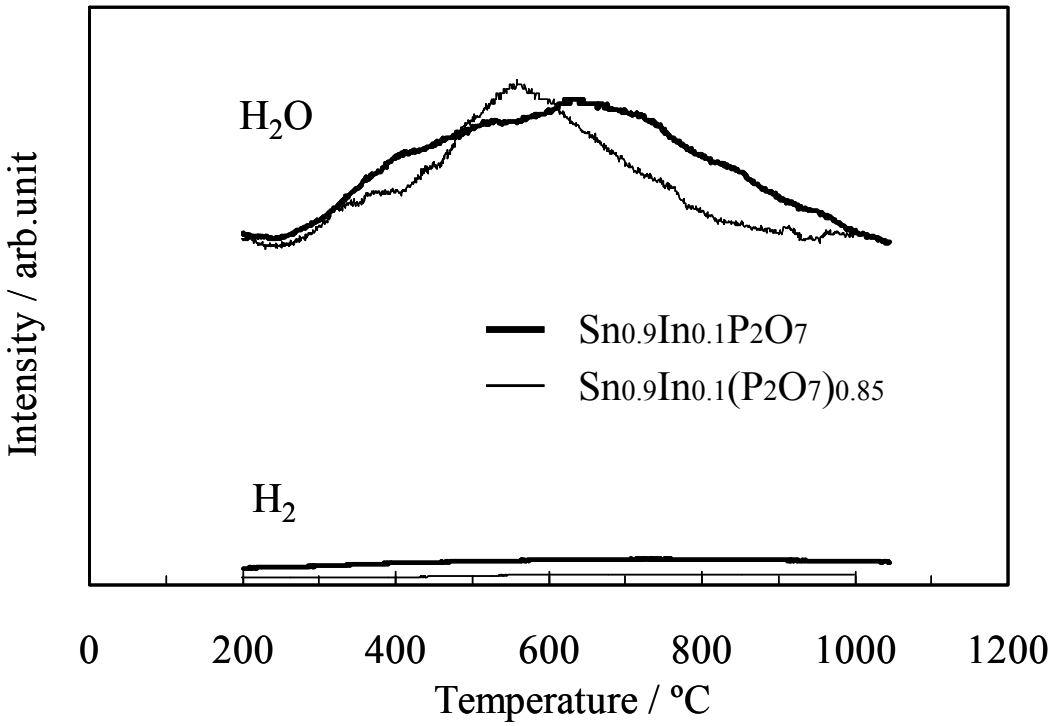

Figure 2-11. TPD spectra of $Sn_{0.9}In_{0.1}P_2O_7$ and $Sn_{0.9}In_{0.1}(P_2O_7)_{0.85}$.

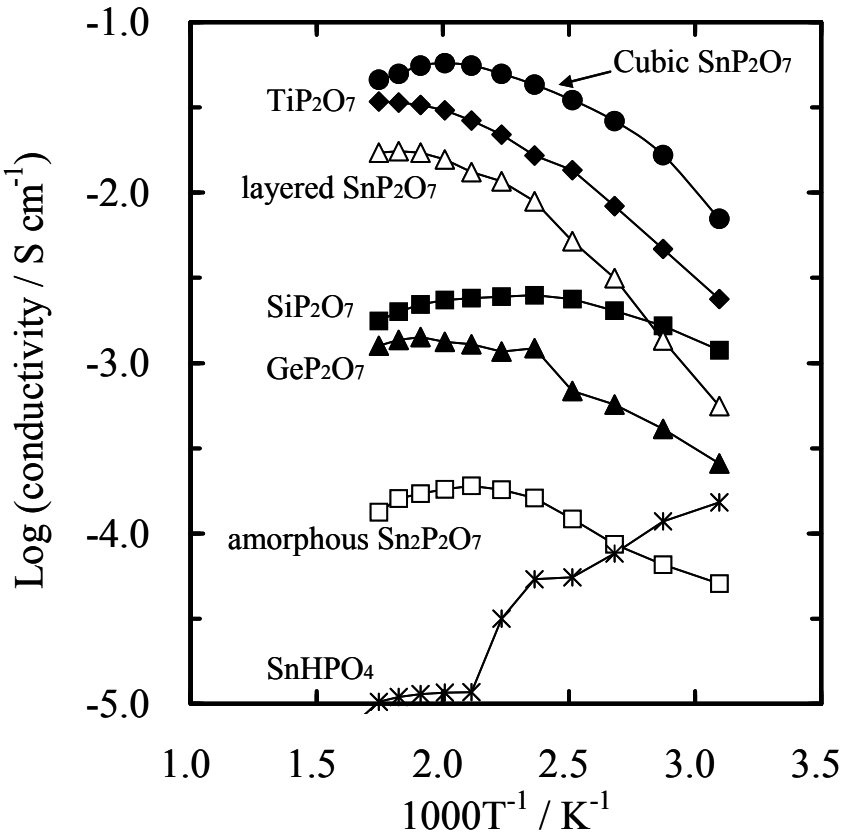

Figure 2-12. Temperature dependence of conductivity of MP_2O_7 (M = Si, Ge, Sn, Ti) in unhumidified air (P_{H2O} = ~ 0.0075 atm).

2.4 Summary

The proton conductivity of In^{3+}-doped SnP_2O_7 was more than 10^{-1} S cm^{-1} between 125 and 300°C. 10 mol% In^{3+}-doped SnP_2O_7 ($Sn_{0.9}In_{0.1}P_2O_7$) showed the highest conductivity among those with various doping levels, where a conductivity value of 1.95 x 10^{-1} S cm^{-1} was achieved at 250°C.

$Sn_{0.9}In_{0.1}P_2O_7$ showed an ionic transport number of almost 1 in the H_2 hydrogen atmosphere, indicating that this material is substantially a pure proton conductor. $Sn_{0.9}In_{0.1}P_2O_7$ exhibited a large H/D isotope effect on conductivity, which demonstrates that the protons are migrating via a hopping mechanism.

The substitution of In^{3+} for Sn^{4+} increased the proton concentration in the bulk, resulting in an increase in proton conductivity. On the other hand, the P_2O_7 deficiency caused extremely low proton conductivity, which was explained by a large increase in energy barrier for proton conduction due to partial disconnection of the P_2O_7 network for proton conduction.

2.5 References

[1] T. Norby, *Nature*, **410**, 877 (2001).

[2] S. M. Haile, D. A. Boysen, C. R. I. Chisholm, R. B. Merle, *Nature*, **410**, 910 (2001).

[3] T. Kenjo, Y. Ogawa, *Solid State Ionics*, **76**, 29 (1995).

[4] T. Matsui, S. Takeshita, Y. Iriyama, T. Abe, M. Inaba, Z. Ogumi, *Electrochem Commun.*, **6**, 180 (2004).

[5] D. A. Boysen, T. Uda, C. R. I. Chisholm, S. M. Haile, *Science*, **303**, 68 (2004).

[6] W. Wieczorek, G. Zukowska, R. Borkowska, S. H. Chung, S. Greenbaum, *Electrochim. Acta*, **46**, 1427 (2001).

[7] A. Matsuda, T. Kanzaki, K. Tadanaga, M. Tatsumisago, T. Minami, *Solid State Ionics*, **154-155**, 687 (2002).

[8] J. D. Kim, I. Honma, *Electrochim. Acta.*, **49**, 3179 (2004).

[9] C. Yang, S. Srinivasan, A. B. Bocarsly, S. Tulyani, J. B. Benziger, *J. Memb. Sci.*, **237**, 145 (2004).

[10] A. Takeuchi, M. Nagao, P. Heo, M. Sano, T. Hibino, A. Tomita, in: Proceedings of Presentation at the 72th Meeting of The Electrochemical Society of Japan, Kumamoto, 1-3 April, 2005, p. 197.

[11] P. K. Gover, N. D. Withers, S. Allen, R. L. Withers,S. O. Evans, *J. Solid State Chem.*, **166**, 42 (2002).
[12] S. Gallini, M. Hänsel, T. Norby, M. T. Colomer, J. R. Jurado, *Solid State Ionics*, **162-163**, 167 (2003).
[13] K. Amezawa, Y. Tomii, N. Yamamoto, *Solid State Ionics*, **162-163**, 175 (2003).
[14] H. Iwahara, T. Yajima, T. Hibino, H. Ushida, *J. Electrochem. Soc.*, **140**, 1687 (1993).
[15] S. Steinsvik, Y. Larring, Truls Norby, *Solid State Ionics*, **143**, 103 (2001).
[16] N. Bonanos, *Solid State Ionics*, **145**, 265 (2001).
[17] H. Uchida, N. Maeda, H. Iwahara, *Solid State Ionics*, **11**, 117 (1983).
[18] T. Norby, *Solid State Ionics*, **40-41**, 857 (1990).
[19] A. S. Nowick, A. V. Vaysleyb, *Solid State Ionics*, **97**, 17 (1997).
[20] C. Yang, P. Costamagna, S. Srinivasan, J. Benziger, A. B. Bocarsly, *J. Power Source*, **103**, 1 (2001).
[21] M. Levent, D. J. Gunn, M. A. El-Bousiffi, *Inter. J. Hydrogen Energy*, **28**, 945 (2003).
[22] T. Hibino, K. Mizutani, T. Yajima, and H. Iwahara, *Solid State Ionics*, **57**, 303 (1992).
[23] H. Uchida, H. Yoshikawa, H. Iwahara, *Solid State Ionics,* **35**, 229 (1989).

3 Performance of an Intermediate-Temperature Fuel Cell Using a Proton-Conducting $Sn_{0.9}In_{0.1}P_2O_7$ Electrolyte

3.1 Introduction

Proton exchange membrane fuel cells (PEMFCs) have received increasing interest in recent years because of their high efficiency and environmentally-friendly characteristics. Proton-conducting fluoropolymers such as Nafion are commonly used as the electrolytes. However, these electrolytes need to be operated below 100ºC, which causes serious CO poisoning of the anode electrocatalyst [1,2]. These electrolytes also require highly humidified conditions to achieve sufficient proton conductivity, and the use of the large water control unit required complicates fuel cell systems [3,4]. Such problems can obviously be avoided by using a proton conductor functioning as the electrolyte above 100ºC under low humidity or dry atmosphere. Thus, considerable efforts have been devoted to developing such proton conductors worldwide [5-10].

Hibino et al. have recently reported a promising anhydrous proton conductor, 10 mol% In^{3+}-doped SnP_2O_7 ($Sn_{0.9}In_{0.1}P_2O_7$), for electrochemical devices in the temperature range of interest [11,12]. In their previous paper [11], SnP_2O_7 showed a cubic structure with SnO_6 octahedra and P_2O_7 units at the corners and the edges, respectively. Such closely packed P_2O_7 units could provide many proton bonding sites and associated transport pathways in the bulk, resulting in high proton conductivities above 0.1 S cm^{-1} between 150 and 350°C under unhumidified conditions. The electromotive force values of a hydrogen concentration cell with this material were very near the theoretical values calculated from Nernst's equation, indicating that the ionic transport number was 0.97. Thus, $Sn_{0.9}In_{0.1}P_2O_7$ was found to be an almost purely ionic conductor in hydrogen atmospheres.

In the present study, I used $Sn_{0.9}In_{0.1}P_2O_7$ as electrolyte material for intermediate-temperature fuel cells. Fuel cell tests were conducted in unhumidified hydrogen and air in the temperature range of 150-350ºC. The internal resistances of the fuel cell were characterized in terms of the ohmic and polarization resistances. The DC conductivity values of the electrolyte were estimated from the IR drops during discharge and compared with the AC conductivity values reported in previous papers [11]. The cathode overpotential, occupying a large portion of the potential drop, was improved by placing an intermediate layer of $Sn_{0.9}In_{0.1}P_2O_7$ and Pt/C catalyst powders at the interface between the electrolyte and electrode. Finally, the tolerance of the fuel cell for CO was evaluated in the presence of 5 and 10% CO.

3.2 Experimental

3.2.1 Materials preparation

Electrolyte preparation – $Sn_{0.9}In_{0.1}P_2O_7$ was prepared as described in chapter 2. Briefly, the corresponding oxides (SnO_2 and In_2O_3), 85% H_3PO_4, and ion-exchanged water were mixed and stirred at 300ºC until a high-viscosity paste was formed. After calcinations of the paste at 650ºC for 2.5 h, the compound was ground with a mortar and pestle. The final P/(Sn+In) molar ratio of the compounds was confirmed to be 2.0 (±0.02) from X-ray fluorescence (XRF). The X-ray diffraction (XRD) patterns of the compound were found to be identical with those reported in the literature [13]. The compound powders were pressed into a pellet under a pressure of 2 x 10^3 kg cm^{-2}. The measured density of the obtained pellet was 3.065 g cm^{-3}, with a relative density of 79.3%.

Electrode and intermediate layer preparation – Both the anode and cathode were made from a catalyst (10 wt% Pt/C, E-TEK) and carbon paper (Toray TGPH-090), in which the Pt loading was about 0.6 mg cm^{-2}. An intermediate layer was prepared by mixing $Sn_{0.9}In_{0.1}P_2O_7$

and Pt/C catalyst powders (the latter prepared in-house) with a 10% poly(vinylidene fluoride) (PVdF) binder in 1-methyl-2-pyrrolidinone (NMP) solvent using a mortar and pestle. The preparation of the Pt/C catalysts (10-40 wt% Pt) was carried out as follows. Carbon powders (Ketjen BLACK EC600JD) were suspended in an ethanol/water solution. A chloroplatinic acid ($H_2PtCl_6 \cdot 6H_2O$) solution and sodium boronhydride ($NaBH_4$) solution were simultaneously added into the suspension at 70ºC with stirring. The mixture solution was stirred for 2 h and washed with distilled water repeatedly until the pH of the filtrate was roughly 7. After drying at 90ºC overnight, the catalyst was heat-treated with a H_2/Ar (10 vol% H_2) atmosphere at 200ºC for 1 h. The intermediate layer was applied homogeneously by doctor blading on the cathode. Microstructure of the intermediate layer was studied by scanning electron microscopy (SEM).

3.2.2 Fuel cell performance tests

Fuel cell tests were performed using the setup as shown in Fig. 3-1. The anode and cathode (area: 0.5 cm^2) were set on both sides of the $Sn_{0.9}In_{0.1}P_2O_7$ electrolyte (1.0 mm thickness unless otherwise specified). Two gas chambers were set up by placing the cell between two alumina tubes. Each chamber was sealed with an inorganic adhesive. The fuel and air chambers were supplied with unhumidified hydrogen and air, respectively, at a flow rate of 30 mL min^{-1}. The I-V curves were measured by the four-probe method (Fig. 3-1b). The potential drop during discharge was analyzed by the current interruption method. In this case, a Pt reference electrode was attached on the side surface of the electrolyte and exposed to open air atmosphere (Fig. 3-1c) [14]. The electrode polarization was also investigated by measuring the impedance spectra between the cathode and reference electrodes. CO tolerance tests were performed by supplying hydrogen or a mixture of 5 or 10% CO and hydrogen to the fuel chamber.

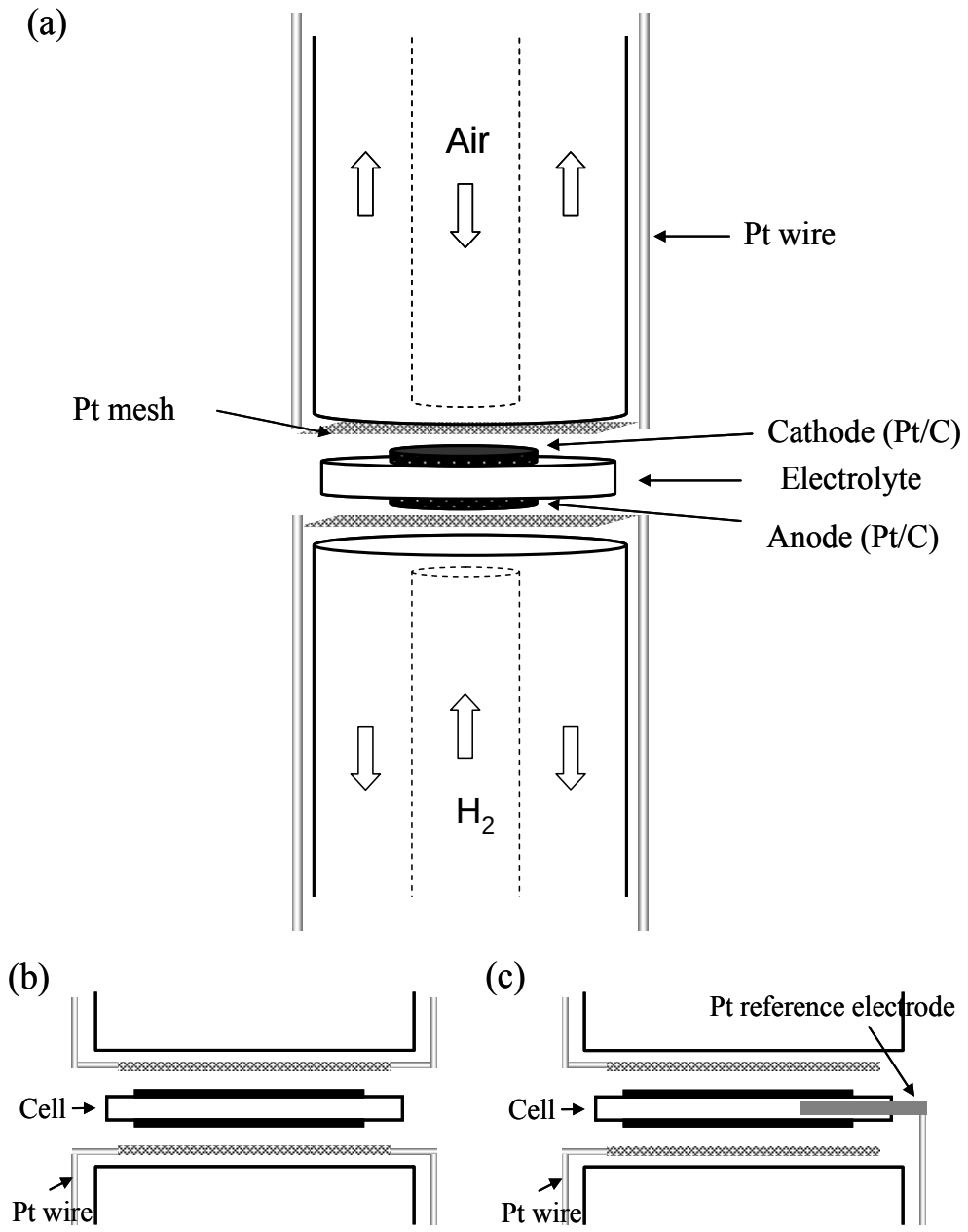

Figure 3-1. Schematic of the setup for fuel cell tests. (a) overall setup and current corrector layouts for (b) 4-probe method and (c) current interruption method.

3.3 Results and Discussion

3.3.1 Cell performance with a Pt/C cathode

Figure 3-2 plots the cell voltage and power density versus the current density at various temperatures using 10 wt% Pt/C (E-TEK) as the cathode under unhumidified conditions (P_{H_2O}

≈ 0.0075 atm). The open circuit voltages (OCVs) were about 920 mV, which were lower than the theoretical value of ~1.1 V. As described in chapter 2, $Sn_{0.9}In_{0.1}P_2O_7$ was an almost purely ionic conductor in reducing atmospheres (P_{O_2} = 10^{-22}-10^{-3} atm), but showed mixed proton and electron-hole conduction in oxidizing atmospheres (P_{O_2} = 10^{-3}-1 atm). Thus, the low OCVs are attributable to the partial electron-hole conduction in the electrolyte, causing an internal short circuit in the cell. Another possible explanation is physical leakage of gas through the electrolyte since the OCVs increased with increasing electrolyte thickness. The fuel cell yielded the peak power density of 85 mW cm^{-2} at 250ºC. However, this power density value was much lower when compared to that expected from the AC conductivity (1.95×10^{-1} S cm^{-1}) of the $Sn_{0.9}In_{0.1}P_2O_7$ electrolyte.

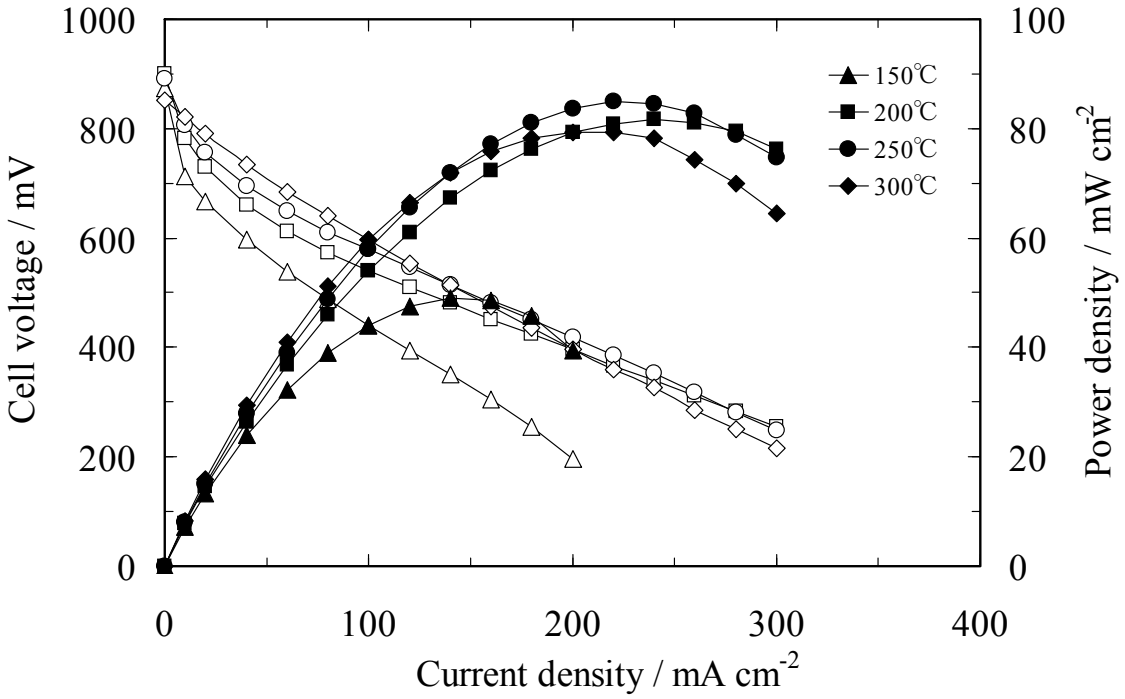

Figure 3-2. Cell voltage and power density vs. current density of the fuel cells using $Sn_{0.9}In_{0.1}P_2O_7$ as the electrolyte between 150 and 300ºC. The thickness of the electrolyte was 1 mm. Unhumidified hydrogen and air were supplied to the anode and cathode, respectively, at a flow rate of 30 ml min^{-1}.

To better understand the above low cell performance, the IR drops of fuel cells with $Sn_{0.9}In_{0.1}P_2O_7$ electrolytes of varying thickness were measured by the current interruption

method. Figure 3-3 shows the IR drops of the electrolytes with thicknesses of 1.0, 1.5, and 2.0 mm measured between 150 and 300ºC. The IR drops were primarily determined by the electrolyte thickness and were less dependent on the temperature. The DC conductivity values of the electrolyte were estimated from the IR drops and compared with the AC conductivity values. The results are shown in Fig. 3-4. The DC conductivity values for the different electrolyte thicknesses were close to each other. At 250ºC for example, the DC conductivity values were 1.35×10^{-1}, 1.43×10^{-1}, and 1.41×10^{-1} S cm^{-1} for the electrolyte thicknesses of 1.0, 1.5, and 2.0 mm, respectively. Furthermore, the DC conductivity values were roughly in agreement with the AC conductivity values at all temperatures tested. The slight difference in conductivity between the DC and AC measurements is probably due to the contact resistance between the electrode and current collector. This agreement means that high proton conductivity values of $Sn_{0.9}In_{0.1}P_2O_7$ were demonstrated under fuel cell operation conditions.

The agreement between the DC and AC measurements also suggests that the low cell performance shown in Fig. 3-2 was caused by a large electrode polarization.

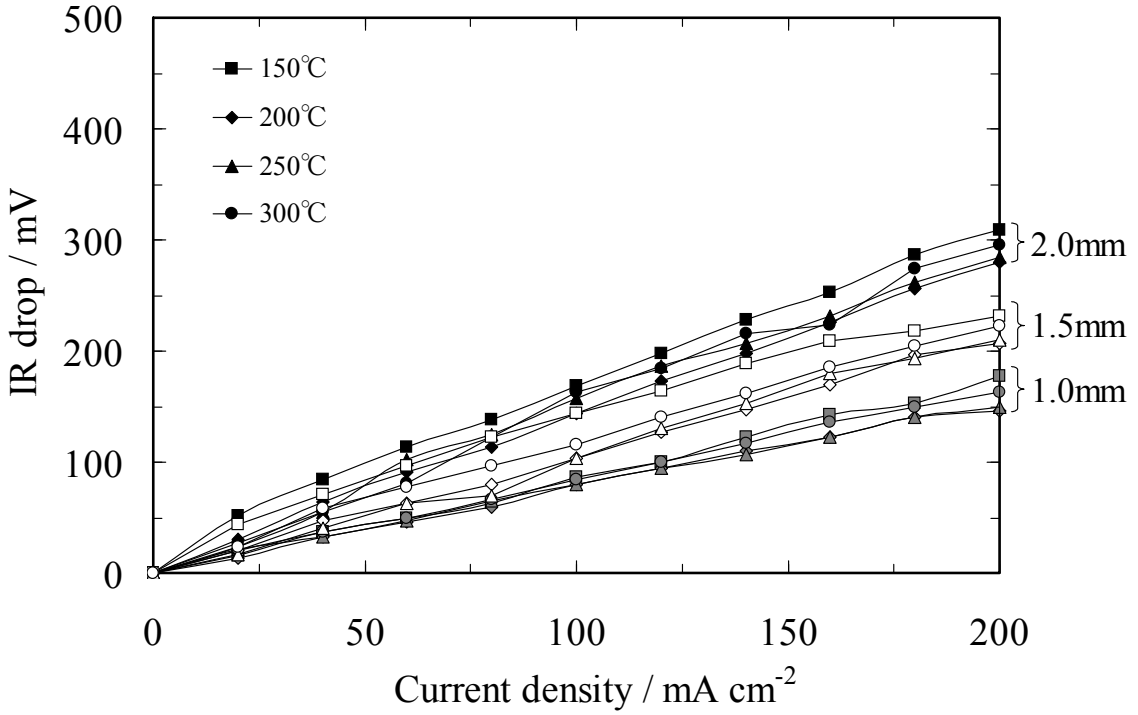

Figure 3-3. IR drops of $Sn_{0.9}In_{0.1}P_2O_7$ electrolytes with thicknesses of 1.0, 1.5, and 2.0 mm between 150 and 300ºC.

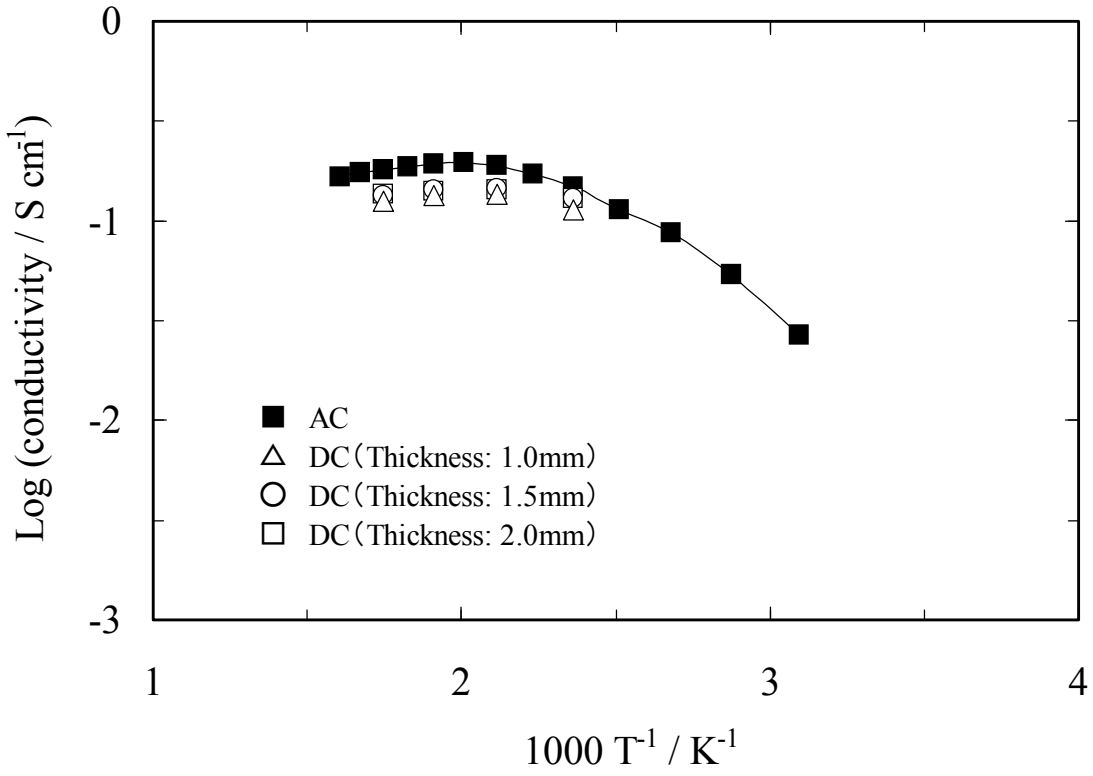

Figure 3-4. Comparison between DC and AC conductivity values of $Sn_{0.9}In_{0.1}P_2O_7$ electrolytes at various temperatures.

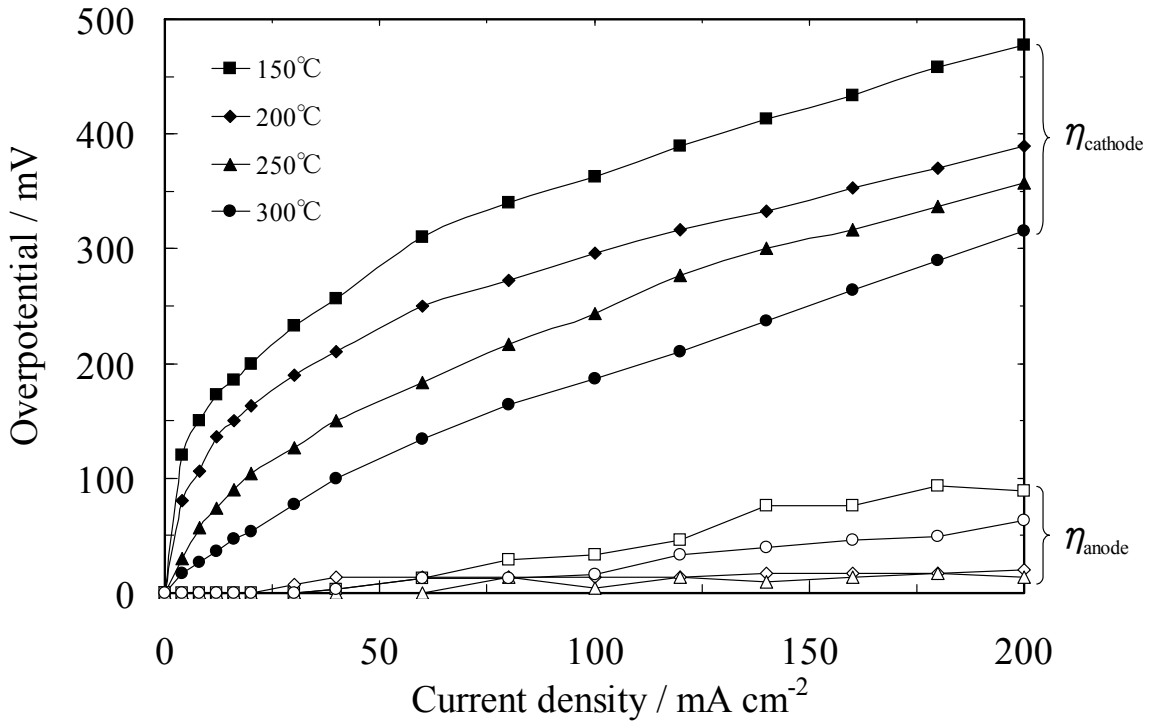

Figure 3-5. Anodic and cathodic overpotentials between 150 and 300°C.

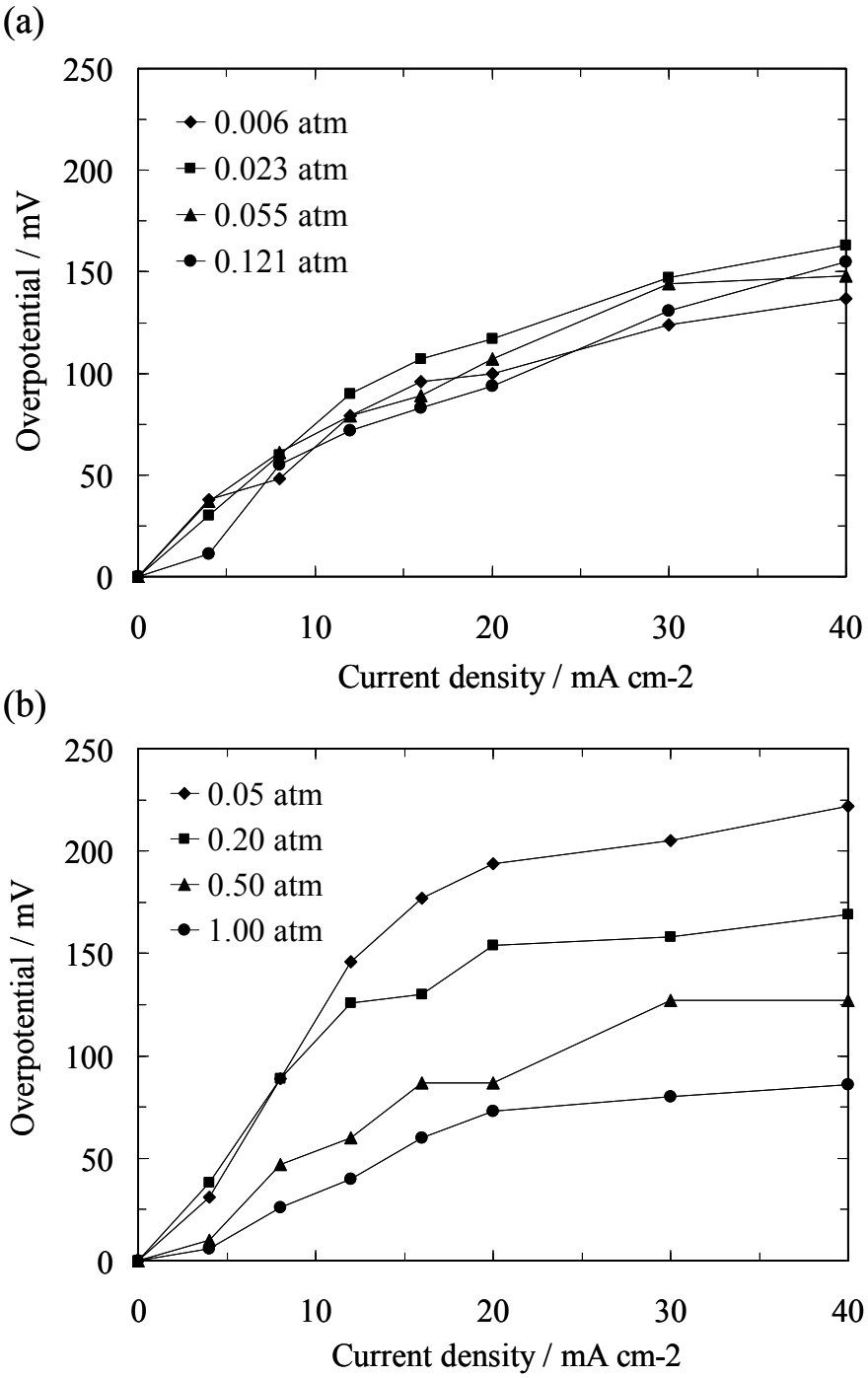

Figure 3-6. Cathodic overpotentials under various (a) P_{H2O} and (b) P_{O2} at 250ºC.

3.3.2 Electrode polarizations

The electrode polarization was measured between 150 and 300ºC. The anodic and cathodic overpotentials as a function of the current density are shown in Fig. 3-5. The cathodic

overpotentials were much larger than the anodic overpotentials over the whole temperature range. Moreover, the cathodic overpotential showed a strong temperature dependence, suggesting that the cathode had a high activation energy for the reduction of oxygen. Clearly, the development of a more active cathode is required to improve the cell performance.

In order to determine the origin of the high overpotential at the cathode, the influence of P_{H2O} and P_{O2} on the cathodic overpotential was measured at 250ºC. As shown in Fig. 3-6(a), the cathodic overpotential was independent of P_{H2O}, indicating that the water formed electrochemically does not affect the subsequent cathode reaction. This is presumably because the water formed is promptly desorbed from the electrode as water vapor under the present conditions. On the other hand, it can be seen from Fig. 3-6(b) that the cathodic overpotentials increased significantly with decreasing P_{O2}. This result is mainly ascribed to the fact the diffusion of oxygen through the electrode or its charge-transfer reaction at the electrolyte/electrode interface proceeds at a very slow rate. Another possible reason may be due to a decrease in p-type electronic conductivity of the electrolyte surface with decreasing P_{O2}.

3.3.3 Intermediate layers for a cathode reaction

It is useful to increase the area of the three-phase boundary for promotion of the cathode reaction. Thus, intermediate layers of $Sn_{0.9}In_{0.1}P_2O_7$ and Pt/C catalyst powders were applied at the interface between the electrolyte and electrode. As a result of the optimization of both the Pt content in the Pt/C catalyst and the weight ratio of the $Sn_{0.9}In_{0.1}P_2O_7$ electrolyte to the Pt/C catalyst, the cathodic overpotential could be the most improved when Pt content = 30 wt% and $Sn_{0.9}In_{0.1}P_2O_7$: Pt/C catalyst = 10:1 at 250ºC (Fig. 3-7). The microstructure of the intermediate layer is shown in Fig. 3-8. Agglomerates of the $Sn_{0.9}In_{0.1}P_2O_7$ electrolyte (agglomerate size: 400-500 nm) were homogeneously dispersed in the Pt/C catalyst powders. It is believed that the intermediate layer provides proton conduction to the cathode, enhancing

the frequency of contact between proton and oxygen.

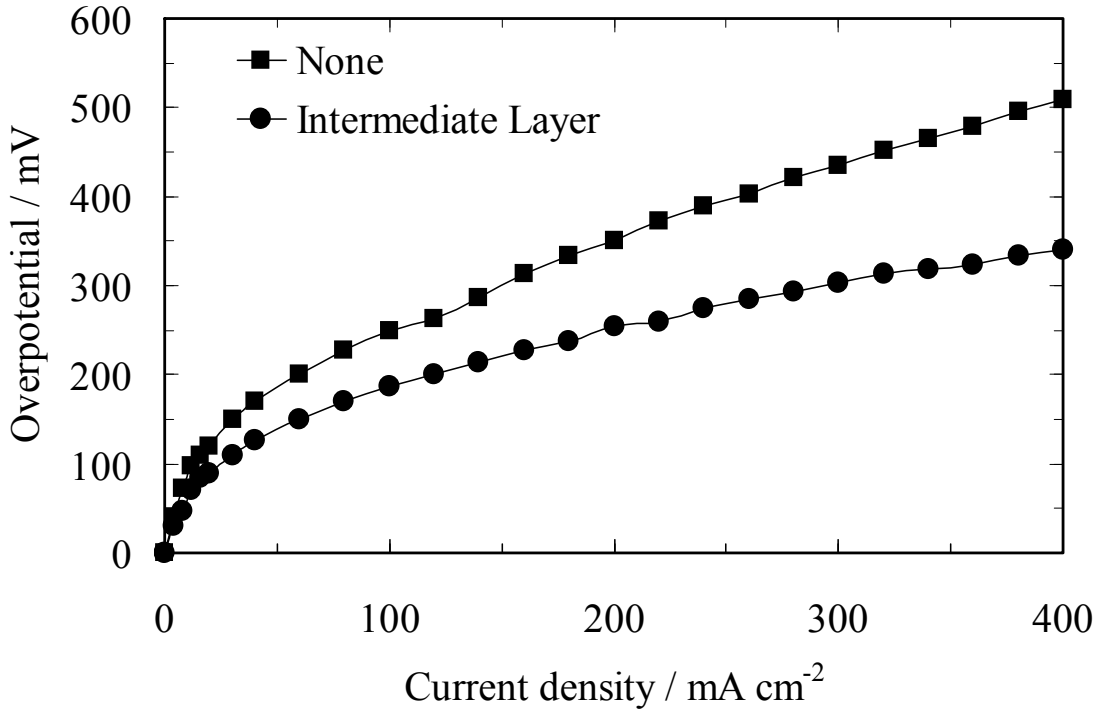

Figure 3-7. Cathodic overpotentials without and with an intermediate layer between the electrolyte and electrode. The intermediate layer composed of $Sn_{0.9}In_{0.1}P_2O7$ and 30 wt.% Pt/C catalyst powders with a weight ratio of 10:1.

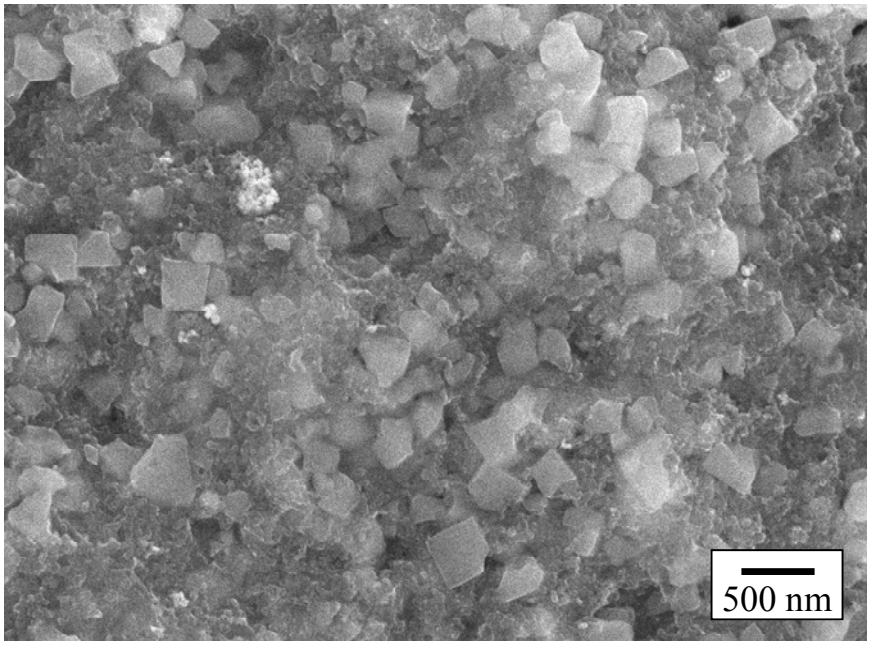

Figure 3-8. SEM micrograph of an intermediate layer of $Sn_{0.9}In_{0.1}P_2O_7$ and 30 wt.% Pt/C catalyst powders.

Performance of the fuel cell with the intermediate layer was evaluated under unhumidified conditions. The experimental conditions were the same as those shown in Fig. 3-2. The results are shown in Fig. 3-9. The voltage drop during discharge was less dependent on the temperature between 200 and 300ºC, which is responsible for the small difference in the proton conductivity of the electrolyte under such conditions. The peak power density ranged from 120 mW cm^{-2} at 150ºC to 152 mW cm^{-2} at 250ºC; these values are considerably higher than those obtained without using the intermediate layer shown in Fig. 3-2. This indicates that the intermediate layer effectively improved the cell performance. Another important contribution of this intermediate layer to cell performance was that the layer increased the proportion of the ohmic resistance in the whole internal resistance compared to the polarization resistance. As a result, the peak power density was enhanced to 264 mW cm^{-2} by reducing the electrolyte thickness to 0.35 mm at 250ºC, as shown in Fig. 3-10.

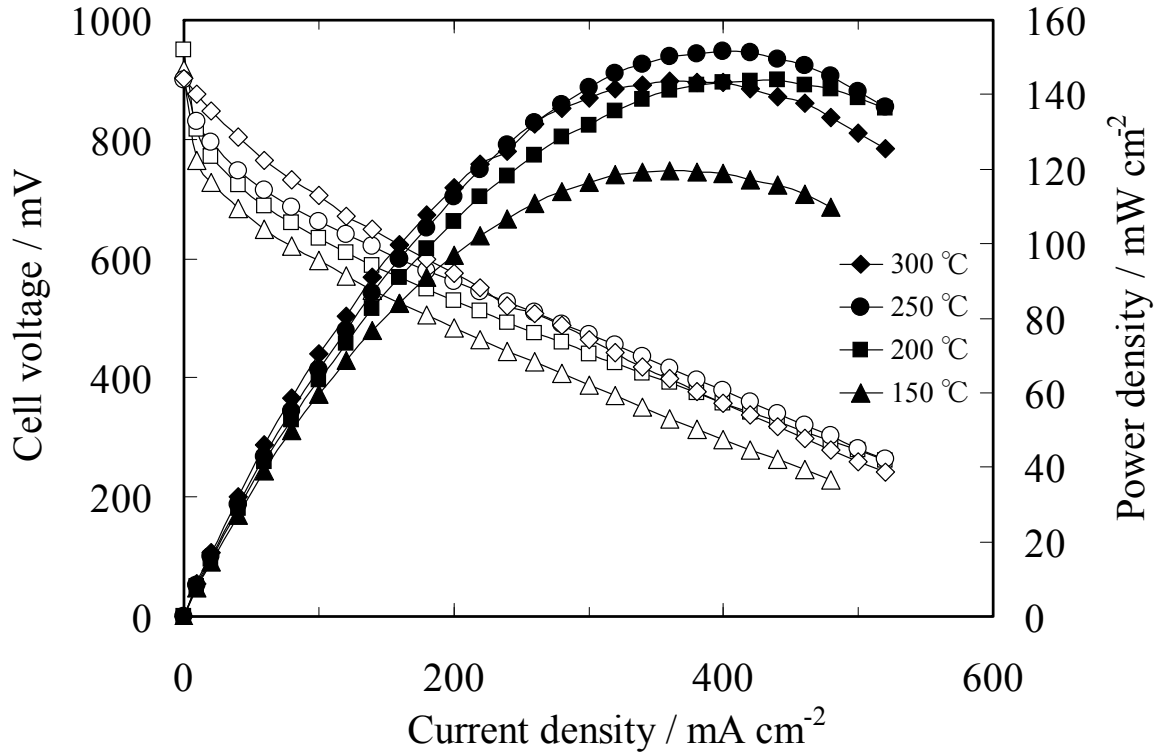

Figure 3-9. Cell voltage and power density vs. current density of the fuel cells of a fuel cell using an intermediate layer of $Sn_{0.9}In_{0.1}P_2O_7$ and 30 wt.% Pt/C catalyst. The thickness of the $Sn_{0.9}In_{0.1}P_2O_7$ electrolyte was 1 mm. The experimental conditions are the same as those shown in Fig. 3-2.

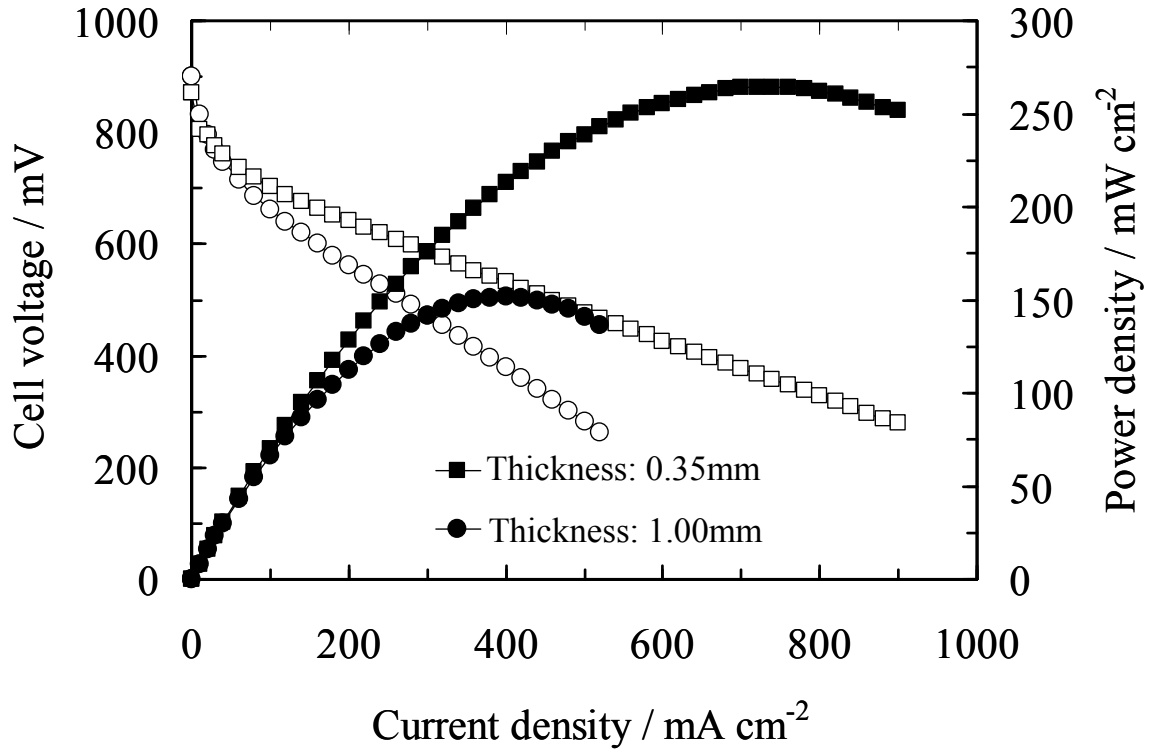

Figure 3-10. Cell voltage and power density vs. current density of the fuel cells using an intermediate layer with different electrolyte thicknesses at 250°C. The experimental conditions are the same as those shown in Fig. 3-2.

3.3.4 CO tolerance

CO tolerance tests of the present fuel cell were investigated by supplying hydrogen or a mixture of 5 or 10% CO and hydrogen to the fuel chamber at 250ºC. The cell performance was clearly not influenced by the presence of CO (Fig. 3-11(a)). Similar results were observed in AC impedance spectra (0.2 V bias voltage) as shown in Fig. 3-11(b), which maintained a polarization resistance of 0.4 Ω cm^2 regardless of the presence of CO. It was also found that the polarization resistances at 100 and 200ºC in the presence of 10% CO were about 25 and 1.8 times larger, respectively, than the values at the same temperatures in pure hydrogen. This temperature dependence on CO poisoning is roughly in agreement with theoretical studies on CO tolerance at high temperatures [15].

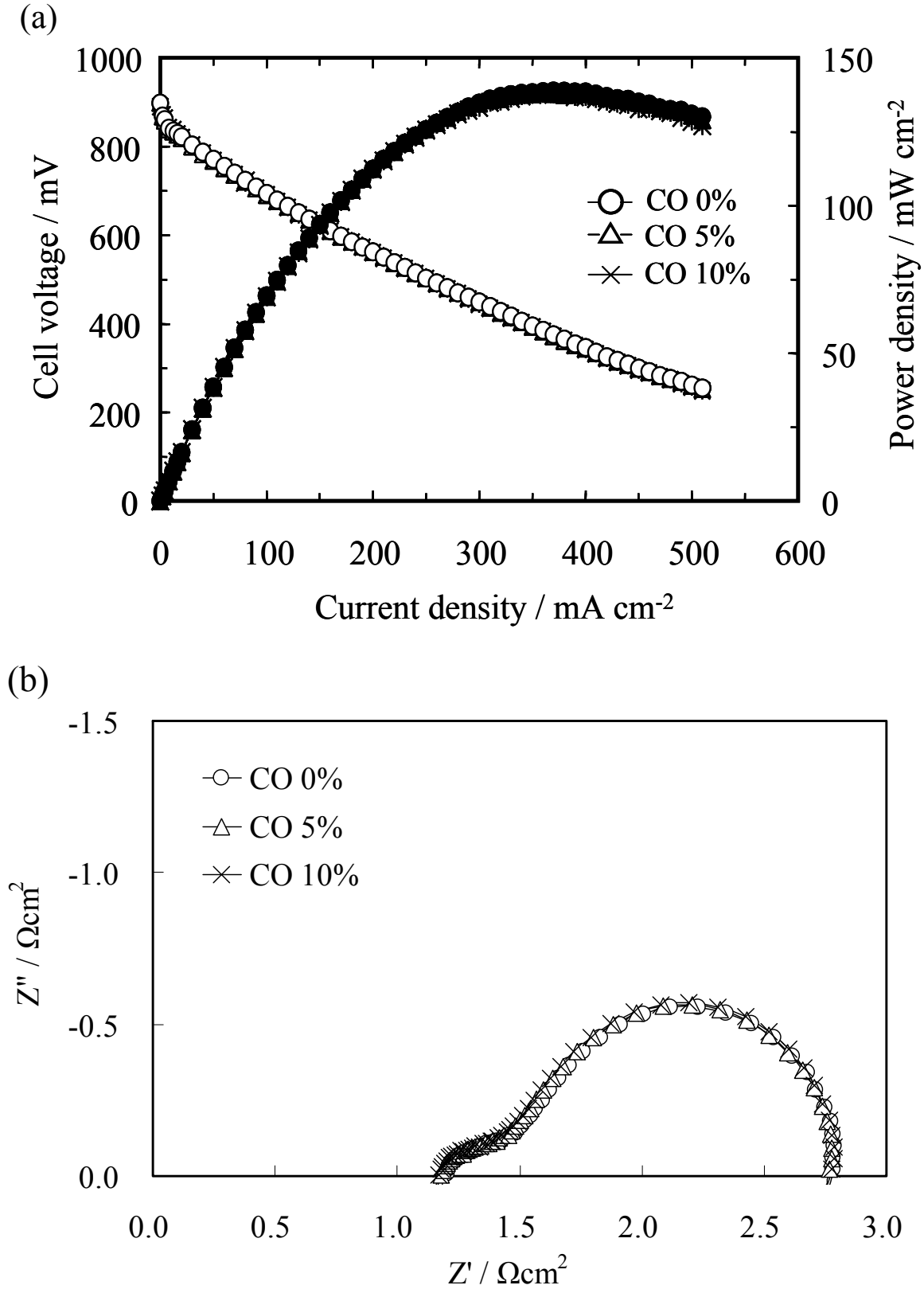

Figure 3-11. Cell voltage and power density vs. current density of the fuel cells of a fuel cell using an intermediate layer of $Sn_{0.9}In_{0.1}P_2O_7$ and 30 wt.% Pt/C catalyst. The thickness of the $Sn_{0.9}In_{0.1}P_2O_7$ electrolyte was 1 mm. The experimental conditions are the same as those shown in Fig. 3-2.

Short-term stability tests were also carried out in the presence of 10% CO at 250ºC. The cell voltage was initially set to 700 mV by drawing current from the cell and then monitored with the current density maintained at a constant value. The cell voltage was almost stable for 60 h (Fig. 3-12). These results indicate that the present fuel cell has excellent CO tolerance for external reformer-based applications, wherein the CO concentration in the outlet gases from conventional reformers is usually 10% [16].

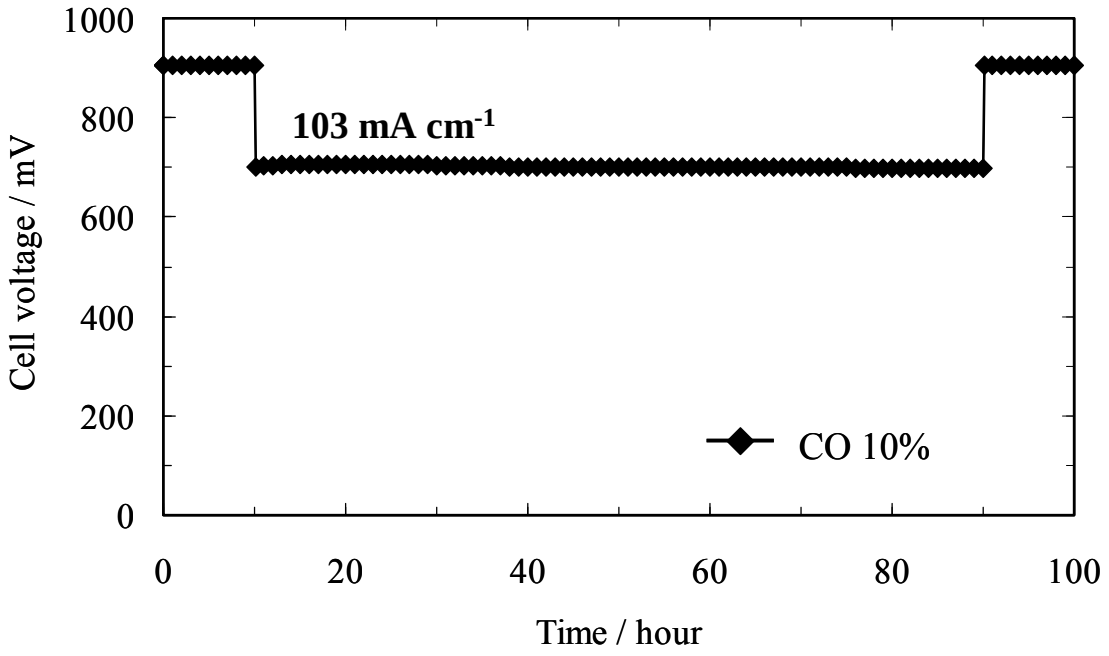

Figure 3-12. Stability of the fuel cell tested using a mixture of 10% CO + H_2 as the fuel gas at 250ºC.

3.3.5 Advantages of the present fuel cell

The fuel cell with the $Sn_{0.9}In_{0.1}P_2O_7$ electrolyte exhibited a more stable performance at low relative humidities and high CO concentrations compared to current PEMFCs, which will make fuel cell systems significantly simpler and more economic. Furthermore, the present fuel cell is expected have additional advantages over PEMFCs, such as higher reaction rates, faster heat rejection rates, and more efficient thermal utilization. These advantages would

greatly enhance the position of intermediate-temperature fuel cells as the preferred power generation technology for practical applications.

3.4 Summary

Performance of a fuel cell that employs $Sn_{0.9}In_{0.1}P_2O_7$ as the electrolyte was evaluated at low relative humidities and in the temperature range of 150-300ºC. The DC conductivity values estimated for the fuel cell were roughly in agreement with the AC conductivity values of the electrolyte over the whole temperature range, demonstrating the high proton conductivity of $Sn_{0.9}In_{0.1}P_2O_7$ under fuel cell operation conditions.

The cathodic polarization was significantly improved by applying an intermediate layer of $Sn_{0.9}In_{0.1}P_2O_7$ and 30 wt% Pt/C catalyst powders at the interface between the electrolyte and cathode. The resulting power density reached 152 mW cm^{-2} and 264 mW cm^{-2} at 250ºC using the electrolytes with 1.00 and 0.35 mm thickness, respectively. More importantly, the present fuel cell showed excellent CO tolerance and good thermal stability in unhumidified conditions. The cell performance and polarization resistances were clearly not influenced by the presence of 10% CO at 250ºC. In the stability test, the cell voltage (700 mV) with a constant current density, maintained at a constant value for 60 h in the presence of 10% CO at 250ºC.

3.5 References

[1] S. Malhotra and R. Datta, *J. Electrochem. Soc.*, **144**, L23 (1997).
[2] Q. Li, R. He, J. A. Gao, J. O. Jensen, and N. J. Bjerrum, *J. Electrochem. Soc.*, **150**, A1599 (2003).
[3] A. Karthikeyan, C. Martindale, and S. W. Martin, *J. Non-Cryst. Solids*, **349**, 215 (2004).
[4] P. Berg, K. Promislow, J. S. Pierre, J. Stumper, and B. Wetton, *J. Electrochem. Soc.*, **151**, A341 (2004).
[5] T. Uda, D. A. Boysen, and S. M. Haile, *Solid State Ionics*, **176**, 127 (2005).
[6] S. M. Haile, D. A. Boysen, C. R. I. Chisholm, and R. B. Merle, *Nature*, **410**, 910 (2001).
[7] D. A. Boysen, T. Uda, C. R. I. Chisholm, and S. M. Haile, *Science*, **303**, 68 (2004).

[8] W. Wieczorek, G. Zukowska, R. Borkowska, S. H. Chung, and S. Greenbaum, *Electrochim. Acta*, **46**, 1427 (2001).
[9] A. Matsuda, T. Kanzaki, K. Tadanaga, M. Tatsumisago, and T. Minami, *Solid State Ionics*, **154-155**, 687 (2002).
[10] J. D. Kim and I. Honma, *Electrochim. Acta.*, **49***,* 3179 (2004).
[11] M. Nagao, A. Takeuchi, P. Heo, T. Hibino, M. Sano, A. Tomita, *Electrochem. Solid-State Lett*., **9**, A105 (2006).
[12] M. Nagao, T. Yoshii, T. Hibino, M. Sano, and A. Tomita, *Electrochem. Solid-State Lett*., **9**, J1 (2006).
[13] P. K. Gover, N. D. Withers, S. Allen, R. L. Withers, and J. S. O. Evans, *J. Solid State Chem.*, **166**, 42 (2002).
[14] M. Nagata, Y. Itoh, and H. Iwahara, *Solid State Ionics*, **67**, 215 (1994).
[15] C. Yang, P. Costamagna, S. Srinivasan, J. Benziger, and A. B. Bocarsly, *J. Power Source*, **103**, 1 (2001).
[16] M. Levent, D. J. Gunn, and M. A. El-Bousiffi, *Inter. J. Hydrogen Energy*, **28**, 945 (2003).

4 Platinum-Free Catalysts for Intermediate-Temperature Fuel Cells

4.1 Introduction

Recently, proton exchange membrane fuel cells (PEMFCs) have received increasing attention as next generation alternative power sources because of their high efficiencies and environmentally-friendly characteristics. However, these electrolytes present some challenges regarding technology and materials costs for the commercialization of PEMFCs [1]. The operating temperature of PEMFCs is limited to the dehydration temperature of ~100ºC, causing serious CO poisoning of the anode elctrocatalysts. The electrolytes also need to be operated in highly humidified conditions, resulting in complicated water management. These challenges would be overcome by using a proton conductor capable of operating above 100ºC under low humidity or dry conditions.

More importantly, the use of Pt-based catalysts is required to catalyze the electrode reactions at such low temperatures. But since the use of Pt causes high materials cost for PEMFCs, new alternatives are sought to replace expensive Pt [2]. High-temperature operation above 100ºC provides the possibility of using Pt-free electrodes in PEMFCs, but alternative materials that show as high of a performance as the Pt-based electrodes, have not been discovered yet.

Recently, it has been reported that an anhydrous proton conductor, 10 mol% In^{3+}-doped SnP_2O_7 ($Sn_{0.9}In_{0.1}P_2O_7$), showed high proton conductivities above 0.1 S cm^{-1} between 150 and 350ºC under unhumidified conditions [3-5]. The electromotive force values of a hydrogen concentration cell using this material were very near the theoretical values calculated by Nernst's equation, indicating that the ionic transport number was 0.97. A hydrogen/air fuel

cell with a 0.35-mm-thick $Sn_{0.9}In_{0.1}P_2O_7$ electrolyte could yield a high power density of 264 mW cm^{-2} at 250ºC. Furthermore, the fuel cell showed excellent tolerance toward 10% CO and good thermal stability under unhumidified conditions. However, there still remains the need to use Pt/C electrodes to achieve reasonable cell performance.

So far, low Pt loadings have been achieved by increasing the utilization of Pt and by alloying Pt with transition metals [6,7]. However, there are no alternative electrodes showing as high a performance as Pt-based electrodes. Transition metal carbides such as Mo_2C and WC have been reported as potential catalysts for many chemical reactions because of their Pt-like behavior at elevated temperatures [8-17]. Mo_2C has also been investigated as an anode catalyst for PEMFCs [18,19], although its catalytic activity for electrochemical hydrogen oxidation is not high enough to meet the criteria for an alternative material. It is likely that the low catalytic activity of this material results from the low-temperature operation below 100ºC.

On the other hands, metal oxynitrides [20] and transition metal macrocycles [21] such as TaON and FeN_4 have been reported as possible non Pt cathode catalysts. However, these catalytic activities for an oxygen reduction reaction (ORR) and chemical stability in acidic media are not high enough [22]. In addition, non Pt catalysts may be easily oxidized at high cathode potentials. Considering these challenges, my attention was focused on the application of metal oxides to the non Pt catalyst for the ORR.

In this study, I report the anode performance of Mo_2C-based catalysts toward hydrogen oxidation at intermediate temperatures between 150 and 300ºC. The overpotential of Mo_2C was compared with those of other transition metal carbides and a Pt catalyst. Moreover, the catalytic activity of Mo_2C was improved by the addition of different metal oxides to the anode. Performance of a fuel cell with the optimized Mo_2C catalyst was evaluated in the temperature range from 150 to 300ºC. I also investigated the cathode performance of various metal oxide catalysts toward the ORR at intermediate temperatures between 150 and 300ºC. The cathode performance was improved by optimizing the heat-treatment temperature for the metal oxide

catalyst. Finally, I reported the intermediate-temperature fuel cell using the Pt-free anode and cathodes.

4.2 Experimental

4.2.1 Electrode preparation

Non Pt anode catalyst – The Mo_2C/C anode catalyst was fabricated as follows. A Mo precursor was impregnated onto a carbon support (Black Pearls, BET surface area = 1500 m^2g^{-1}), wherein the slurry of $MoCl_5$ in a carbon suspension was evaporated and dried at 100ºC with stirring. The impregnated sample was reduced in a 10 vol% H_2/Ar mixture at 500ºC for 2 h and then carburized in a 20 vol% CH_4/H_2 mixture at 700ºC for 3 h. Other transition metal carbides, MxC/C (M = W, Ni, Co), were prepared in a similar manner, although their carburization temperatures ranged from 700 to 1000ºC, depending on the materials. The loadings of the carbide on the carbon support were 30 mg cm^{-2} for 50 wt.% MxC/C catalyst. The Mo_2C/C anode catalyst was also modified by impregnating $MoCl_5$ along with various other metal chlorides or oxychlorides, such as $ZrCl_2O{\cdot}8H_2O$. Subsequent treatments were the same as those for Mo_2C.

Non Pt cathode catalyst – The MOx/C cathode catalysts (M=Zr, W, Ni, Ce) were prepared by precipitation method with ammonia using aqueous solution of metal oxychlorides or chlorides, such as $ZrCl_2O{\cdot}8H_2O$ and $NiCl_2$. An aqueous ammonia solution was slowly added into the solutions of corresponding metal salts dispersed with a carbon support (Black Pearls) with stirring until the pH of the solution was 10. The obtained precipitates were filtered, and then washed with ion-exchanged water. After drying at 100ºC for 12h, the impregnation powders were heat-treated in Ar at the temperature from 300 to 750ºC. The loadings of the oxide on the carbon support were 0.8~2.0 mg cm^{-2} for 10~50 wt.% MOx/C catalysts.

Pt electrode and characterization of catalysts – Pt/C catalysts (30 wt% Pt/C, Tanaka

Kikinzoku Kogyo) were used for the comparison of the anode and cathode catalysts. The microstructure of the catalysts was analyzed using X-ray diffraction (XRD, Shimazu XRD-600) and transmission electron microscopy (TEM, Hitachi H-800).

Electrode preparation – Anode and cathode catalyst powders were mixed with poly(tetrafluoroethylene) (PTFE) dispersion (30-J, Dupont – Mitsui Fluorochemicals) and glycerol as a binder and a solvent, respectively. The catalyst inks were coated on a gas diffusion layer (SGL carbon GDL35BC). These samples were heated in Ar at 150ºC for 3 h to remove the glycerol solvent in the catalyst layer. After pressing at 50 kg cm^{-2}, the samples were heated in Ar at 350ºC for 1 h to disperse PTFE in the catalyst layer. Commercial Pt/C electrodes (10 wt% Pt/C, 0.6 mg Pt cm^{-2}, E-TEK) were used as counter electrodes for the anode and cathode, respectively.

4.2.2 Fuel cell tests

Electrolyte preparation – $Sn_{0.9}In_{0.1}P_2O_7$ was prepared as described in chapter 2. Briefly, the corresponding oxides (SnO_2 and In_2O_3), 85% H_3PO_4, and ion-exchanged water were mixed and stirred at 300ºC until a high-viscosity paste was formed. After calcinations of the paste at 650ºC for 2.5 h, the compound was ground with a mortar and pestle. The compound powders were pressed into a pellet 1.0 mm in thickness and 14.0 mm in diameter under a pressure of 2×10^3 kg cm^{-2}.

Fuel cell tests – Fuel cell tests were performed as described in chapter 3. Briefly, the anode and cathode (area: 0.5 cm^2) were set on both sides of the $Sn_{0.9}In_{0.1}P_2O_7$ electrolyte. The fuel and air chambers were supplied with unhumidified hydrogen and air, respectively, at a flow rate of 30 mL min^{-1}. The anodic and cathodic overpotentials were analyzed by the current interruption method. In this case, a Pt reference electrode was attached on the side surface of the electrolyte and exposed to open air atmosphere. The voltage-current density curves were measured by the four-probe method between 150 and 300ºC.

4.3 Results and Discussion

4.3.1 Non Pt anode

The anodic overpotentials of carbon-supported transition metal carbide anodes at 250ºC are plotted in Fig. 4-1, including the results for Pt/C and carbon anodes. While the Pt/C anode showed negligibly small overpotentials, the carbon anode had significantly large overpotentials. The polarization resistances estimated from the slope of the potential vs. the current density were 0.16 Ω cm^2 for Pt/C and 33.13 Ω cm^2 for carbon. Clearly, the catalyst-free hydrogen oxidation proceeded at a very slow rate even at 250ºC. On the other hand, all the metal carbide anodes showed lower overpotentials than that of the carbon anode. In particular, the Mo_2C/C anode exhibited the best performance among the carbides tested; the polarization resistance was 2.13 Ω cm^2. It is known that Mo_2C shows significant catalytic activities toward hydrogenation [12-14], dehydrogenation [15], hydrodenitrogenation [16], and water gas shift reactions [17], compared with the other metal carbides. It is also reported

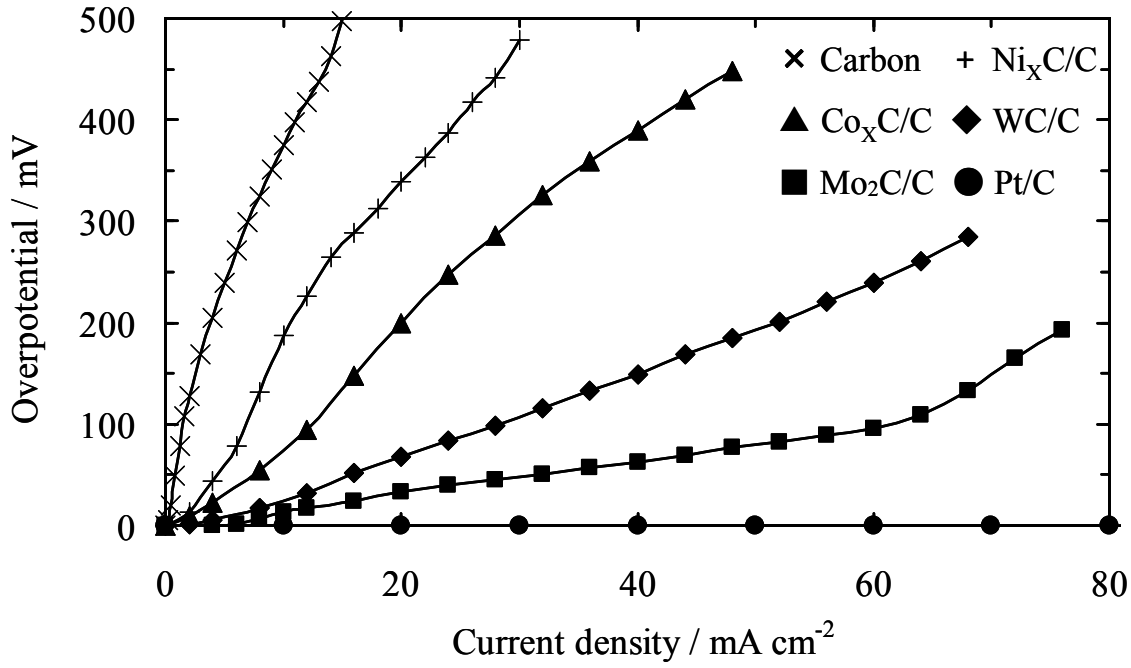

Figure 4-1. Anodic overpotentials of various carbon-supported transition metal carbide catalysts at 250ºC. For comparison, the results obtained for Pt/C and carbon anodes are shown as well.

that Mo_2C has catalytic characteristics similar to those of Pt-group metals. J. S. Choi et al. have explained the unique catalytic activity of Mo_2C by the change in the electron density of the d-band of Mo upon its carburization [10]. The introduction of C atoms into the Mo metal lattice leads to an increase in the lattice parameters, causing a contraction of the d-band and thus an enhanced d-electron density in the d-electron density levels of noble metals. However, Fig. 4-1 also showed that the performance of the Mo_2C/C anode was still considerably inferior to that of the Pt/C anode. In addition, there was an increase in the overpotential of the Mo_2C/C anode at high current densities, indicating a significant concentration overpotential based on mass transportation limitation. This may be due to an insufficient spill-over of hydrogen, causing a low hydrogen diffusion rate.

An attempt was made to improve the Mo_2C catalyst by the addition of various promoters to the catalyst. The chlorides or oxychlorides of Sn, Ce, W, and Zr were impregnated together with $MoCl_5$ onto a carbon support and then carburized at 700ºC. As described later, the promoters were confirmed to be oxides rather than carbides after carburization. Figure 4-2 shows the anodic overpotentials of the unmodified and modified Mo_2C/C anodes at 250ºC.

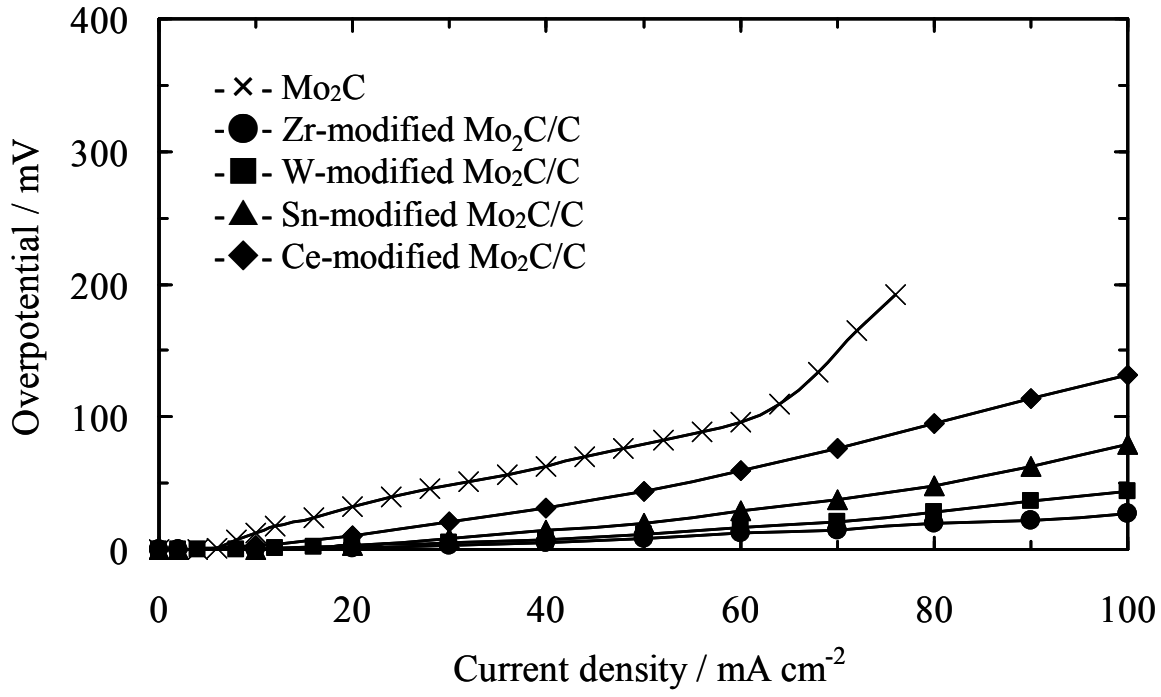

Figure 4-2. Anodic overpotentials of modified Mo_2C/C anodes at 250ºC.

All the modified Mo_2C/C anodes, in particular Mo_2C-ZrO_2/C, showed considerably lower overpotentials compared to the unmodified Mo_2C/C anode. Moreover, there were no large increases in overpotential at high current densities. I chose ZrO_2, which showed the best performance, as a promoter for subsequent experiments.

4.3.2 Anode performance of the Mo_2C-ZrO_2/C catalyst

Figure 4-3 shows the anodic overpotentials of the modified Mo_2C/C anodes with different weight ratios of Mo_2C to ZrO_2 at 250ºC. The overpotential decreased with increasing amount of ZrO_2 and reached a minimum at a weight ratio of Mo_2C:ZrO_2 of 1:0.2. The polarization resistance was 0.28 Ω cm^2, which was approximately one order of magnitude lower than that of the unmodified Mo_2C/C anode. On the other hand, the overpotential of the ZrO_2/C anode was much higher than that of the Mo_2C/C anode; the polarization resistance was 9.7 Ω cm^2. This result indicates that the effect of ZrO_2 shown in Fig. 4-3 is not attributable to the catalytic activity of ZrO_2 itself toward hydrogen oxidation.

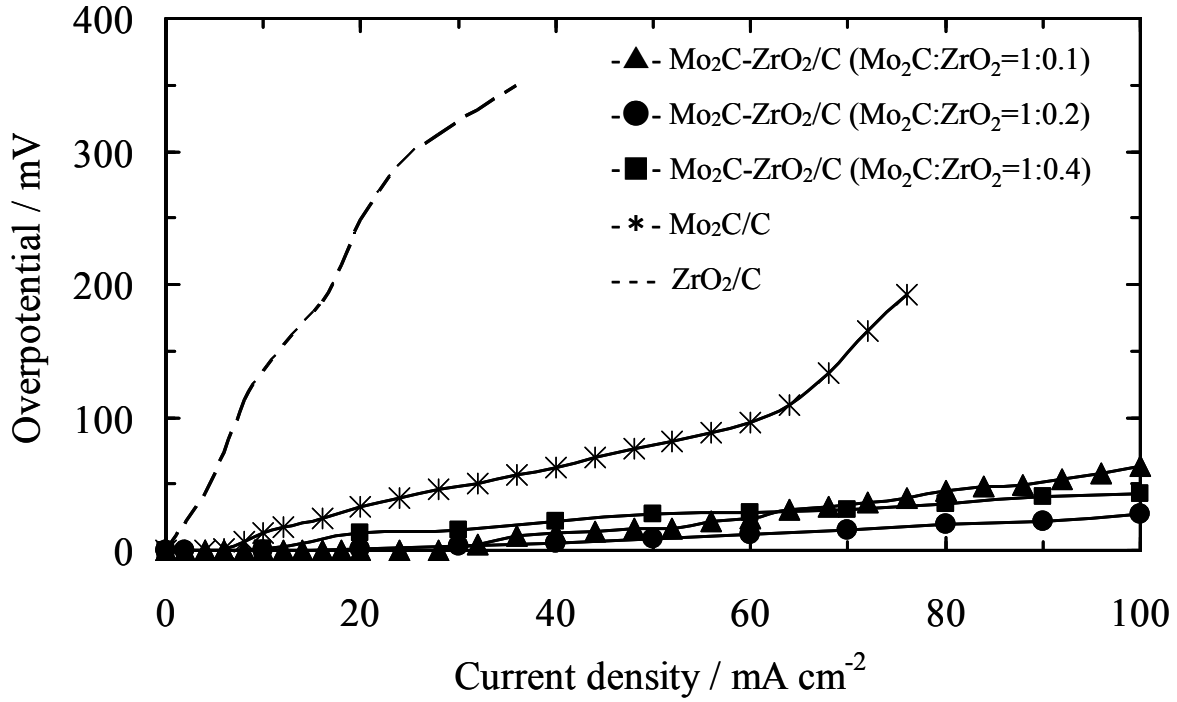

Figure 4-3. Anodic overpotentials of Mo_2C-ZrO_2/C anodes with different weight ratios of Mo_2C to ZrO_2 at 250ºC.

To better understand the above effect of ZrO_2, the microstructure of the Mo_2C-ZrO_2/C catalyst was characterized by XRD and TEM measurements. Figure 4-4 shows XRD profiles of the Mo_2C/C and Mo_2C-ZrO_2/C catalysts. In the XRD profile of Mo_2C/C, all the diffraction peaks were identical to those reported for Mo_2C in the literature [10] and no peaks of Mo metal and oxides were detected. The XRD profile of Mo_2C-ZrO_2/C revealed that the added Zr species was present as ZrO_2. In addition, the diffraction peaks of Mo_2C were not shifted by the addition of ZrO_2 to the catalyst, suggesting no incorporation of Zr into the crystalline lattice of Mo_2C. The Scherrer formula was used to estimate the particle size of Mo_2C. The estimated particle sizes were 28 and 13 nm for Mo_2C/C and Mo_2C-ZrO_2/C, respectively. A similar difference was observed in the particle size of Mo_2C, as revealed by TEM measurements of the two catalysts. As shown in Fig. 4-5, the TEM images indicated that the particle sizes of Mo_2C were 16-34 nm and 10-16 nm for Mo_2C/C and Mo_2C-ZrO_2/C, respectively. These results indicate that the Mo_2C particles showed a higher dispersion with

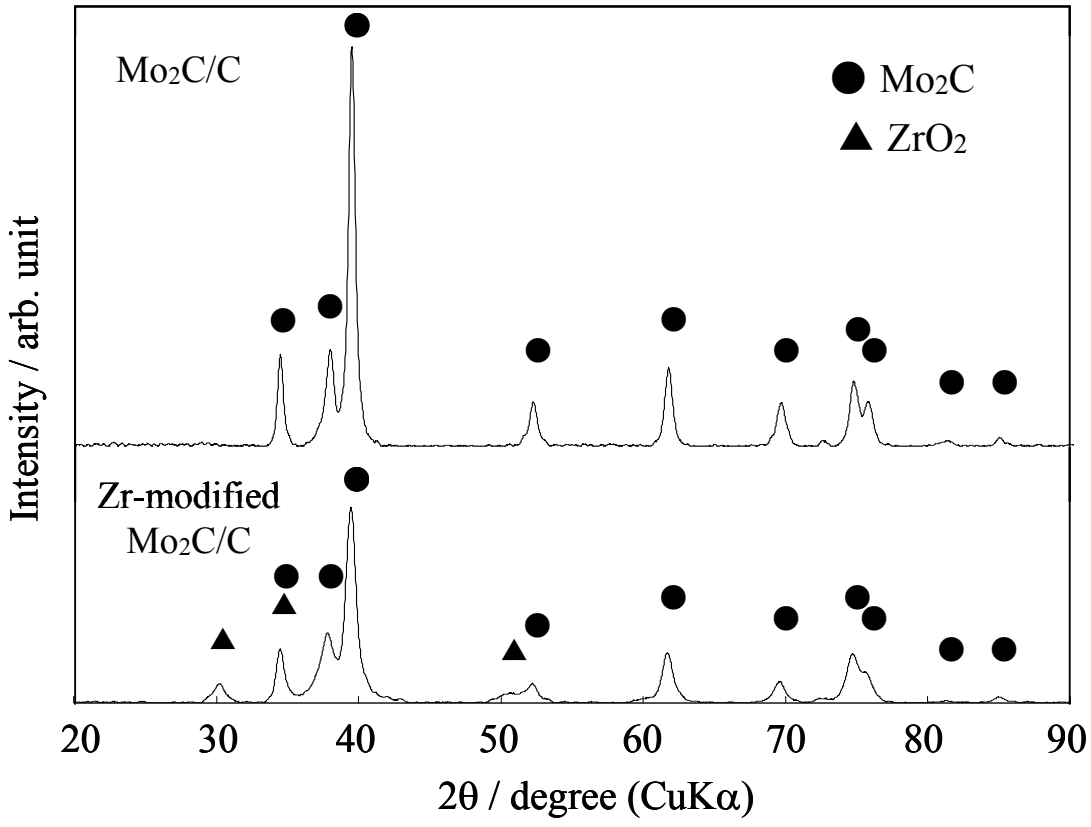

Figure 4-4. XRD profiles of Mo_2C/C and Mo_2C-ZrO_2/C.

ZrO_2 than without ZrO_2. It is likely that excessive sintering of Mo_2C during carburization is inhibited in the presence of ZrO_2, resulting in the significantly improved catalytic activity of Mo_2C toward hydrogen oxidation. Naito et al. have reported that ZrO_2 was an effective support for Mo_2C in the reforming of CH_4 by CO_2 compared to other support materials such as SiO_2, Al_2O_3, ZrO_2, TiO_2, and CeO_2 [13]. XPS analysis revealed a strong electronic interaction between Mo_2C and ZrO_2 in the Mo_2C/ZrO_2 catalyst. This interaction may be another reason for the promotive effect of ZrO_2 on Mo_2C.

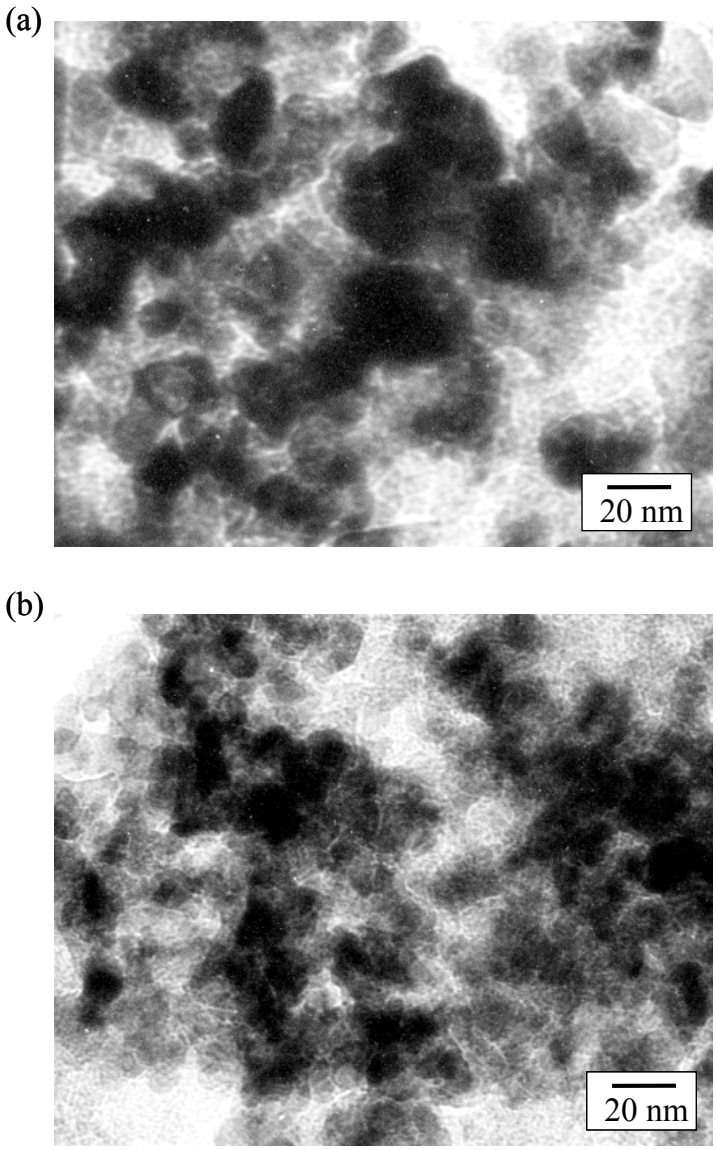

Figure 4-5. TEM images of Mo_2C/C and Mo_2C-ZrO_2/C. The catalysts and carbons are shown as black and gray, respectively.

Cell performance using the Mo_2C-ZrO_2/C anode was evaluated at 250ºC under unhumidified H_2/air fuel cell conditions. Figure 4-6 compares the cell performance using the Mo_2C-ZrO_2/C anode with those using the Mo_2C/C, Pt/C, and carbon anodes at 250ºC. The open-circuit voltages (OCVs) of all the fuel cells tested were between 0.80 and 0.85 V, which are lower than the theoretical value of ~1.1 V. The low OCVs are due to the physical leakage of gas through the electrolyte and partial electron-hole conduction in the electrolyte, as described in chapter 2. It is important to note that while limiting current behavior was observed for the Mo_2C/C anode at high current densities, no change in the current-voltage slope was observed for the Mo_2C-ZrO_2/C anode, suggesting an enhanced hydrogen spill-over on the highly dispersed Mo_2C. More importantly, there is not a large difference in cell performance between the Mo_2C-ZrO_2/C anode and the Pt/C anode; the power density was 67 mW cm^{-2} for Mo_2C-ZrO_2/C and 84 mW cm^{-2} for Pt/C. This demonstrates that Mo_2C-ZrO_2/C

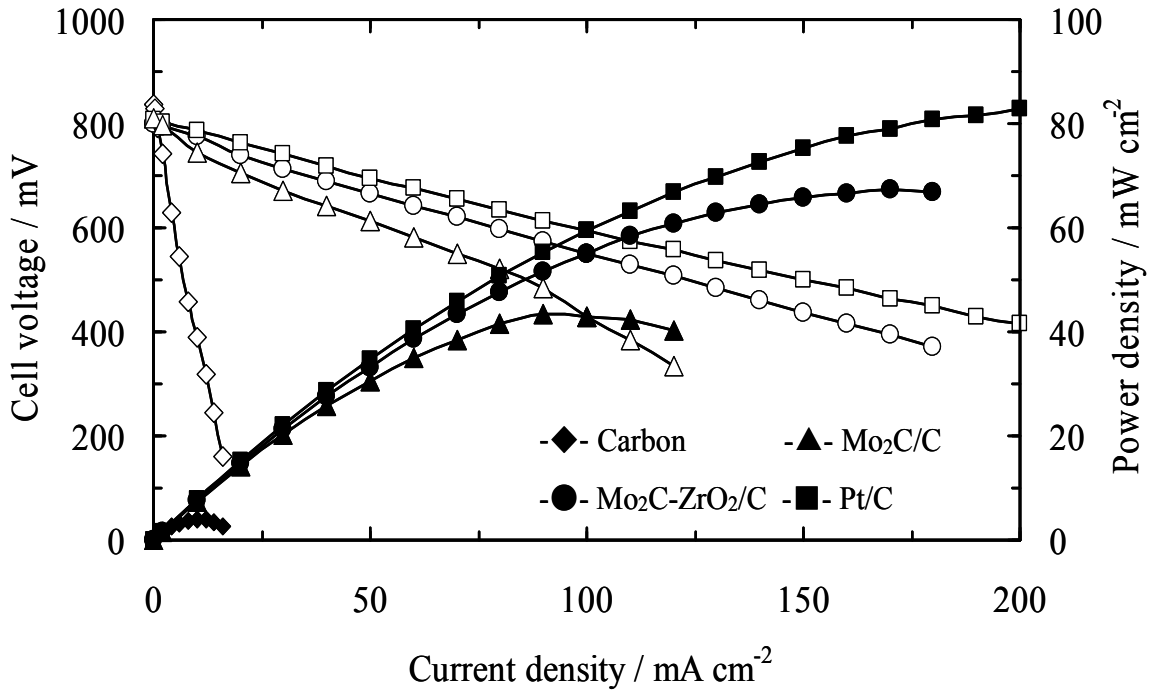

Figure 4-6. Cell voltage and power density vs. current density of fuel cells with Mo_2C/C, Mo_2C-ZrO_2/C, Pt/C, and carbon anodes at 250ºC. The thickness of the $Sn_{0.9}In_{0.1}P_2O_7$ electrolyte was 1 mm. The fuel and air chambers were supplied with unhumidified hydrogen and air, respectively, at a flow rate of 30 mL min^{-1}.

has a high potential as an anode catalyst for PEMFCs. However, this is not applicable to operation below 250ºC. It can be seen from Fig. 4-7 that the cell performance with the Mo_2C-ZrO_2/C anode was strongly dependent on the operating temperature; the peak power density reached 76 mW cm^{-2} at 300ºC, but was significantly decreased at 200ºC (35 mW cm^{-2}) and 150ºC (28 mW cm^{-2}). The anodic overpotential measurements showed that the polarization resistance increased significantly with decreasing temperature, especially below 200ºC; the polarization resistance was 1.57 Ω cm^2 at 200ºC and 2.15 Ω cm^2 at 150ºC. Thus, it is concluded that the Mo_2C-ZrO_2/C anode needs to be operated above 200ºC in order for it to be an effective alternative to Pt-based anodes.

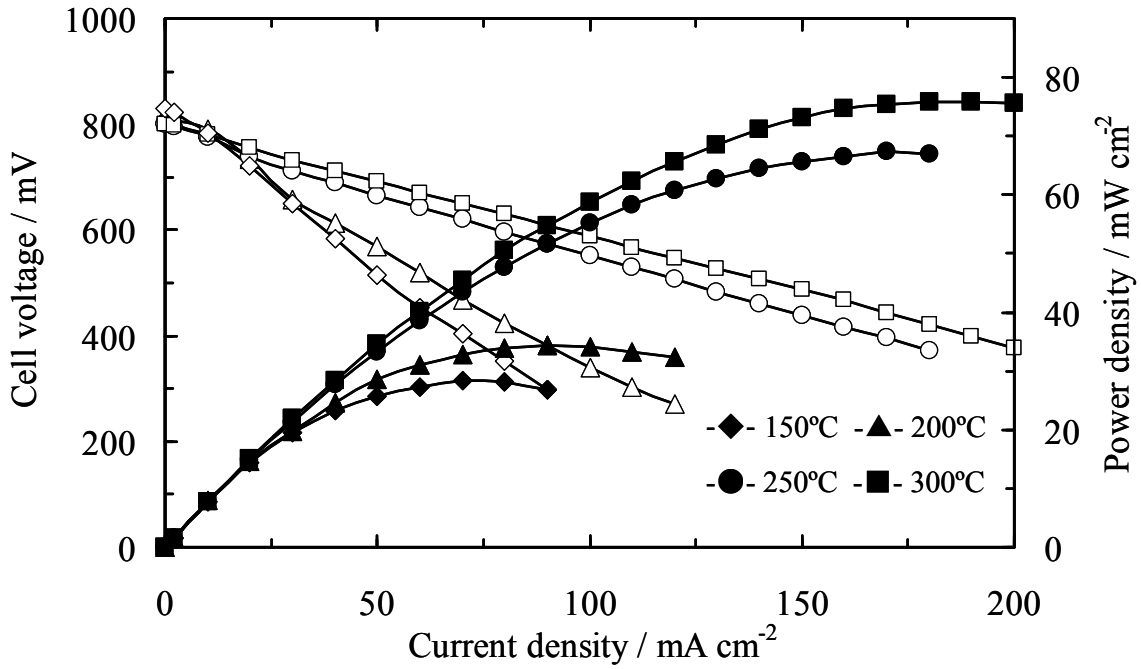

Figure 4-7. Cell voltage and power density vs. current density of fuel cells with Mo_2C-ZrO_2/C anode at different temperatures. The experimental conditions are the same as those shown in Fig. 4-6.

4.3.3 Non Pt cathode

The cathodic overpotentials of Pt/C and carbon cathodes at 250ºC are shown in Fig. 4-8. The overpotentials of these cathodes were much larger than the overpotentials of the corresponding anodes, as described earlier. The polarization resistances were estimated to be 3.18 and 108.50 Ω cm^2 for the Pt/C and carbon cathodes, respectively. Figure 4-8 also shows various transitional metal oxides (50wt.% MOx impregnated on a carbon support by the heat-treatment at 500ºC. These metal oxide cathodes exhibited lower overpotentials than that of the carbon cathode, indicating that the metal oxides tested catalyzed the oxygen reduction reaction (ORR). In particular, the catalytic activity of ZrO_2 catalyst was the highest toward the ORR among the metal oxides tested. Y. Liu also reported that the ZrOx catalyst sputtered on a glassy carbon had a certain catalytic activity for the ORR based on half-cell test in sulfuric acid [22]. However, the performance of the ZrO_2/C cathode shown in Fig. 4-8 is still insufficient, compared with that of the Pt/C cathode.

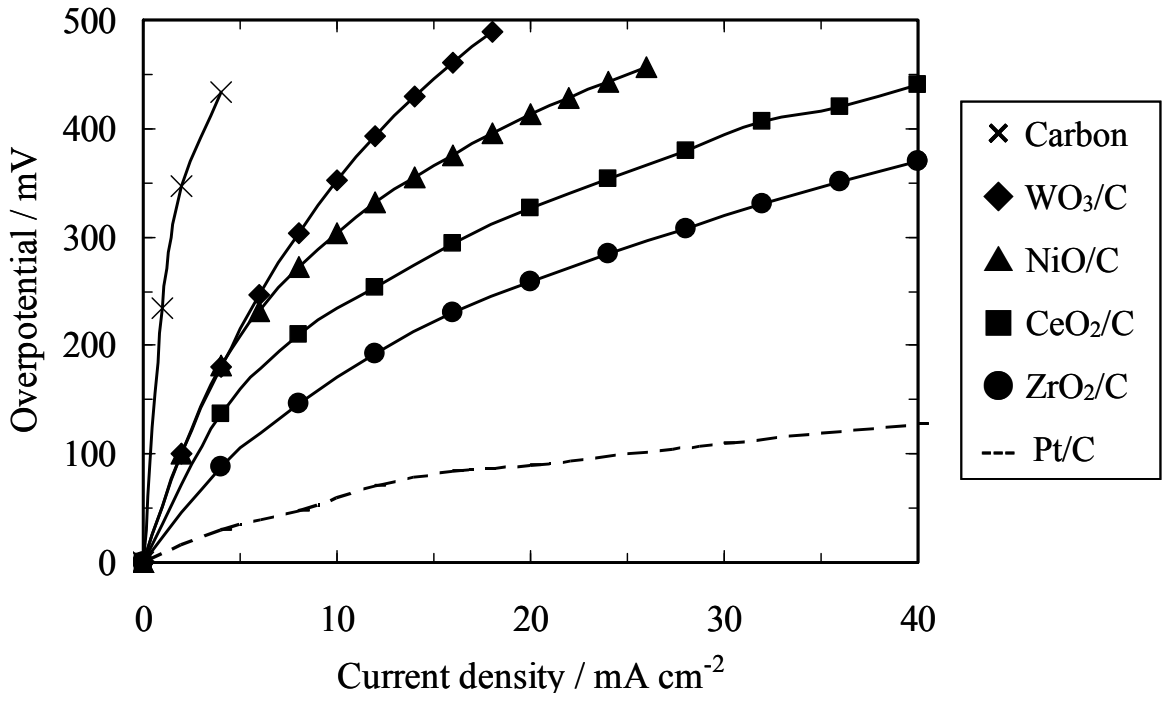

Figure 4-8. Cathodic overpotentials of various carbon-supported transition metal oxide catalysts at 250ºC. Oxide contents in the catalysts were 50 wt.%. For comparison, the results obtained for Pt/C and carbon cathodes are shown as well.

4.3.4 Cathode performance of the ZrO_2/C catalyst

The effect of ZrO_2 content on the cathode performance of the ZrO_2/C catalyst was examined. Figure 4-9 shows the cathodic overpotentials at 250ºC for ZrO_2/C with different ZrO_2 contents between 10 and 50 wt.%. The overpotential of ZrO_2/C decreased with the decreasing of the ZrO_2 content. The lowest overpotential was obtained at 20 wt.% and then the overpotential increased with the decreasing of the weight percent. These results are considered to be because the appropriate ZrO_2 content (20 wt.%) allowed both an electrically conductive electrode and its higher dispersion on a carbon support. Therefore, I chose 20 wt.% ZrO_2/C as the cathode for subsequent experiments.

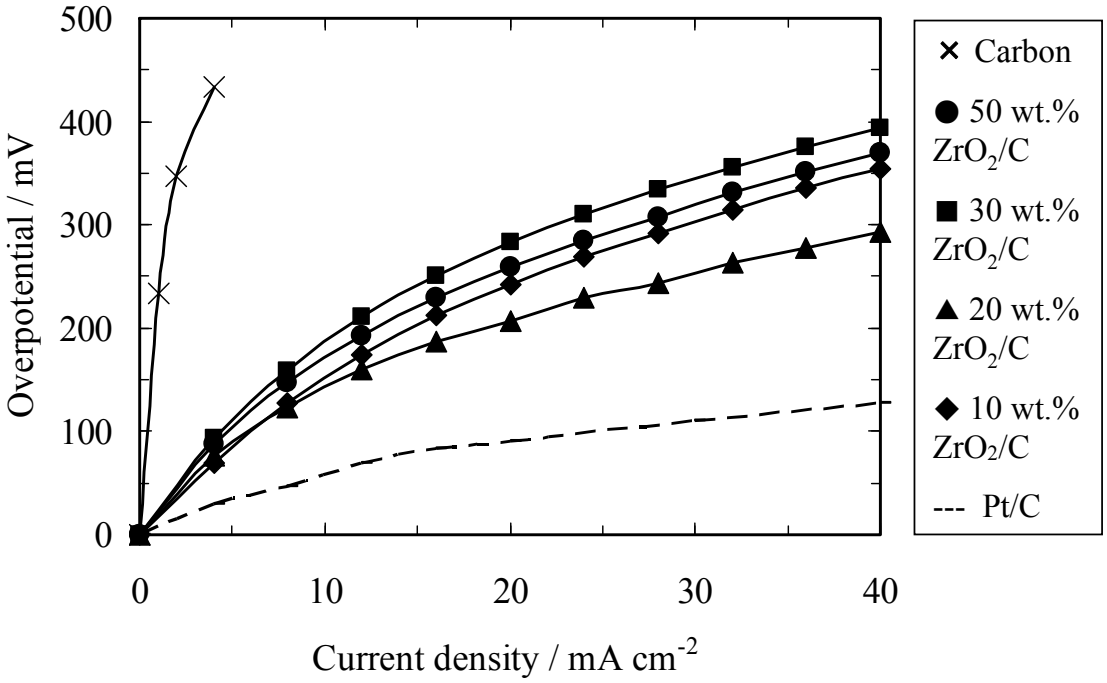

Figure 4-9. Cathodic overpotentials of ZrO_2/C catalysts with different ZrO_2 contents at 250ºC. For comparison, the result obtained for Pt/C and carbon cathodes are shown as well.

To further improve the catalytic activity of the ZrO_2 catalyst, I attempted to control the heat-treatment temperature for ZrO_2/C. Figure 4-10 shows the cathodic overpotentials at 250ºC for ZrO_2/C being heat-treated between 300 and 750ºC. The overpotential of ZrO_2/C decreased with the increasing of the heat-treatment temperature, reaching a minimum value at

650ºC, and then increased above 650ºC. As a result, the lowest polarization resistance of ZrO_2/C cathode of 6.37 Ω cm^2 was obtained at 650ºC. The ZrO_2/C catalysts treated at various temperatures were characterized by XRD to investigate the effect of the heat-treatment on the catalytic activities for ZrO_2/C. XRD profiles of these ZrO_2/C catalysts are shown in Fig. 4-11. ZrO_2 had two crystalline phases, tetragonal and monoclinic ZrO_2. The relative ratio of tetragonal to monoclinic ZrO_2 was found to be the highest when the heat-treatment was performed at 650ºC, which is consistent with the treatment-temperature effect on the catalytic activity of ZrO_2/C for the ORR shown in Fig. 4-10. Thus, it is likely that the high catalytic activity of ZrO_2 is attributed to the crystal structure of tetragonal ZrO_2. A similar correlation between the catalytic activity and crystal structure of ZrO_2 catalysts was observed for synthesis of dimethyl carbonate from methanol and CO_2 [23].

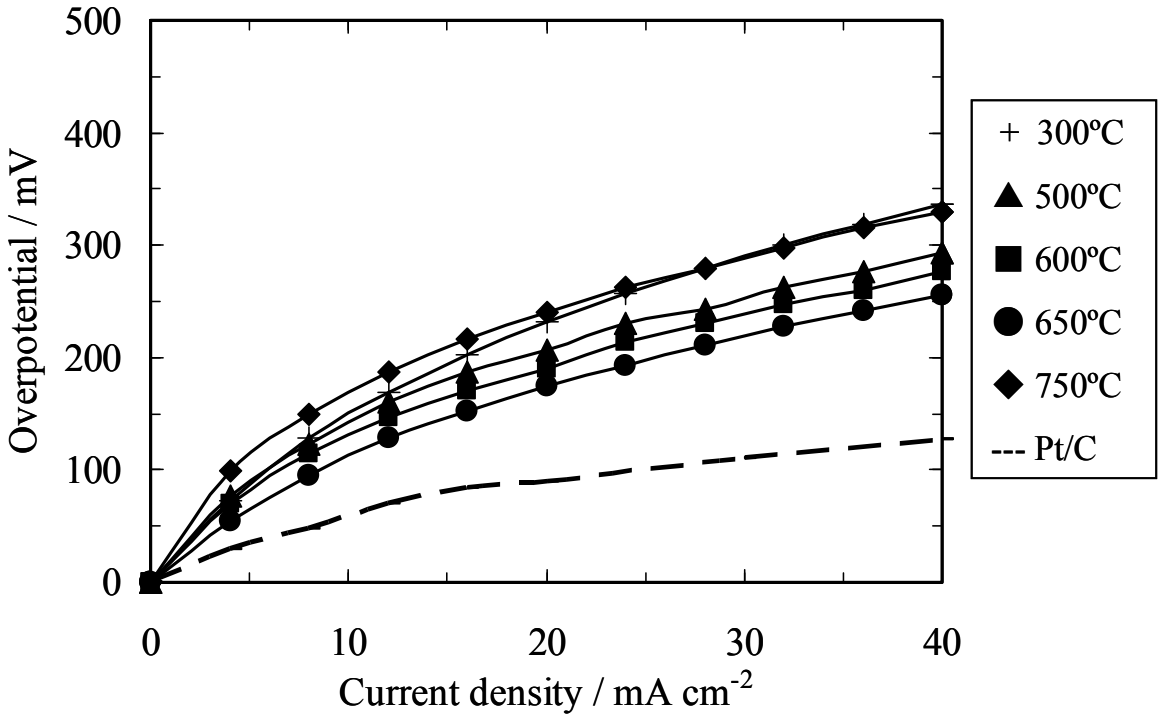

Figure 4-10. Cathodic overpotentials of ZrO_2/C catalysts with different heat-treat temperatures at 250ºC. For comparison, the result obtained for a Pt/C anode is shown.

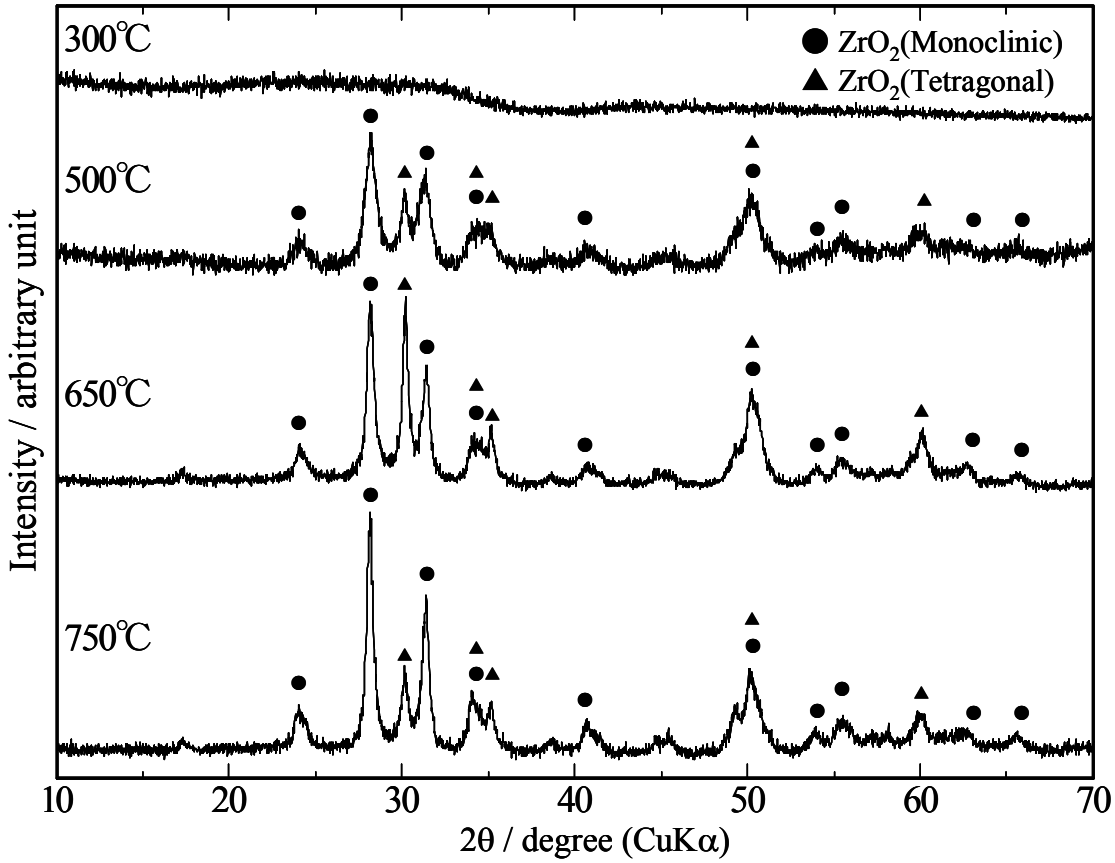

Figure 4-11. XRD profiles of ZrO_2/C catalysts with different heat-treat temperatures.

4.3.5 Pt-free fuel cell

Performance of four fuel cells using the Pt/C, Mo_2C-ZrO_2/C, and ZrO_2/C electrodes was evaluated using a 1.0-mm-thick $Sn_{0.9}In_{0.1}P_2O_7$ electrolyte at 250ºC under unhumidified H_2/air fuel cell conditions (Fig. 4-12). There was not a large difference in performance between Pt/C|electrolyte|Pt/C and Mo_2C-ZrO_2/C|electrolyte|Pt/C cells; the power density was 84 mW cm^{-2} for the Pt/C anode and 67 mW cm^{-2} for the Mo_2C-ZrO_2/C anode. The performances of Pt/C|electrolyte|ZrO_2/C and Mo_2C-ZrO_2/C|electrolyte|ZrO_2/C cells were about one-third of those of the Pt/C|electrolyte|Pt/C and the Mo_2C-ZrO_2/C|electrolyte|Pt/C cells, respectively. The peak power density was 33 mW cm^{-2} for the Pt/C|electrolyte|ZrO_2/C cell and 23 mW cm^{-2} for the Mo_2C-ZrO_2/C|electrolyte|ZrO_2/C cell. These results suggest that a further improvement of the present cathode is required for higher performance of the Pt-free fuel cell.

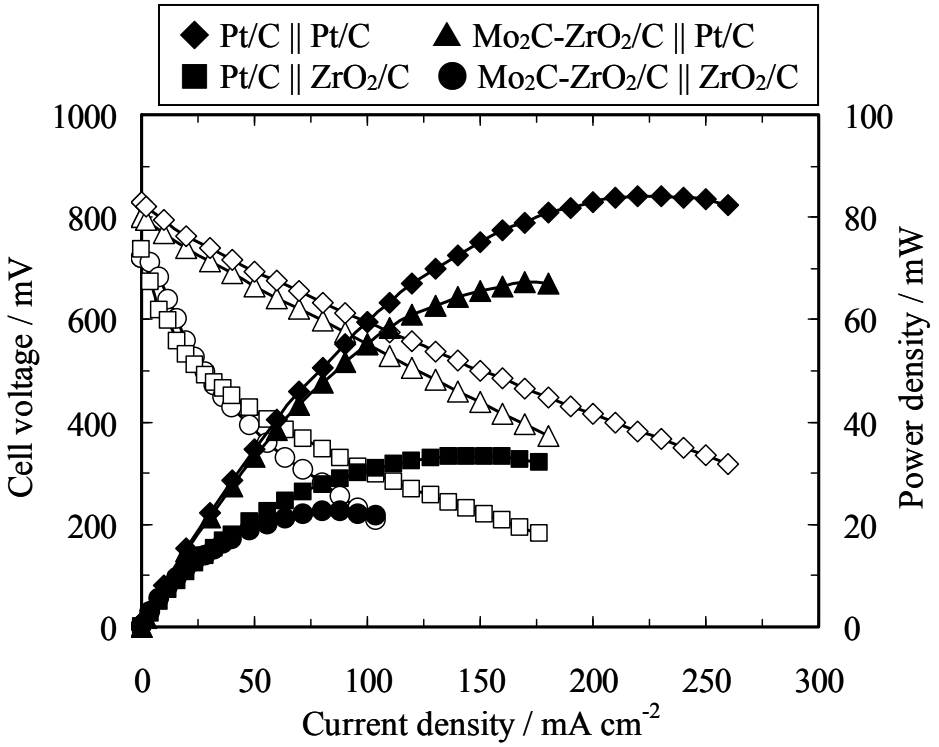

Figure 4-12. Cell voltage and power density vs. current density of fuel cells using Pt/C, Mo_2C-ZrO_2/C, and ZrO_2/C electrodes at 250°C. The experimental conditions are the same as those shown in Fig. 4-6.

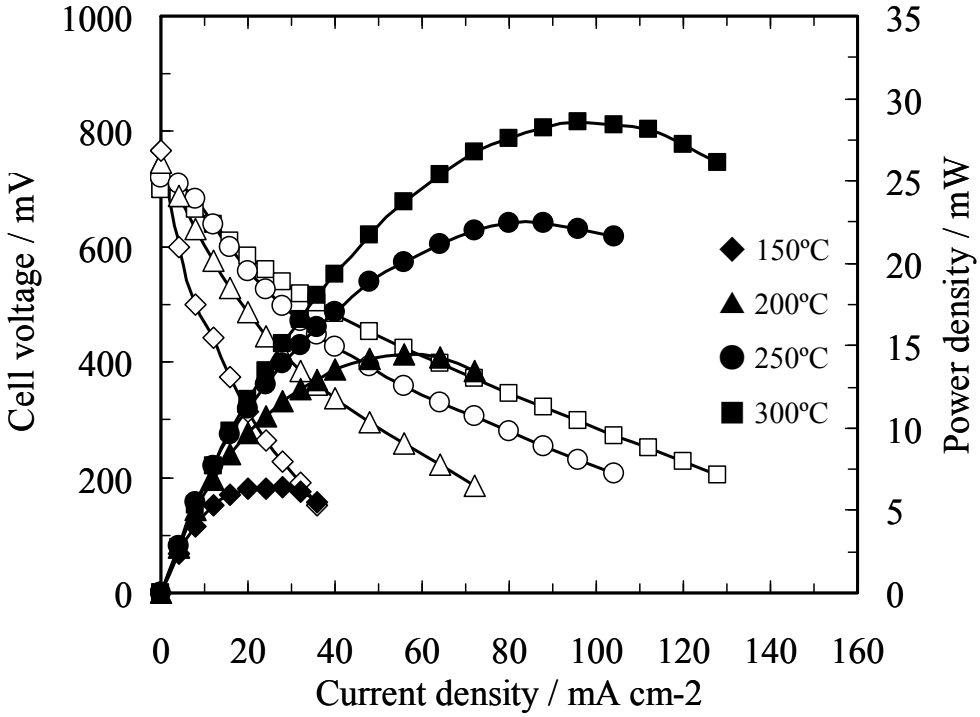

Figure 4-13. Cell voltage and power density vs. current density of Pt-free fuel cells using the Mo_2C-ZrO_2/C anode and the ZrO_2/C cathode at different temperatures. The experimental conditions are the same as those shown in Fig. 4-6.

Figure 4-13 shows performance of the Pt-free fuel cell, Mo_2C-ZrO_2/C|electrolyte|ZrO_2/C, between 150 and 300ºC. At all the tested temperatures, no limiting current behavior was observed at high current densities. The performance of the Pt-free fuel cell was strongly dependent on the operating temperature; the peak power density reached 29 mW cm^{-2} at 300ºC, but was significantly reduced to 6 mW cm^{-2} at 150ºC. Consequently, the present Pt-free electrodes need to be operated above 200ºC in order for them to be an effective alternative to Pt-based electrodes.

4.4 Summary

The Pt-free catalysts were investigated at intermediate temperatures between 150 and 300ºC. As the Pt-free catalysts, the Mo_2C-ZrO_2/C showed high anode performance toward the hydrogen oxidation (The polarization resistances were 0.28 Ω cm^2 for the Mo_2C-ZrO_2/C and 0.16 Ω cm^2 for the Pt/C at 250ºC) and the ZrO_2/C showed high cathode performance for the ORR (The polarization resistances were 6.37 Ω cm^2 for the ZrO_2/C and 3.18 Ω cm^2 for the Pt/C at 250ºC), respectively.

The Mo_2C anode catalyst showed the lowest polarization resistance at 250ºC among all the transition metal carbide catalysts tested. The addition of ZrO_2 to the catalyst allowed the Mo_2C to become highly dispersed on the carbon support, so that the catalytic activity could be improved to the level of the Pt catalyst. A fuel cell using the Mo_2C-ZrO_2/C and $Sn_{0.9}In_{0.1}P_2O_7$ as the anode and electrolyte, respectively, yielded a peak power density of 67 mW cm^{-2} at 250ºC, which was close to the peak power density of 84 mW cm^{-2} obtained using a fuel cell with the Pt/C anode.

The ZrO_2/C cathode catalyst showed the lowest overpotential among all the transition metal oxide catalysts tested. The catalytic activity of ZrO_2 for the ORR was considerably influenced by the ZrO_2 content on a carbon support and the heat-treatment for the ZrO_2/C, wherein the

20 wt.% ZrO_2/C that was heat-treated at 650ºC exhibited the best performance.

Performance of a Pt-free fuel cell using the Mo_2C-ZrO_2/C and ZrO_2/C as the anode and cathodes, respectively, was strongly dependent on the operating temperature. The peak power density reached 29 mW cm^{-2} at 300ºC, but was significantly decreased to 6 mW cm^{-2} at 150ºC. Its relatively high performance was achieved by operating the Pt-free fuel cell at intermediate temperatures above 200ºC.

4.5 References

[1] B. C. H. Steele and A. Heinzel, *Nature*, **414**, 345 (2001).

[2] B. R. Limoges, R. J. Stanis, J. A. Turner, A. M. Herring, *Electrochim. Acta.*, **50**, 1169 (2005).

[3] M. Nagao, A. Takeuchi, P. Heo, T. Hibino, M. Sano, A. Tomita, *Electrochem. Solid-State Lett*., **9**, A105 (2006).

[4] M. Nagao, T. Kamiya, P. Heo, A. Tomita, T. Hibino, M. Sano, *J. Electrochem. Soc.*, **153**, A1604 (2006).

[5] P. Heo, H. Shibata, M. Nagao, T. Hibino, M. Sano, *J. Electrochem. Soc.*, **153**, A897 (2006).

[6] M. S. Wilson, S. Gottesfeld, *J. Appl. Electrochem.*, **22**, 1 (1992).

[7] N. Cunningham, E. Irissou, M. Lefevre, M. C. Denis, D. Guay, J. P. Dodelet, *J. Electrochem. Soc.*, **6**, A125 (2003).

[8] J. H. Sinfelt, D. J. C. Yates, *Nature Phys. Sci.*, **229**, 27 (1971).

[9] R. B. Levy, M. Boudart, *Science*, **181**, 547 (1973).

[10] J. S. Choi, G. Bugli, G. Djega-Mariadassou, *J. Catal.*, **193**, 238 (2000).

[11] J. R. Kitchin, J. K. Norskov, M. A. Barteau, J. G. Chen, *Catal. Today*, **105**, 66 (2005).

[12] D. C. LaMont and W. J. Thomson, *Chem. Eng. Sci.*, **60**, 3553 (2005).

[13] S. Naito, M. Tsuji, and T. Miyao, *Catal. Today*, **77**, 161 (2002).

[14] C. Sayag, M. Benkhaled, S. Suppan, J. Trawczynski, G. Djega-Mariadassou, *Appl. Catal.*, **275**, 15 (2004).

[15] F. Solymosi, R. Nemeth, L. Ovari, and L. Egri, *J. Catal.*, **195**, 316 (2000).

[16] S. Ramanathan and S. T. Oyama, *J. Phys. Chem.*, **99**, 16365 (1995).

[17] J. Patt, D. J. Moon, C. Phillips, and L. Thomson, *Catal. Lett.*, **65**, 193 (2000).

[18] E. C. Weigert, N. A. Smith, B. G. Willis, A. Amorelli, J. G. Chen, *Electrochem. Solid-State Lett*., **8**, A337 (2005).

[19] T. Matsumoto, Y. Nagashima, T. Yamazaki, J. Nakamura, *Electrochem. Solid-State Lett*.,

9, A160 (2006).
[20] A. Ishihara, K. Lee, S. Doi, S. Mitsushima, N. Kamiya, M. Hara, K. Domen, K. Fukuda, and K. Ota, *Electrochem. Solid-State Lett*., **8**, A201 (2005).
[21] M. Lefevre and J. P. Dodelet, *Electrochim. Acta.*, **48**, 2749 (2003).
[22] Y. Liu, A. Ishihara, S. Mitsushima, N. Kamiya, and K. Ota, *Electrochem. Solid-State Lett*., **8**, A400 (2005).
[23] K. Tomishige, Y. Ikeda, T. Sakaihori, and K. Fujimoto, *J. Catal.*, **192**, 355 (2000).

5 Direct Dimethyl ether and Hydrocarbon Fuel Cells at Intermediate Temperatures

5.1 Introduction

Proton exchange membrane fuel cells (PEMFCs) have received increasing attention for residential and vehicular applications because of their high efficiencies and environmentally friendly characteristics. Although hydrogen, which is commonly used as fuel, provides the best performance and is the most efficient of the fuels, it presents several problems, such as low storage density, high production cost, and lack of distribution infrastructure [1]. While the local chemical reforming of hydrocarbons such as methane to produce hydrogen is regarded as a more acceptable option, a major disadvantage of this strategy is the considerable complexity and expense that reform-and-shift reactor adds to the system [2]. The reformer system represents an additional cost of at least 30% of the total cost of the fuel cell system. Thus, considerable effort has been devoted to developing fuel cells using alternative fuels as a direct fuel [3-5]. The use of alcohols as a direct fuel is advantageous in terms of fuel storage and handlings because they are liquid fuels. Among the different possible alcohols, methanol is the most promising organic fuel due to high theoretical density of energy (6 kWh/kg) [6]. Therefore, direct methanol fuel cell (DMFC) based on PEMFCs has been expensively investigated, especially, for portable applications. However, the DMFC remains critical challenges such as anode poisoning by CO formed during methanol oxidation and methanol cross-over through the membranes, causing significant efficiency losses. Moreover, methanol has some particular disadvantages, e.g. it is relatively toxic, inflammable with a low boiling point (65 °C).

Dimethyl ether (DME) is regarded as a promising candidate owing to its advantages in

terms of production, storage and toxicity as well. DME can be produced from various resources, including fossil and biomass fuels [7], and stored as a higher density liquid (it is typically stored at 0.6 MPa in standard propane tanks) [1]. Additionally, the low toxicity of DME is comparable to that of liquid propane.

Some direct DME fuel cells (DDMEFCs) have been studied using Nafion as an electrolyte [8-12]. The oxidation of DME to CO_2 follows equation (5-1)

$$(CH_3)_2O + 3H_2O \rightarrow 2CO_2 + 12H^+ + 12e^- \quad (5\text{-}1)$$

According to the literature, the kinetics of this reaction is strongly dependent on the temperature [8]. The reaction rate is slow near room temperature, causing DDMEFCs to show poor performance. Kerangueven et al. reported that the peak power density of the DDMEFC was below 2 mW cm^{-2} at an operating temperature of 50ºC and a pressure of 1 atm [9]. They also found that increasing the temperature from 50 to 90ºC led to a power density enhanced by a factor of almost 10 (16 mW cm^{-2} at 90ºC). These results suggest that operation at higher temperatures is favorable for DDMEFCs.

Another potential fuel to alternate hydrogen is hydrocarbons such as propane. The fuel cells using hydrocarbons as a direct fuel would be the most advantageous in term of an infrastructure for fuel distribution. Like DME, hydrocarbons can be also stored in liquid form in pressure vessels and their energy densities are higher than the energy density of methanol [2]. Although the direct hydrocarbon fuel cell has such a lot of advantages, very little study has been reported on PEMFC using hydrocarbons as a direct fuel. However, Li et al. reported the ethane/oxygen fuel cell using Nafion as an electrolyte, although its cell performance was very poor; the peak power density is 0.0024 mW cm^{-2} at 90ºC [13]. This result is due to very low kinetics for the oxidation of hydrocarbons at the low temperature below 100ºC and thus the higher temperature operation is required for the direct hydrocarbon fuel cells. However, the operating temperature of Nafion-based fuel cells is commonly limited to the dehydration temperature of ~100ºC because protons attach themselves to water and diffuse as H_3O^+ ions

through the Nafion electrolyte.

Recently, it has been found that an anhydrous proton conductor, 10 mol% In^{3+}-doped SnP_2O_7 ($Sn_{0.9}In_{0.1}P_2O_7$), shows high proton conductivities above 0.1 S cm^{-1} between 150 and 350ºC under unhumidified conditions [14-17]. The charge carriers of this material were not H_3O^+ ions, but protons which migrated between the lattice oxide ions according to a hopping mechanism. A hydrogen/air fuel cell with a 0.35-mm-thick $Sn_{0.9}In_{0.1}P_2O_7$ electrolyte could yield a high power density of 264 mW cm^{-2} at 250ºC. Furthermore, the fuel cell showed excellent tolerance toward 10% CO and good thermal stability under unhumidified conditions.

In this study, I investigated DDMEFCs and direct hydrocarbon fuel cells using $Sn_{0.9}In_{0.1}P_2O_7$ as an electrolyte at intermediate temperatures between 150 and 350ºC. The anode reaction of DME and hydrocarbons in the fuel cells was evaluated by analyzing anodic overpotentials and anode products.

5.2 Experimental

5.2.1 Materials preparation

Electrolyte preparation – $Sn_{0.9}In_{0.1}P_2O_7$ was prepared as described in chapter 2. Briefly, the corresponding oxides (SnO_2 and In_2O_3), 85% H_3PO_4, and ion-exchanged water were mixed and stirred at 300ºC until a high-viscosity paste was formed. After calcinations of the paste at 650ºC for 2.5 h, the compound was ground with a mortar and pestle. The compound powders were pressed into a pellet 1.0 mm in thickness and 14.0 mm in diameter under a pressure of 2×10^3 kg cm^{-2}.

Electrode preparation – For DDMEFCs, the anode was made from 60 wt.% Pt/C catalyst (E-TEK) and carbon papers (Toray TGPH-090). PtMe/C (Me=Pd,Rh,Ru; atomic ratio of PtMe=1:1, E-TEK) were also used as anode catalysts. The Pt and PtMe loadings were about 4

mg cm^{-2} for the anodes.

For direct hydrocarbon fuel cells, 30~70 wt.% Pt/C (Tanaka Kikinzoku Kogyo) and 50~80 wt.% Mo_2C-ZrO_2/C were used for anode catalysts. Mo_2C-ZrO_2/C was prepared as described in chapter 4. Anode catalyst powders were mixed with poly(tetrafluoroethylene) (PTFE) and glycerol as a binder and a solvent, respectively. The catalyst inks were coated on a gas diffusion layer (SGL carbon GDL35BC). These samples were heated in Ar at 150ºC for 3 h to remove the glycerol solvent in the catalyst layer. After pressing at 50 kg cm^{-2}, the samples were heated in Ar at 350ºC for 1 h to disperse PTFE in the catalyst layer.

Intermediate layers prepared by mixing the electrolyte ($Sn_{0.9}In_{0.1}P_2O_7$) and catalyst (Pt/C or PtMe) powders were applied at the interface between the electrolyte and electrode as described in chapter 3. Commercial Pt/C electrodes (10 wt% Pt/C, 0.6 mg Pt cm^{-2}, E-TEK) were used as a counter electrode for a cathode.

5.2.2 Fuel cell tests

The anode and cathode (area: 0.5 cm^2) were attached on opposite sides of the $Sn_{0.9}In_{0.1}P_2O_7$ electrolyte (thickness: 1.0 mm). The fuel and air chambers were set up by placing a cell between two alumina tubes. Each chamber was sealed with an inorganic adhesive. A mixture of DME or hydrocarbons and water vapor was supplied to the fuel chamber at a flow rate of 60 mL min^{-1}. The pressure ratio of water vapor (0.3 atm) to DME or hydrocarbons (0.1 atm) was 3. The applied hydrocarbons are methane, ethane, propane, and butane. Unhumidified air was supplied to the air chamber at a flow rate of 30 mL min^{-1}. The outlet gas from the fuel cells was analyzed using on-line gas chromatography (GC). The anodic overpotentials were measured by the current interruption method. For this measurement, a Pt reference electrode was attached on the side surface of the electrolyte and exposed to open air atmosphere. The voltage-current density curves were measured by the four-probe method. The operating temperature was maintained between 150 and 350ºC.

5.3 Results and discussion

5.3.1 Direct DME fuel cells

Figure 5-1 shows the open-circuit voltages (OCVs) of DDMEFCs using Pt/C as anode between room temperature and 300ºC. At temperatures below 150ºC, the OCVs were lower than the values obtained by Mench et al. (700-800 mV) using Nafion-based DDMEFCs [1]. This is presumably due to the difference in experimental conditions: while Mench et al. conducted their fuel cell tests at high DME pressures of ~3 atm, I employed a low DME pressure of 0.1 atm. On the other hand, as shown in Fig. 5-1, the OCVs increased with increasing temperature and reached about 800 mV at 200ºC or higher. The increase in OCVs

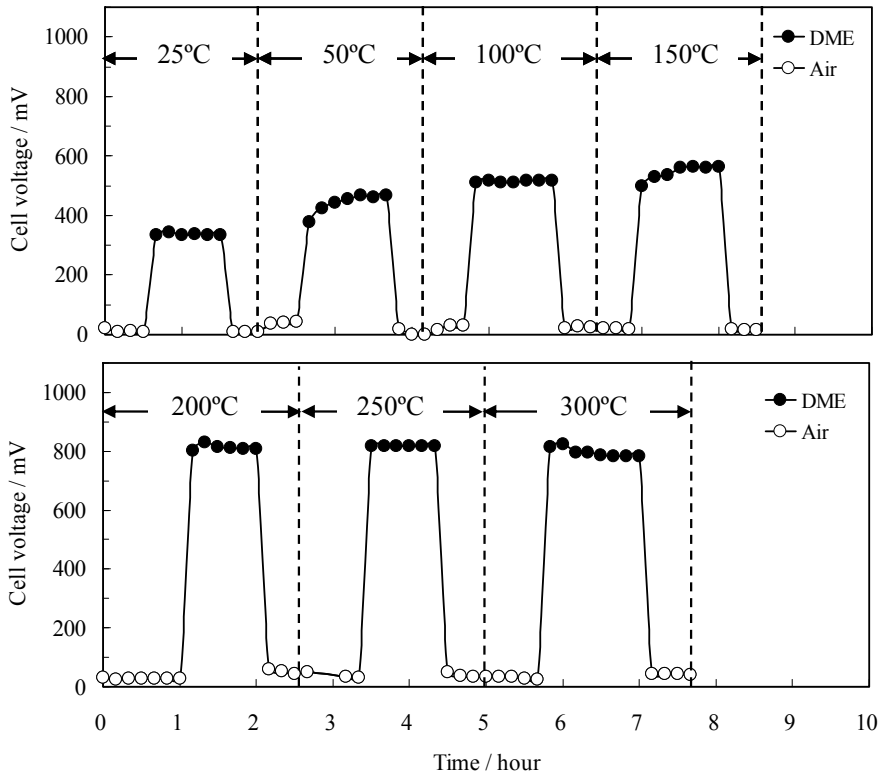

Figure 5-1. Open-circuit voltages (OCVs) of DDMEFCs using $Sn_{0.9}In_{0.1}P_2O_7$ and Pt/C as electrolyte and anode, respectively, between room temperature and 300ºC. The thickness of the $Sn_{0.9}In_{0.1}P_2O_7$ electrolyte was 1 mm. A mixture of DME and water vapor was supplied to the anode at a flow rate of 60 mL min^{-1}, in which the DME partial pressure was 0.1 atm. The supplied gas was switched from unhumidified air to fuel, and back to unhumidified air at each temperature.

can be explained by assuming that the oxidation reaction shown in Eq. (5-1) was activated under these conditions. The high CO tolerance of the DDMEFCs at elevated temperatures is also responsible for the relatively high OCVs, as will be described later. Thus, in subsequent experiments, I operated the fuel cell at intermediate temperatures between 150 and 300ºC.

The anodic overpotentials of the Pt/C anode for the anode reaction of DME were measured between 150 and 300ºC, as shown in Fig. 5-2. The anodic overpotentials decreased considerably with increasing temperature. The decrease in overpotential was found to be particularly marked above 200ºC: the overpotentials at 100 mA cm^{-2} were 287, 260, and 167 mV at 150, 200, and 250ºC, respectively. A similar temperature dependence was observed for the cell performance of the DDMEFCs. Figure 5-3 plots the current-voltage curves of the DDMEFCs at various temperatures. While the peak power density was 9 mW cm^{-2} at 150ºC, it could be improved to 41 mW cm^{-2} at 300ºC.

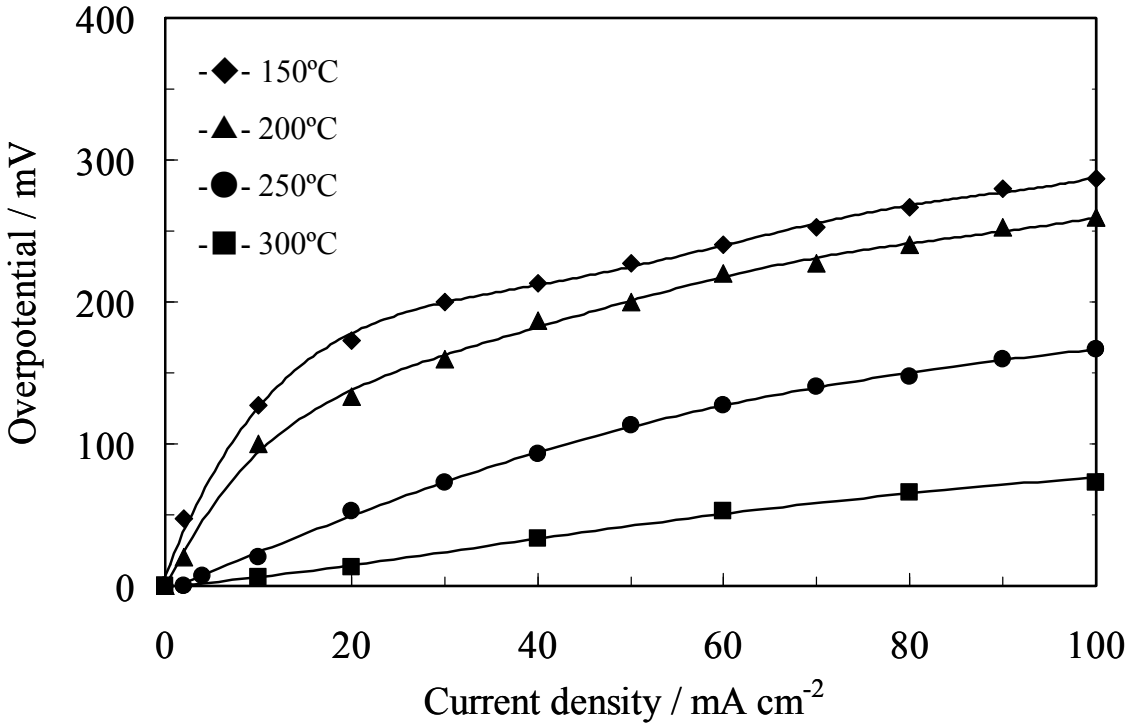

Figure 5-2. Anodic overpotentials of the Pt/C anode for the anode reaction of DME between 150 and 300ºC.

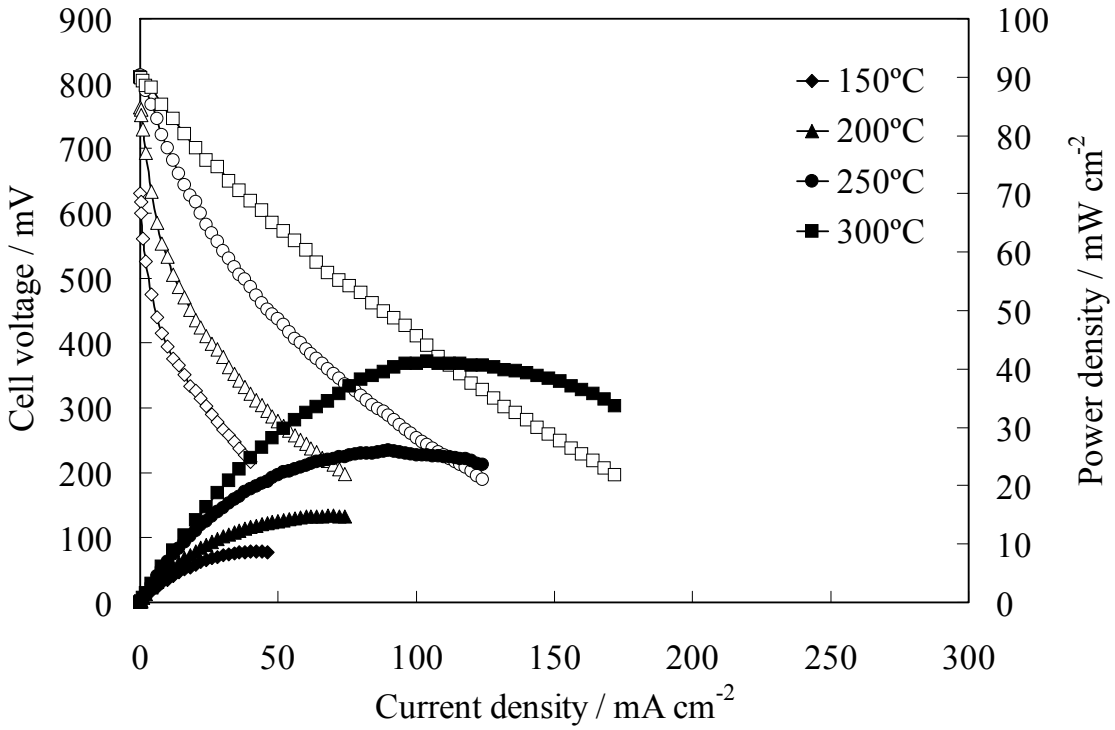

Figure 5-3. Cell voltage and power density vs. current density of DDMEFCs with Pt/C anode between 150 and 300ºC. The thickness of the $Sn_{0.9}In_{0.1}P_2O_7$ electrolyte was 1 mm. A mixture of DME and water vapor was supplied to the anode at a flow rate of 60 mL min^{-1}, in which the DME partial pressure was 0.1 atm.

To better understand the anode reaction of DME at the Pt/C anode, the anode products in the outlet gas from the DDMEFCs were analyzed at 250ºC. The gas concentrations of the anode products as a function of current density at 250ºC are plotted in Fig. 5-4, including the theoretical value of CO_2 concentration for 100% faradic efficiency (i.e., complete oxidation of DME). The CO_2 concentration increased linearly with current density and was very near its theoretical values, indicating that DME is converted into CO_2 according to the oxidation reaction shown in Eq. (5-1). However, small amounts of CO and H_2 were also produced in the open circuit, suggesting that the following reforming reaction of DME occurs to a small extent along with the direct oxidation reaction of DME.

$$(CH_3)_2O + H_2O \rightarrow 4H_2 + 2CO \qquad (5\text{-}2)\ [18]$$

Liu et al. has reported that the CO formed during the anode reaction of DME functions as poisonous species for a Pt catalyst [8]. Thus, I investigated the CO tolerance of the Pt/C

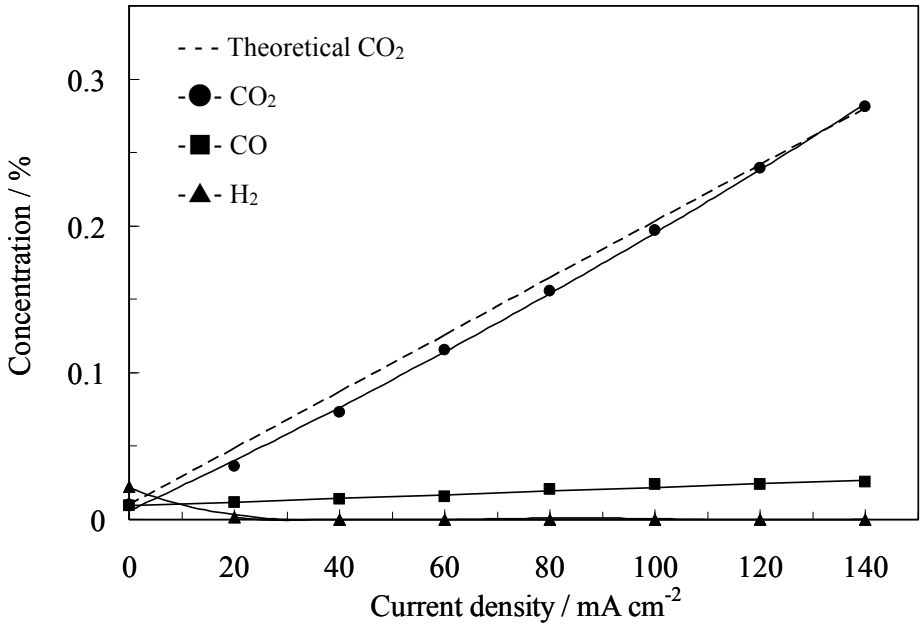

Figure 5-4. Gas concentrations of anode products as a function of current density over the Pt/C anode at 250ºC. The data were obtained by analyzing the outlet gas from the DDMEFCs, including the theoretical value of CO_2 concentration for 100% faradic efficiency.

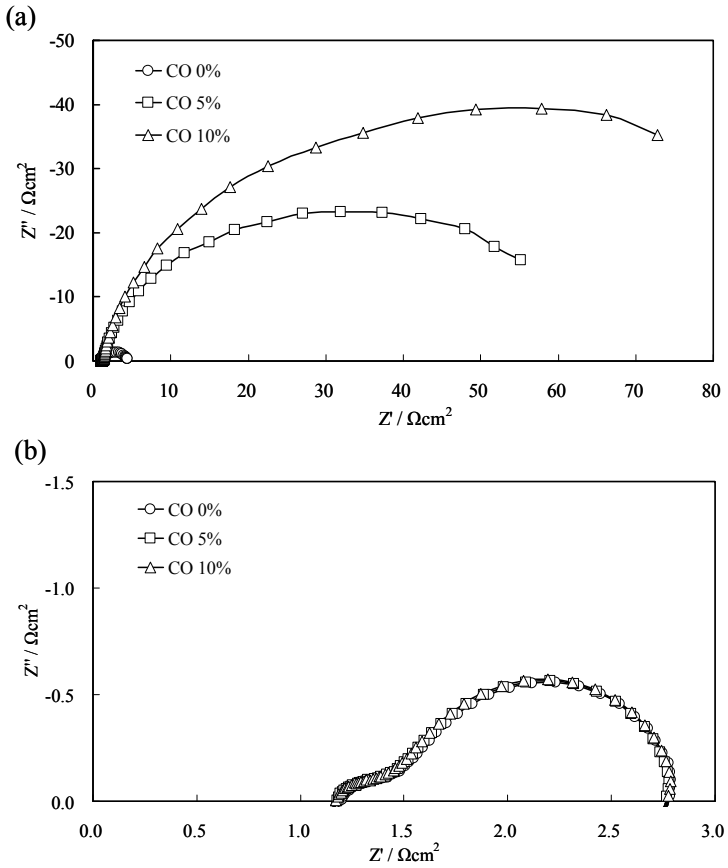

Figure 5-5. Impedance spectra of the fuel cell using H_2 and a mixture of 5 or 10% CO + H_2 as the fuel gas at (a) 100 and (b) 250ºC.

anode by supplying hydrogen or a mixture of 5 or 10% CO and hydrogen to the fuel chamber at 100 and 250ºC, respectively. The impedance spectra of the fuel cells are shown in Fig. 5-5. Although the polarization resistance increased significantly with increasing CO concentration in the fuel at 100ºC, it was maintained constant regardless of the presence of even 10% CO at 250ºC. These results indicate that the Pt/C anode was not at all poisoned by the CO formed during the anode reaction of DME. The results also suggest that this high CO tolerance allowed the Pt/C anode to have a sufficiently high catalytic activity to achieve both the high OCVs and the cell performance observed at 250ºC and above.

The addition of various metals to Pt was attempted to improve the anode reaction. Figure 5-6 shows the anodic overpotentials of Pt/C and PtMe/C (Me=Pd,Rh,Ru) anodes at 250ºC. Among the anodes tested, the PtRu/C anode showed the highest catalytic activity for the anode reaction of DME. The anodic overpotential at the PtRu/C anode was reduced to approximately one-half of that at the Pt/C anode (from 167 mV to 73 mV at 100 mA cm^{-2}).

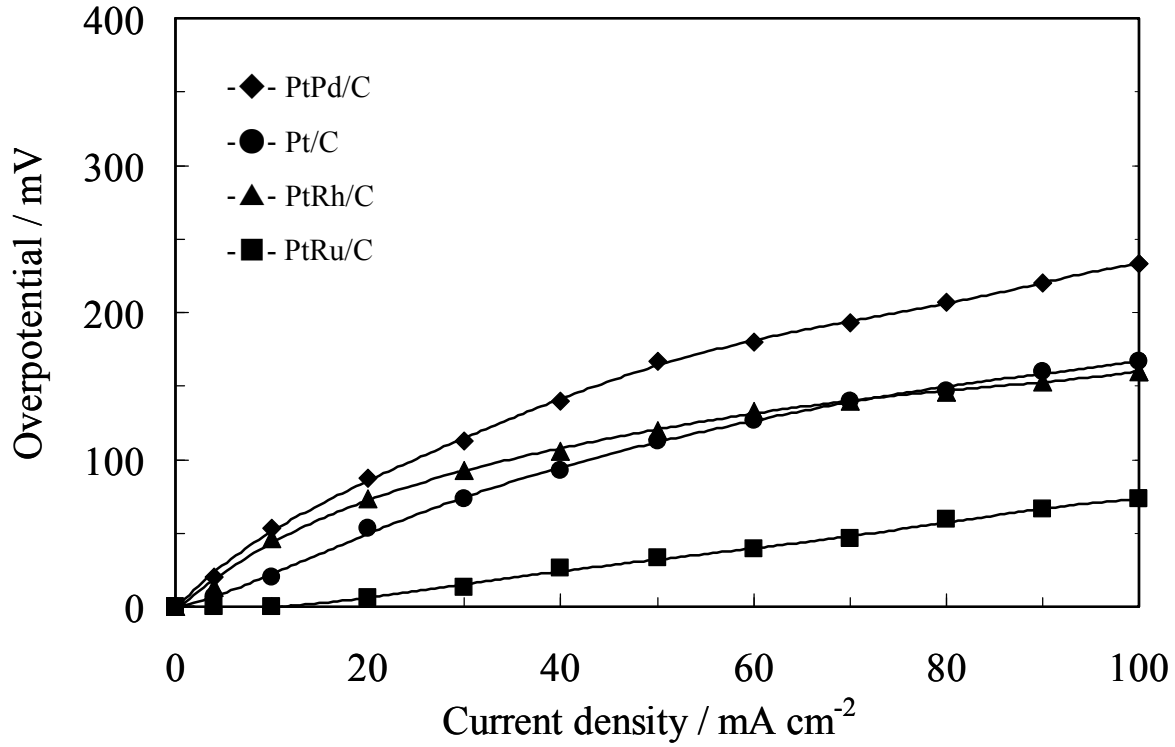

Figure 5-6. Anodic overpotentials of Pt/C and PtMe/C (Me=Pd,Rh,Ru) anodes for the anode reaction of DME at 250ºC.

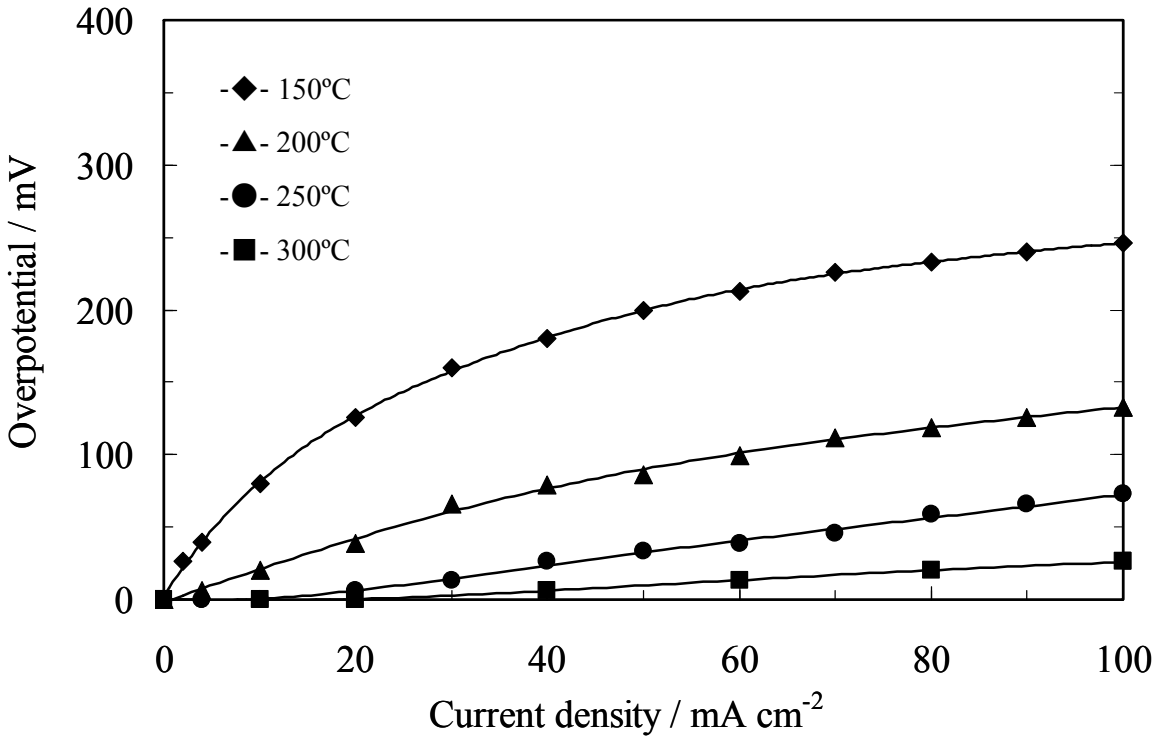

Figure 5-7. Anodic overpotentials of the PtRu/C anode for the anode reaction of DME between 150 and 300ºC.

The anodic overpotential was also improved at various temperatures, as shown in Fig. 5-7. The decrease in the overpotential was found to be particularly marked above 150ºC. On the other hand, the apparent activation energy for the anode reaction of DME can be determined from Arrhenius plots of the reciprocal of polarization resistances for the anodes [19,20]. Polarization resistances of the Pt/C and PtRu/C anodes were estimated from the slopes of anodic overpotentials in Figs. 5-2 and 5-7, respectively. As can be seen from Fig. 5-8, double reciprocal plots of the polarization resistances and operating temperatures gave two lines with different slopes. The apparent activation energies for the anode reaction of DME at the two anodes were calculated from the corresponding slopes. The values obtained were 19 and 26 kJ/mol for the Pt/C and PtRu/C anodes, respectively. This difference can be explained by the difference in the mechanism for the anode reaction between the two anodes. I will discuss this point later.

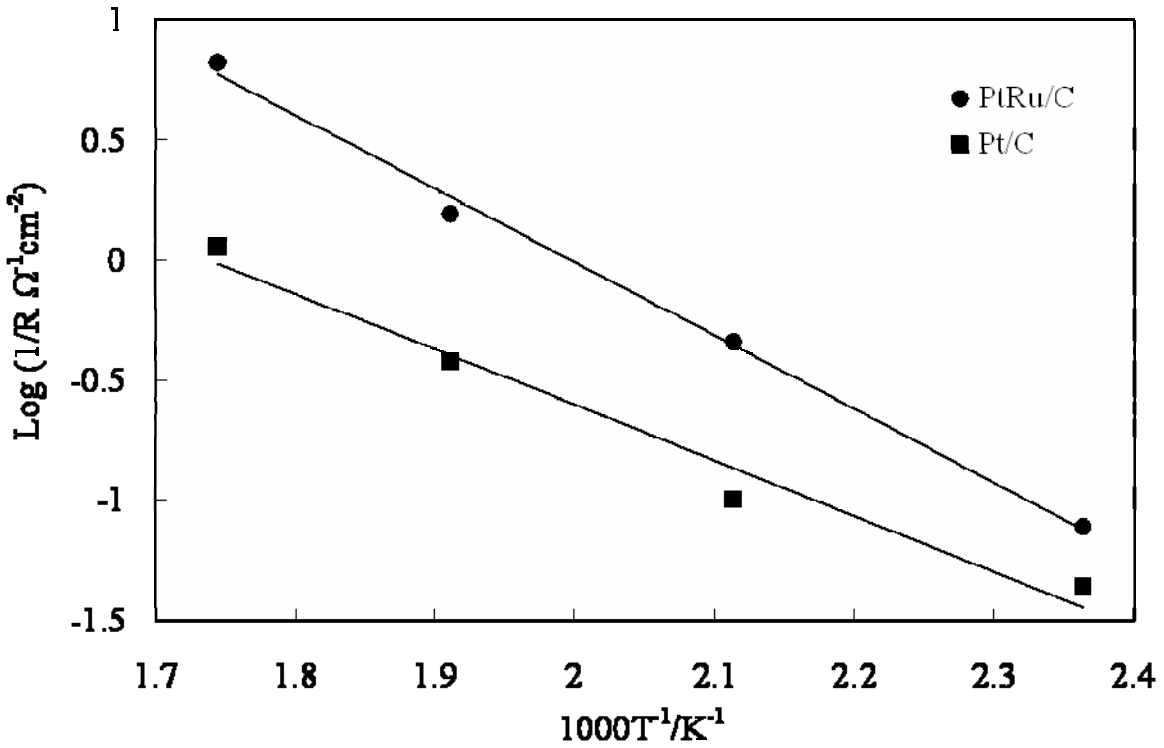

Figure 5-8. The apparent activation energies for the anode reaction of DME at Pt/C and PtRu/C anodes. The polarization resistances of Pt/C and PtRu/C anodes were estimated from the slopes of the anodic overpotentials in Figs. 5-2 and 5-7, respectively.

The performance of the DDMEFCs with a PtRu/C anode is shown in Fig. 5-9. The peak power density ranged from 31 mW cm^{-2} at 200ºC to 78 mW cm^{-2} at 300ºC; these values are about twice those obtained with the Pt/C anode shown in Fig. 5-3. Liu et al. and Yoo et al. reported that the use of PtRu/C anodes improved the cell performance of Nafion-based DDMEFCs as compared to the case of the Pt/C anode [8,12]. In these studies, the improvement was mainly attributed to the bi-functional effect. The Ru activates the water molecule to form OH species, which oxidize poisonous species such as CO and thus reduce the poisoning on the Pt sites. In the present case, the effect of the Ru addition does not appear to be due to the bi-functional effect because no CO poisoning occurred on the Pt catalyst at intermediate temperatures, as shown in Fig. 5-5. It can be seen from the composition analysis of the anode outlet gas in Fig. 5-10 that the amount of H_2 generated over the PtRu/C anode in the open circuit was considerably higher than that over the Pt/C anode. The amount of H_2 was

reduced with current density, indicating that the H_2 produced was electrochemically consumed in the fuel cell. Thus, the effect of the added Ru on the anode reaction is attributable to the activated reforming reaction of DME shown in Eq. (5-2) and the subsequent electrochemical oxidation of the H_2 produced. Since it is an endothermic reaction, the reforming reaction of DME requires a higher activation energy of the anode reaction for the PtRu/C anode compared to that for the Pt/C anode, which can explain the result shown in Fig 5-8. In other words, the anode reaction becomes more favorable as the temperature is increased. Indeed, the cell performance of the DDMEFC at 300ºC was comparable to that of a fuel cell using H_2 as fuel: the power density was 78 mW cm^{-2} for DME and 100 mW cm^{-2} for H_2 at 300ºC.

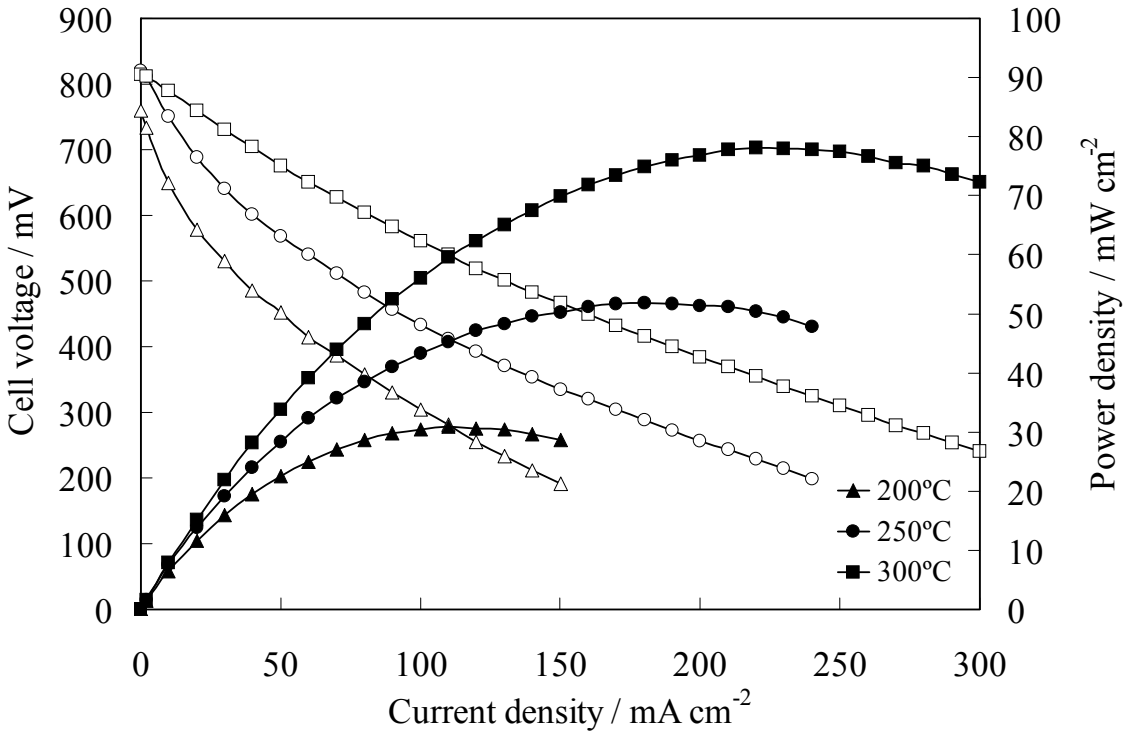

Figure 5-9. Cell voltage and power density vs. current density of DDMEFCs with PtRu/C anode between 200 and 300ºC. The experimental conditions are the same as those in Fig. 5-3.

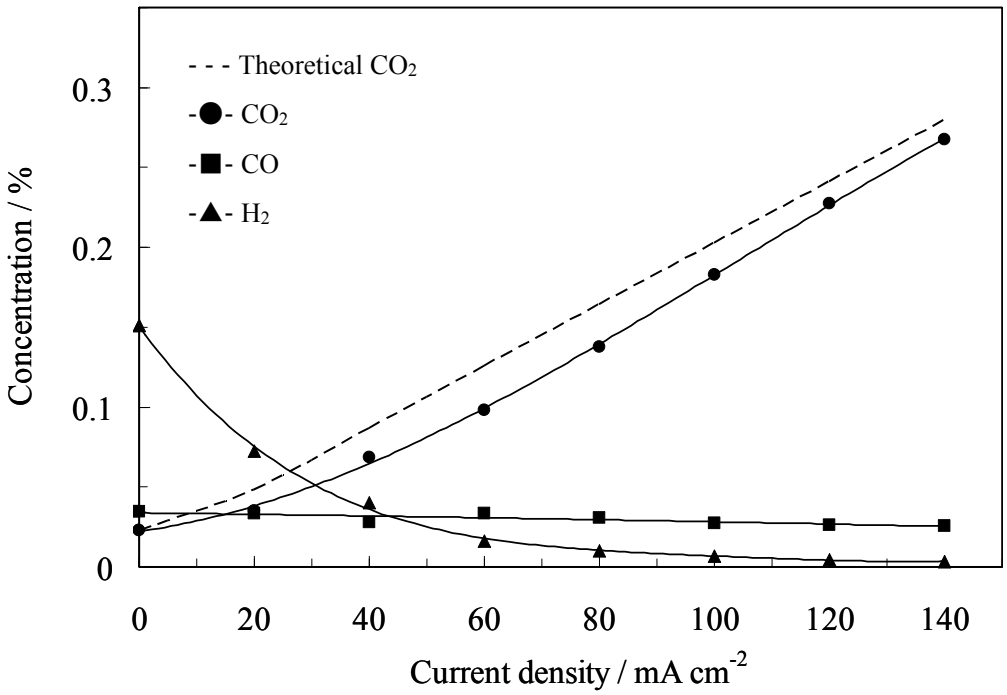

Figure 5-10. Gas concentrations of anode products as a function of current density over the PtRu anode at 250ºC. The experimental conditions are the same as those in Fig. 5-4.

5.3.2 Direct hydrocarbon fuel cells

Operation of direct hydrocarbon fuel cells was evaluated using methane, ethane, propane, and butane as fuels. Figure 5-11 shows the open-circuit voltages (OCVs) of the fuel cells using 50 wt.% Pt/C as anode between 50 and 400ºC. The OCVs increased with increasing temperature and reached about 650 mV at 150ºC or higher. The increase in OCVs may be caused by reactivities for the oxidation reactions for the corresponding hydrocarbons. This suggests that the fuel cells needed to be operated at intermediate temperatures above 150ºC. The performances of the direct hydrocarbon fuel cells at 300ºC are shown in Fig. 5-12. In the fuel cells, except for methane, no limiting current behavior was observed at high current densities. Higher cell performances were obtained with higher hydrocarbons, while the fuel cells with butane, propane, and ethane exhibited comparable performances. The peak power densities were 23 mW cm^{-2} for methane, 35 mW cm^{-2} for ethane, 36 mW cm^{-2} for propane, and 38 mW cm^{-2} for butane.

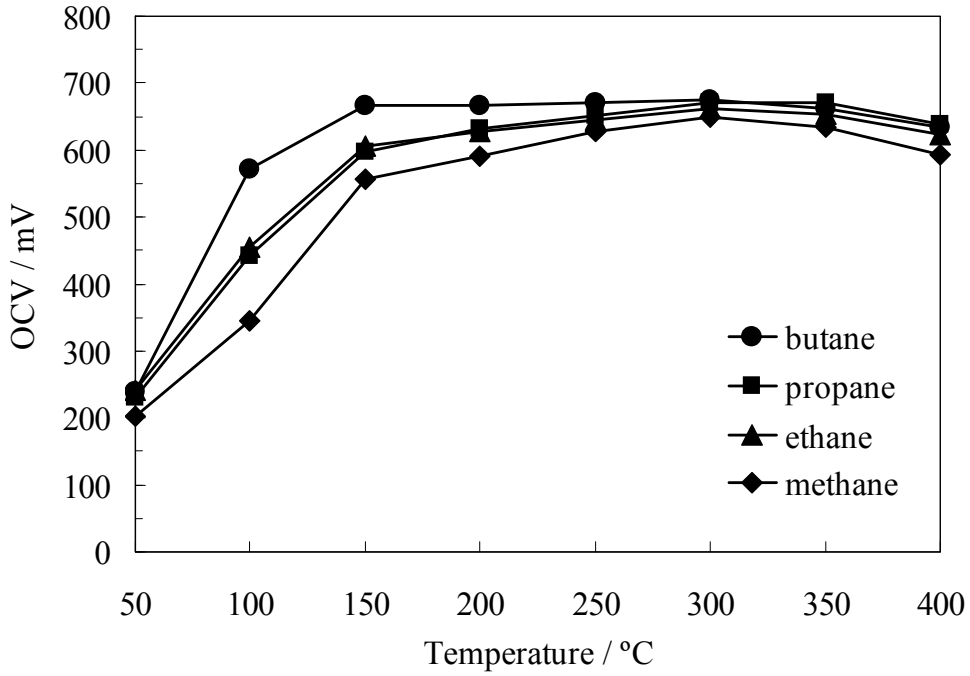

Figure 5-11. Open-circuit voltages (OCVs) of direct hydrocarbon fuel cells with Pt/C anode between 50 and 300°C. The thickness of the $Sn_{0.9}In_{0.1}P_2O_7$ electrolyte was 1 mm. A mixture of hydrocarbon and water vapor was supplied to the anode at a flow rate of 60 mL min^{-1}, in which the partial pressure of hydrocarbon was 0.1 atm.

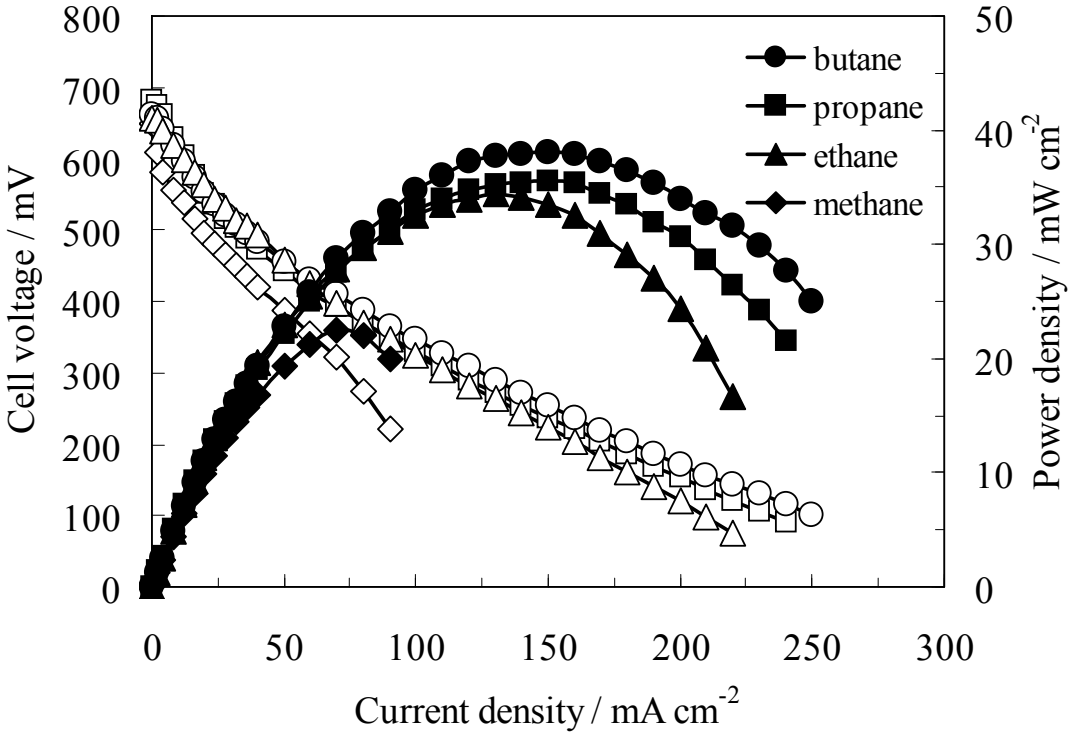

Figure 5-12. Cell voltage and power density vs. current density of direct hydrocarbon fuel cells with Pt/C anode at 300°C. The Pt loadings in the Pt/C anodes are between 5.5 and 6.0 mg/cm^2. The experimental conditions are the same as those in Fig. 5-11.

The anode products in the outlet gas from the fuel cells were analyzed by gas chromatography. The gas concentrations of the anode products as a function of current density at 250ºC are plotted in Fig. 5-13, including the theoretical value of CO_2 concentration for 100% faradic efficiency (i.e., complete oxidation of hydrocarbons). Negligibly amount of CO_2 were formed at OCVs and no by-products were observed for all the fuel cell with hydrocarbons. The CO_2 concentrations increased linearly with current density and were very near its theoretical values. Therefore, in the present fuel cells, all the hydrocarbons are electrochemically converted into CO_2 along with the direct oxidation reaction;

$$C_xH_y + 2xH_2O \rightarrow xCO_2 + (4x+y)H^+ + (4x+y)e^- \quad (5\text{-}3)$$

In case of propane,

$$C_3H_8 + 6H_2O \rightarrow 3CO_2 + 20H^+ + 20e^- \quad (5\text{-}4)$$

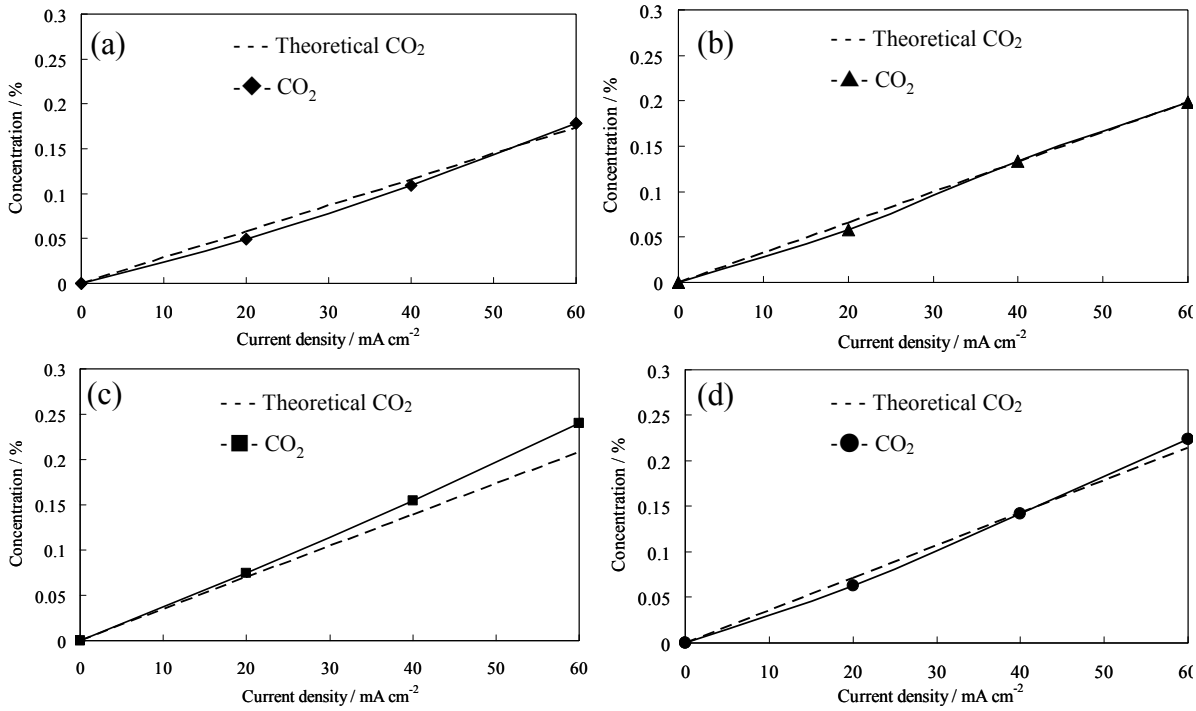

Figure 5-13. Gas concentrations of anode products as a function of current density at Pt/C anodes at 300ºC. The data were obtained by analyzing the outlet gas from the direct hydrocarbon fuel cells with (a) methane, (b) ethane, (c) propane, and (d) butane, including the theoretical values of CO_2 concentration for 100% faradic efficiency.

Similar result was shown in earlier report based on PAFC [21]. In a propane/oxygen fuel cell using H_3PO_4 as an electrolyte, the CO_2 yielded from propane was about 95% at 150ºC. On the other hand, I examined the dependence of Pt loadings in the Pt/C anodes on the performance of the present fuel cells. In direct propane fuel cell (DPFC), the performance was considerably enhanced with increasing Pt loadings in the Pt/C anodes (Fig. 5-14); the peak power densities were 27 mW cm^{-2} for 1.4 mg Pt cm^{-2}, 36 mW cm^{-2} for 5.9 mg Pt cm^{-2}, and 50 mW cm^{-2} for 8.5 mg Pt cm^{-2}. This result indicates an increase in the active surface area of Pt for the direct oxidation reaction of propane.

However, the use of Pt catalyst causes high materials cost for fuel cells. In previous study (chapter 4), I found that the Mo_2C-ZrO_2/C showed high anode performance toward the hydrogen oxidation at intermediate temperatures. I thus attempted to apply the Mo_2C-ZrO_2/C as an anode for the direct hydrocarbon fuel cell. Performance of DPFC with the Mo_2C-ZrO_2/C

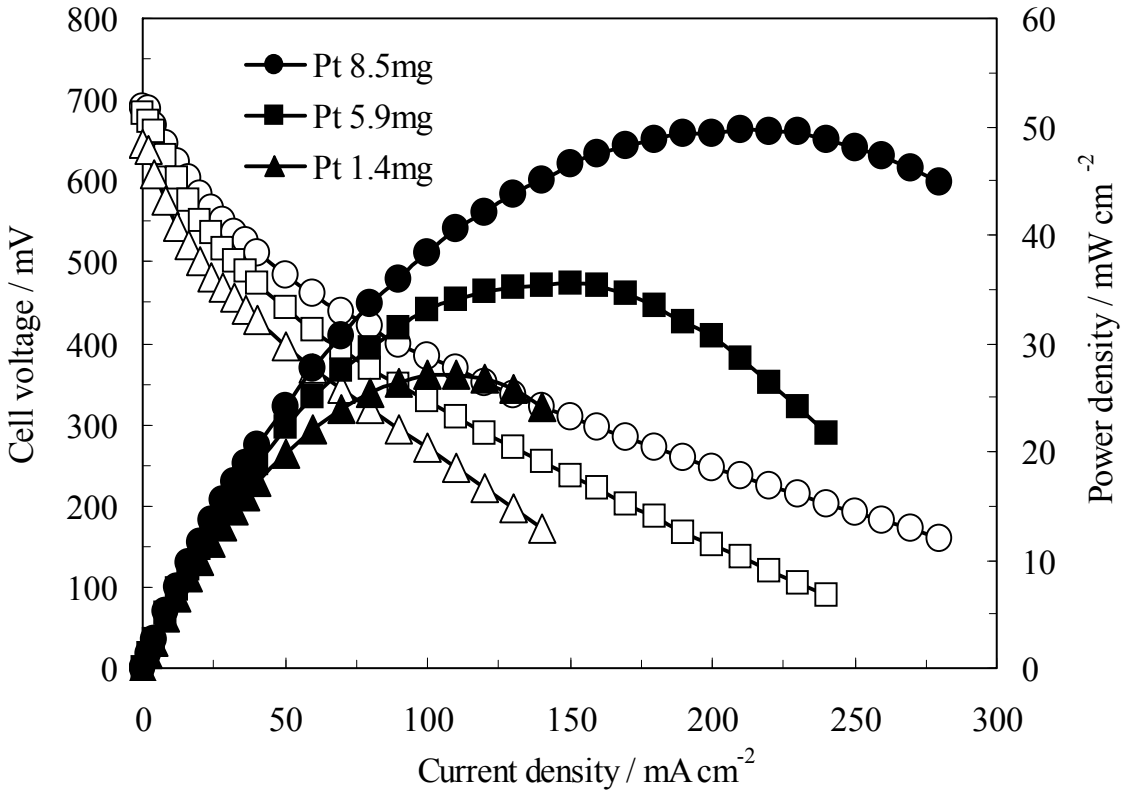

Figure 5-14. Cell voltage and power density vs. current density of DPFCs with Pt/C anode at 300ºC. The experimental conditions are the same as those in Fig. 5-11.

anode at 300ºC was shown in Fig. 5-15. The performances of DPFC were improved by changing the weight ratio of ZrO_2 to Mo_2C in the catalyst. As a result, Mo_2C-ZrO_2/C with a weight ratio of Mo_2C:ZrO_2 = 1:0.3 showed the highest anode performance; the peak power density reached 37 mW cm^{-2}. It can be known that this performance was comparable to that for the Pt/C anode shown in Fig. 5-14.

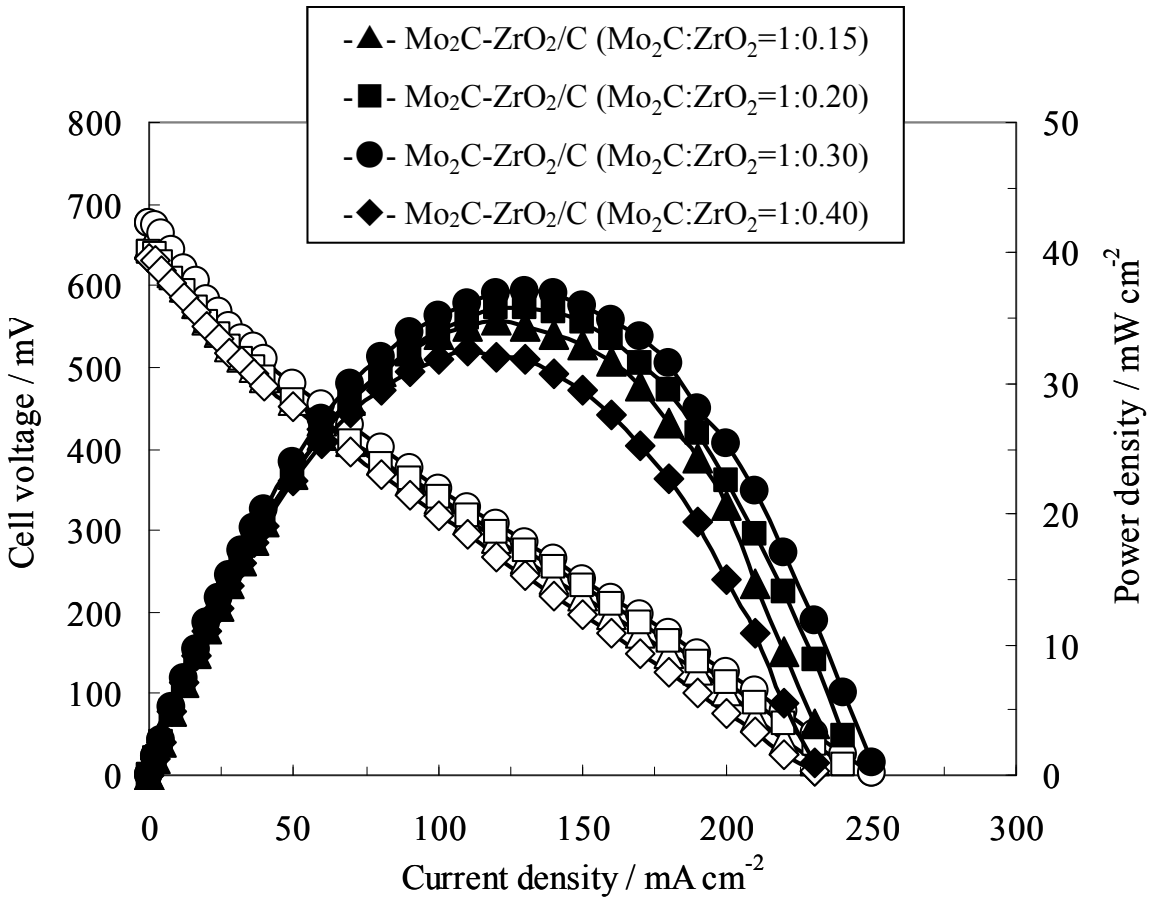

Figure 5-15. Cell voltage and power density vs. current density of DPFCs using Mo_2C-ZrO_2/C anode with different weight ratio of ZrO_2 to Mo_2C at 300ºC. The experimental conditions are the same as those in Fig. 5-11.

5.3.3 Advantages of the present fuel cell

The present fuel cells using DME and hydrocarbons as direct fuels do not require the reforming process of the fuels, which will provide significant simplicity and reduced costs in the fuel cell system. In addition, the use of non Pt anode catalysts in these fuel cells makes it possible to reduce the materials cost of the fuel cell. Furthermore, the present fuel cell is

expected have additional advantages over the current PEMFCs, such as higher reaction rates, faster heat rejection rates, and more efficient thermal utilization. These advantages would greatly enhance the position of intermediate-temperature fuel cells as the preferred power generation technology for practical applications.

5.4 Summary

DDMEFCs and direct hydrocarbon fuel cells were investigated using $Sn_{0.9}In_{0.1}P_2O_7$ as electrolyte at intermediate temperatures between 150 and 300ºC. In these fuel cells, all the DME and hydrocarbons were electrochemically converted into CO_2 along with their direct oxidation. DDMEFCs with the Pt/C anode showed high OCVs above 800 mV at 200ºC and above, below which low OCVs were obtained. The anodic overpotentials of the Pt/C anode for the anode reaction of DME could be improved by the addition of Ru to Pt. In DDMEFCs with the PtRu/C anode, the peak power density ranged from 31 mW cm^{-2} at 200ºC to 78 mW cm^{-2} at 300ºC, which are about twice those obtained with the Pt/C anode. The addition of Ru to the Pt catalyst activated the reforming reaction of DME, especially at intermediate temperatures. The electrochemical oxidation of the H_2 produced by the reforming reaction proceeded concurrently with the direct oxidation reaction of DME.

Direct hydrocarbon fuel cells with the Pt/C anode achieved OCVs above 600 mV at 150ºC and above. Higher cell performances were obtained with higher hydrocarbons, while the fuel cells with butane, propane, and ethane exhibited comparable performances. The peak power densities were 23 mW cm^{-2} for methane, 35 mW cm^{-2} for ethane, 36 mW cm^{-2} for propane, and 38 mW cm^{-2} for butane at 300ºC, while these performances were enhanced with increasing Pt loadings in the Pt/C anodes. DPFC with the Mo_2C-ZrO_2/C anode yielded the peak power density of 37 mW cm^{-2} at 300ºC, which is comparable to that obtained with the Pt/C anode.

5.5 References

[1] M. M. Mench, H. M. Chance, and C. Y. Wang, *J. Electrochem. Soc.*, **151**, A144 (2004).

[2] O. Savadogo and F. J. R. Varela, *J. New Mater. Electrochem. Syst.*, **4**, 93 (2001).

[3] K. Taneda and Y. Yamazaki, *J. Power Sources*, **157**, 177 (2006).

[4] A. S. Arico, P. Creti, P. L. Antonucci, and V. Antonucci, *Electrochem. Solid-State Lett.*, **9**, 66 (1998).

[5] Y. Zhu, Z. Khan, and R. I. Masel, *J. Power Sources*, **139**, 15 (2005).

[6] C. Lamy, A. Lima, V. LeRhun, F. Delime, C. Coutanceau, and J. M. Leger, *J. Power Sources*, **105**, 283 (2002).

[7] T. A. Semelsberger, R. L. Borup, and H. L. Greene, *J. Power Sources*, **156**, 497 (2006).

[8] Y. Liu, S. Mitsushima, K. Ota, and N. Kamiya, *Electrochim. Acta.*, **51***,* 6503 (2006).

[9] G. Kerangueven, C. Coutanceau, E. Sibert, J. -M. Leger, and C. Lamy, *J. Power Sources*, **157**, 318 (2006).

[10] J. T. Muller, P. M. Urban, W. F. Holderich, K. M. Colbow, J. Zhang, and D. P. Wilkinson, *J. Electrochem. Soc.*, **147**, 4058 (2000).

[11] I. Mizutani, Y. Liu, S. Mitsushima, K. Ota, and N. Kamiya, *J. Power Sources*, **156**, 183 (2006).

[12] J. H. Yoo, H. G. Choi, C. H. Chung, and S. M. Cho, *J. Power Sources*, **163**, 103 (2006).

[13] W. S. Li, D. S. Lu, J. L. Luo, and K. T. Chuang, *J. Power Sources*, **145**, 376 (2005).

[14] M. Nagao, A. Takeuchi, P. Heo, T. Hibino, M. Sano, and A. Tomita, *Electrochem. Solid-State Lett.*, **9**, A105 (2006).

[15] M. Nagao, T. Kamiya, P. Heo, A. Tomita, T. Hibino, and M. Sano, *J. Electrochem. Soc.*, **153**, A1604 (2006).

[16] P. Heo, H. Shibata, M. Nagao, T. Hibino, and M. Sano, *J. Electrochem. Soc.,* **153**, A897 (2006).

[17] P. Heo, M. Nagao, M. Sano, T. Hibino, *J. Electrochem. Soc.*, **154**, B53 (2007).

[18] T. A. Semelsberger and R. L. Borup, *J. Power Sources*, **155**, 340 (2006).

[19] S. Hashimoto, K. Kammer, P. H. Karsen, F. W. Poulsen, and M. Mogensen, S*olid State Ionics*, **176**, 1013 (2005).

[20] T. Horita, K. Yamaji, N. Sakai, H. Yokokawa, A. Weber, and E. I. Tiffee, *Electrochim. Acta.*, **46**, 1837 (2001).

[21] W. T. Grubb and C. J. Michalske, *J. Electrochem. Soc.*, **111**, 1015 (1964).

6 $Sn_{0.9}In_{0.1}P_2O_7$-Based Organic/Inorganic Composite membranes

6.1 Introduction

Considerable efforts are being currently expended toward the development of anhydrous proton conductors capable of operating under dry conditions and at intermediate temperatures above 100ºC [1-6], because the fuel cells using such anhydrous proton conductors as an electrolyte membrane have various advantages over the current proton exchange membrane fuel cells (PEMFCs) [7].

Recently, it has been found that an anhydrous proton conductor, 10 mol% In^{3+}-doped SnP_2O_7 ($Sn_{0.9}In_{0.1}P_2O_7$), shows high proton conductivities above 10^{-1} S cm^{-1} between 100 and 300ºC under water-free conditions (see chapter 2). This material was also explored for use as an electrolyte in some electrochemical devices. A fuel cell using the 0.35-mm thick $Sn_{0.9}In_{0.1}P_2O_7$ electrolyte membrane yielded a power density of 264 mW cm^{-2} under unhumidified H_2/air conditions (see chapter 3). This material was also used as an electrolyte membrane in a deNOx reactor [8] and a NOx gas sensor [9]. However, the electrolyte membranes used in these previous studies were merely prepared by pressing $Sn_{0.9}In_{0.1}P_2O_7$ powders into pellets, due to the difficulty in preparing sintered compacts of this material. The synthesis of a dense, flexible, and heat-resistant electrolyte membrane is a crucial requirement for practical applications of this material.

Forming hybrids of organic and inorganic materials is one of the promising methods that meet the above requirements, since they offer the possibility of improving mechanical and thermal properties of various difficult-to-consolidate inorganic materials [10]. Indeed, several inorganic proton conductors have been investigated using composite materials prepared by

blending them with organic polymers [11-17]. This approach also has an additional advantage of combining the positive features of each component via interactions at the molecular level. High proton transfer between clusters of the proton conductor in the matrix is expected if a material having acidic functions as proton sites is added as the third component.

In this study, I investigated the proton-conducting properties of organic/inorganic hybrid composite materials based on $Sn_{0.9}In_{0.1}P_2O_7$ in anhydrous environments. The starting materials chosen as the second and third components were 1,8-bis(triethoxysilyl)octane (TES-Oct) and 3-(trihydroxysilyl)-1-propanesulfonic acid ((THS)Pro-SO_3H), respectively, which have previously been demonstrated to be excellent hybrid components [18,19]. I also evaluated the performance of a fuel cell using the optimized composite material as an electrolyte membrane, wherein my interest is centered on fuel cell performance between 100 and 200ºC under unhumidified conditions.

6.2 Experimental

6.2.1 Materials preparation

Synthesis of $Sn_{0.9}In_{0.1}P_2O_7$ - $Sn_{0.9}In_{0.1}P_2O_7$ was prepared as follows. SnO_2 and In_2O_3 powders were mixed with 85% H_3PO_4 and ion-exchanged water and held with stirring at 300ºC until the mixture formed a high viscosity paste. In this case, the H_3PO_4/MO_x (M=Sn and In) molar ratio was controlled to be 2.8, since a fraction of H_3PO_4 was lost by the subsequent heating treatment. The pastes were calcined in an alumina pot at 650ºC for 2.5 hours and then ground with a mortar and pestle. The final P/(Sn+In) molar ratio of the compounds was confirmed to be 2.0 (±0.02) from X-ray fluorescence (XRF) measurements. For comparison with the composite membranes, the compound powders were pressed into pellets under a pressure of 2×10^3 kg cm^{-2}, as shown in Fig. 6-1 (b).

Synthesis of hybrid composite membranes - TES-Oct (Gelest. Inc., 0.14 g) was mixed

with an equimolar amount of (THS)Pro-SO_3H (Gelest. Inc.) in 2-propanol according to procedures described in literature [19]. $Sn_{0.9}In_{0.1}P_2O_7$ (1.15-2.19 g) and PTFE (0.06 g) was added to the solution and then kneaded in a mortar and pestle for further hydrolysis and condensation. The solution was cast onto a Teflon sheet and then cold-rolled to different thicknesses from 60 to 200 μm using a laboratory rolling mill. After peeling off the membrane, samples were cut with scissors with a size of 2 cm x 2 cm, as shown in Fig. 6-1 (a). A reference composite membrane free of (THS)Pro-SO_3H was also prepared using the same procedure as above.

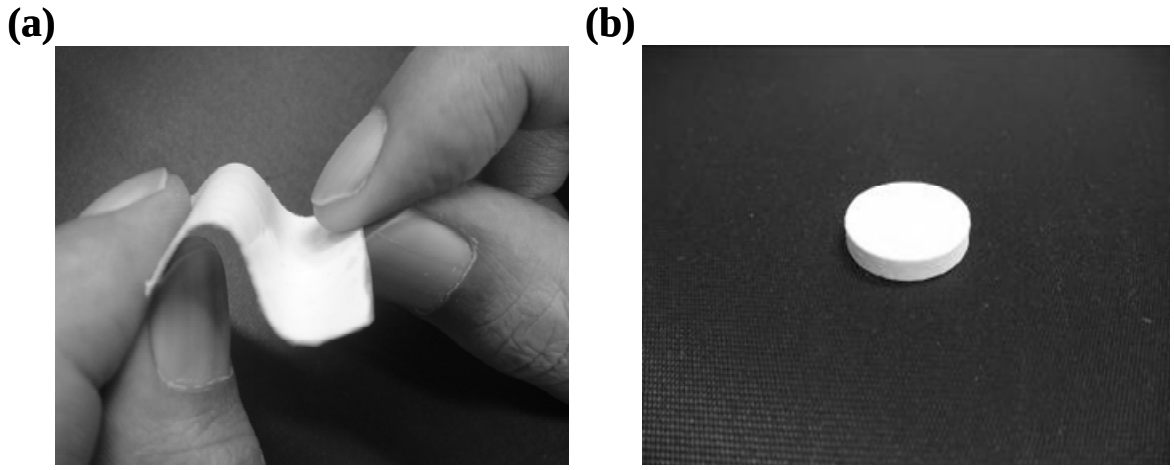

Figure 6-1. Photographs of (a) composite membrane ($Sn_{0.9}In_{0.1}P_2O_7$ content = 90 wt.%) and (b) pellet samples.

6.2.2 Measurements

The surface morphology of the membranes was determined using scanning electron microscopy (SEM) at a magnification of 10,000x. The crystalline structure of the membranes was confirmed by X-ray diffraction (XRD). Impedance spectra measurements were carried out by the standard four probe method. The frequency range was 0.1 - 10^6 Hz, and the AC amplitude was 10 mV. Two types of galvanic cells, a H_2 concentration cell and a H_2/air fuel cell, were fabricated using composite membranes with different thicknesses. Both the anode and cathode (area: 0.5 cm^2) consisted of a catalyst (10 wt.% Pt/C, E-TEK) and carbon paper

(Toray TGPH-090), wherein the Pt loading was 0.6 mg cm^{-2}. The electromotive forces (EMFs) of the H_2 concentration cell were monitored as a function of temperature. The current-voltage curves of the fuel cell were measured by supplying unhumidified H_2 and air to the anode and cathode, respectively, at a flow rate of 30 mL min^{-1}. The Ohmic and polarization resistances were separated using a current interruption method. In this case, a Pt reference electrode was attached to one side of the electrolyte membrane and exposed to open air atmosphere, as illustrated in Fig. 6-2.

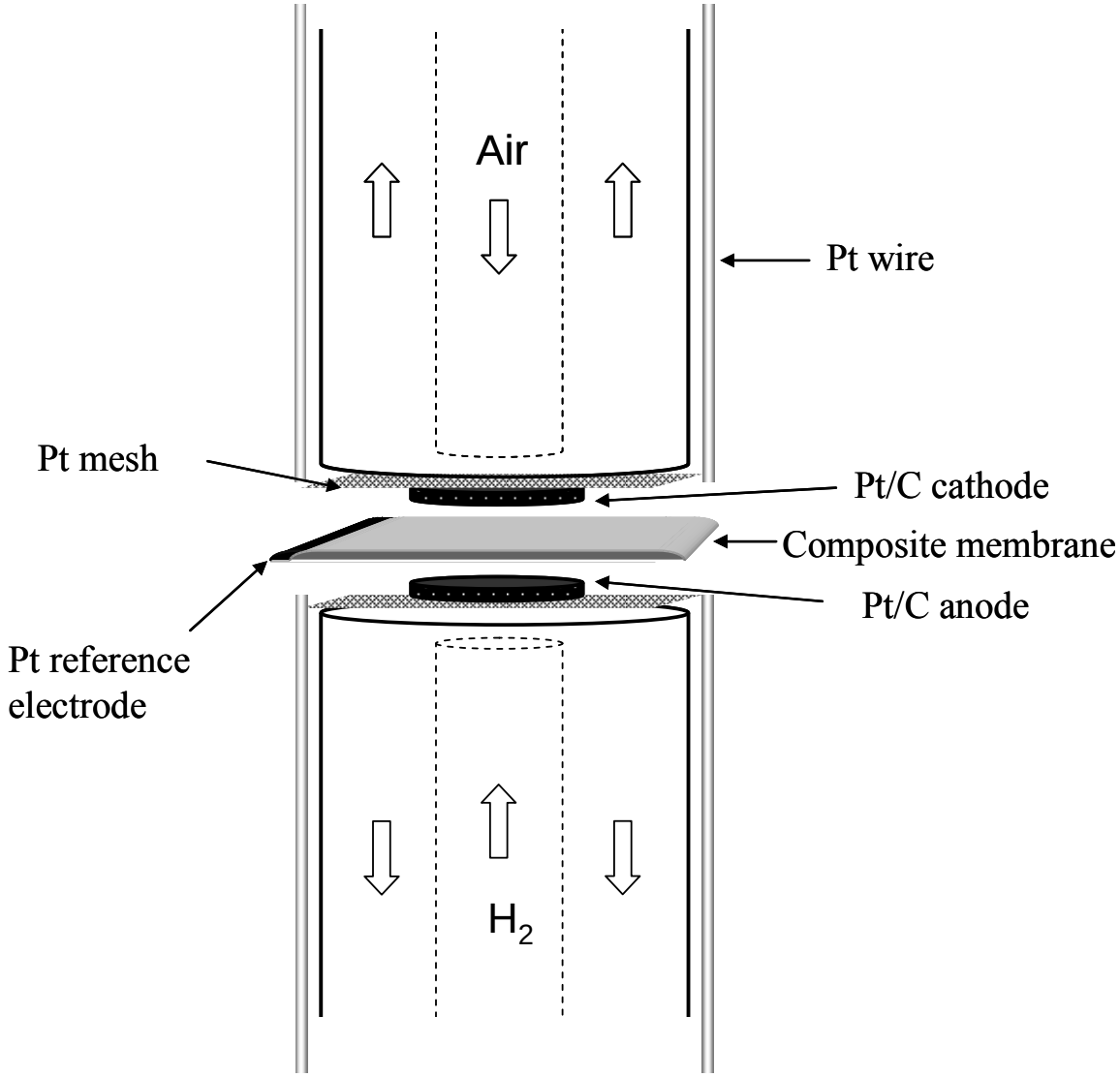

Figure 6-2. Schematic of the fuel cell testing assembly.

6.3 Results and Discussion

6.3.1 Conductivity of the composite membrane

Figure 6-3 shows the Arrhenius plots of the conductivity of the composite membrane samples with various $Sn_{0.9}In_{0.1}P_2O_7$ contents in unhumidified air (P_{H2O}=~0.0075 atm), including the data for a $Sn_{0.9}In_{0.1}P_2O_7$ pellet sample prepared by pressing the powders. All the composite membrane samples showed complex temperature dependence on conductivity. While the data were reproducible over temperature cycles between 100 and 200ºC, hysteresis behavior of the conductivity was observed upon heating and cooling between 200 and 250ºC. I reasoned that the complex temperature dependences of the conductivity are likely due to the reversible dehydration of the membrane below 200ºC and due to thermal decomposition of components such as PTFE above 200ºC, suggesting that the operating temperature of the composite membrane samples is limited to less than 200ºC. On the other hand, the conductivity of the $Sn_{0.9}In_{0.1}P_2O_7$-free composite membrane sample was approximately 2 x 10^{-4} S cm^{-1} at all the tested temperatures, which is about two orders of magnitude lower than the values reported by Nishikawa et al. at the same temperatures [19]. This can be explained by the differences in experimental conditions; Nishikawa et al. conducted their conductivity measurements at 100% relative humidity. The doping of $Sn_{0.9}In_{0.1}P_2O_7$ into the composite membrane significantly enhanced the conductivity, indicating that the doped $Sn_{0.9}In_{0.1}P_2O_7$ showed proton conduction in the whole matrix. As a result, conductivities as high as 0.06 and 0.04 S cm^{-1} were obtained for $Sn_{0.9}In_{0.1}P_2O_7$ contents of 95 and 90 wt.%, respectively, between 150 and 200ºC. However, the flexibility of the composite membrane samples became low when the $Sn_{0.9}In_{0.1}P_2O_7$ content was 95 wt.%. This may be indicative that the organic polymer was no longer interconnected between the $Sn_{0.9}In_{0.1}P_2O_7$ clusters or particles, so that the hybrid effect appeared to disappear. In order to maintain both the conductivity and flexibility as high as possible, the optimum content of $Sn_{0.9}In_{0.1}P_2O_7$ was determined to be 90

wt.% and this content was used in subsequent experiments. Another significant result is that the composite membrane sample with 90 wt.% $Sn_{0.9}In_{0.1}P_2O_7$ showed a lower conductivity of 0.02 S cm^{-1} in the absence of the (THS)Pro-SO_3H component, compared to a conductivity of 0.04 S cm^{-1} in the presence of the component. Given the structural similarity of the two composite membranes, the observed difference can be ascribed to the $–SO_3H$ groups available for proton transfer. The $–SO_3H$ group likely formed a proton-conducting pathway from one $Sn_{0.9}In_{0.1}P_2O_7$ cluster to another.

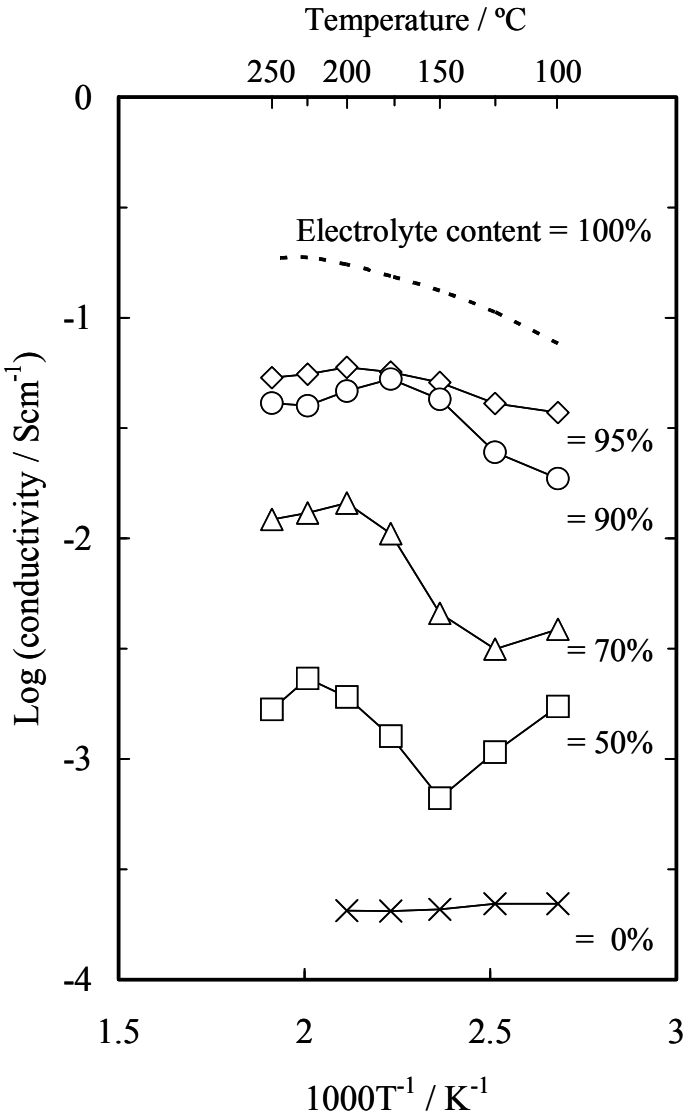

Figure 6-3. Arrhenius plots for conductivities of composite membrane samples having different $Sn_{0.9}In_{0.1}P_2O_7$ contents and the pellet sample. The samples were measured in unhumidified air.

6.3.2 Material characteristics

Figure 3 also showed that the composite membrane samples, especially with $Sn_{0.9}In_{0.1}P_2O_7$ contents of 50 and 70 wt.%, revealed complex temperature dependence on the conductivity between 100 and 200ºC, which was reproducible over temperature cycles. Moreover, the conductivities of all the composite membrane samples decreased with increasing temperature from 200 to 250ºC, which was irreversible upon heating and cooling. I reasoned that while the former behavior is due to the dehydration of the membrane below 200ºC, the later behavior is due to the thermal decomposition of components such as PTFE above 200ºC. Evidence for this reasoning is provided by the thermogravimetry (TG) analysis of the composite membrane and pellet samples. As can be seen from Fig. 6-4, the composite membrane sample with 50 wt.% $Sn_{0.9}In_{0.1}P_2O_7$ showed a large decrease in the weight fraction below 100ºC resulting from the desorption of water. In addition, the weight fractions of both the composite membrane samples were slightly more decreased above 250ºC than that of the pellet sample, indicating the weight loss of components except for $Sn_{0.9}In_{0.1}P_2O_7$. From the above results, the composite membrane sample with 90 wt.% $Sn_{0.9}In_{0.1}P_2O_7$ was used below 200ºC in subsequent experiments.

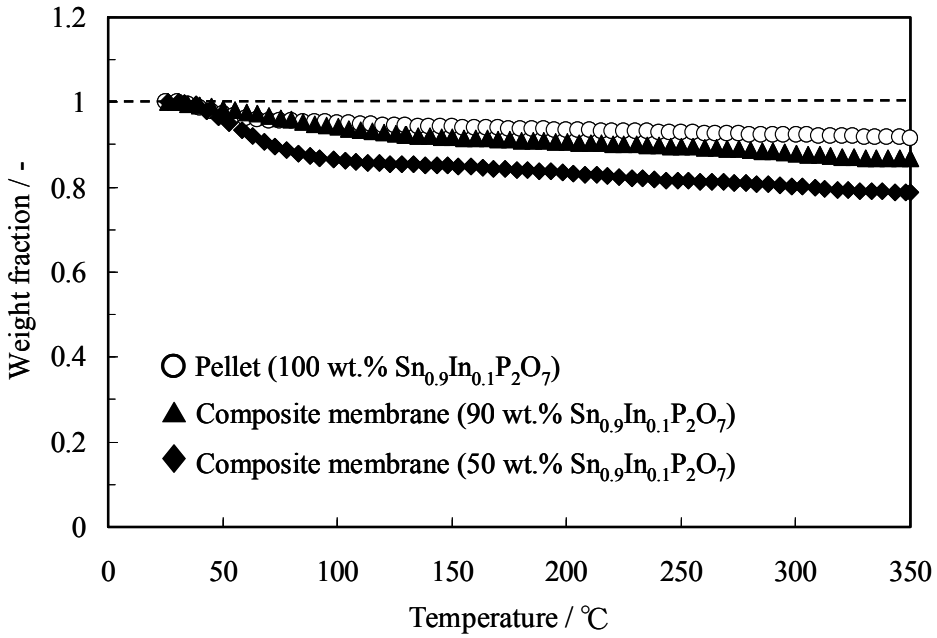

Figure 6-4. TG curves of $Sn_{0.9}In_{0.1}P_2O_7$ composite membrane and pellet samples.

Structural and morphological characterization of the $Sn_{0.9}In_{0.1}P_2O_7$ composite membrane and pellet samples was carried out using XRD and SEM, respectively. Figure 6-5 (a) and (b) show XRD profiles of the composite membrane and pellet samples, respectively. The pellet sample showed the same patterns as those for SnP_2O_7 reported in the literature [20]. Also, a slight shift toward lower angles was observed in the peaks for my sample with respect to SnP_2O_7, indicating an increasing lattice constant due to the doping of In^{3+} in place of Sn^{4+}. On the other hand, the peaks observed for the composite membrane sample were almost identical to those of the pellet sample. This suggests that the polymer components exist as an amorphous phase in the matrix. Figures 6-6 (a) and (b) show SEM micrographs of the composite membrane and pellet sample, respectively. As can be seen, the surface of the pellet sample was highly porous, which corresponds to the relative density value of 79.3% determined by dividing the bulk density of the sample by the theoretical density. However, the composite membrane was rather compact, as observed in Fig. 6-6(a), suggesting that the

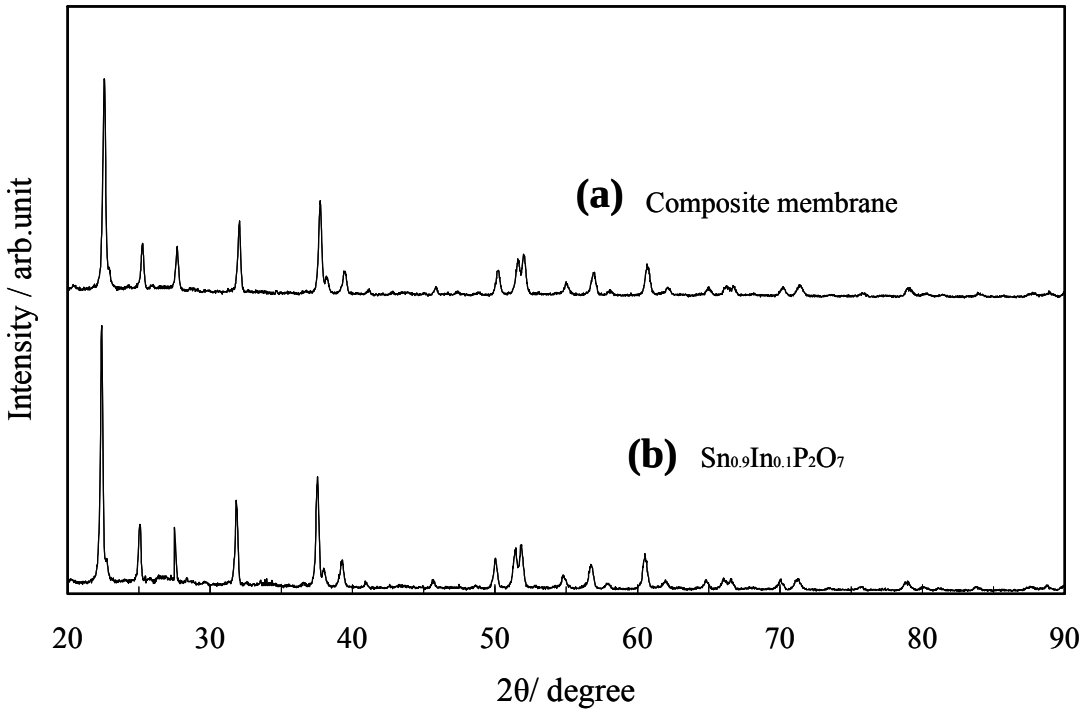

Figure 6-5. XRD patterns of (a) $Sn_{0.9}In_{0.1}P_2O_7$ composite membrane and (b) pellet samples.

polymer functioned as a binder at the interface. Although the distribution of $Sn_{0.9}In_{0.1}P_2O_7$ in the matrix is difficult to visualize by surface SEM, homogeneity ranging from several micrometers to several decades of micrometers was likely established, as will be described later.

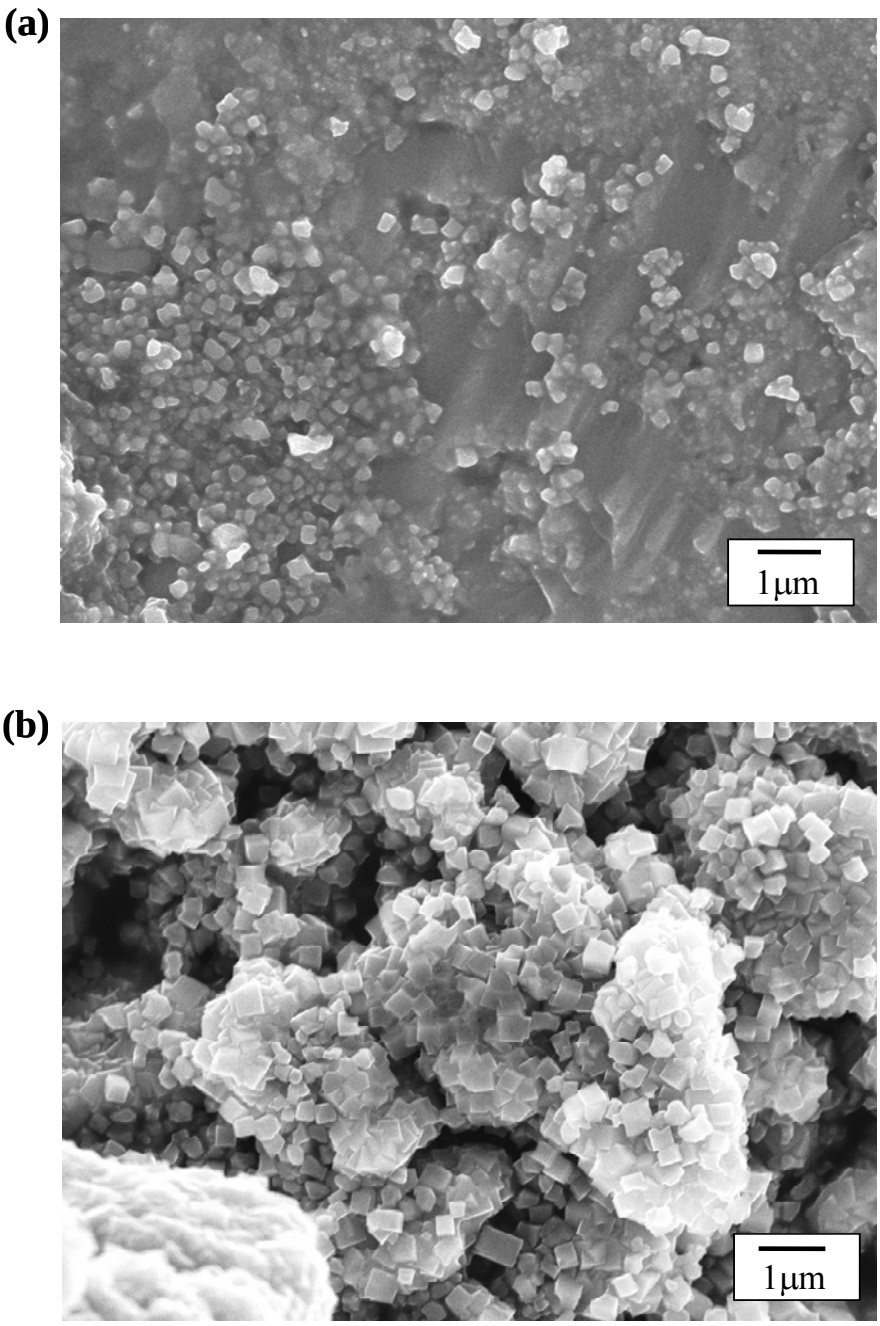

Figure 6-6. XRD patterns of (a) $Sn_{0.9}In_{0.1}P_2O_7$ composite membrane and (b) pellet samples.

6.3.3 Electrochemical characterization

The galvanic cell method was used for the electrochemical characterization of the $Sn_{0.9}In_{0.1}P_2O_7$ composite membrane and pellet samples. The following galvanic cell was fabricated using each sample as an electrolyte:

$$H_2 \text{ (1 atm), Pt/C} \mid \text{electrolyte} \mid \text{Pt/C, } H_2\text{+Ar (0.1 atm)} \quad (6\text{-}1)$$

Here, I used relatively thick electrolyte samples in order to reduce the influence of gas leakage through the electrolyte; 200 μm for the composite membrane and 2.1 mm for the pellet. A comparison of the measured EMF values with the theoretical values calculated from Nernst's equation between 100 and 200ºC is shown in Fig. 6-7. It was found that all the EMF values obtained for both samples were very close to the corresponding theoretical values. I estimated the proton transport number from the ratio of the EMF value to the theoretical value as below;

$$T_{H^+} = EMF_{observed}/EMF_{theoretical} \quad (6\text{-}2)$$

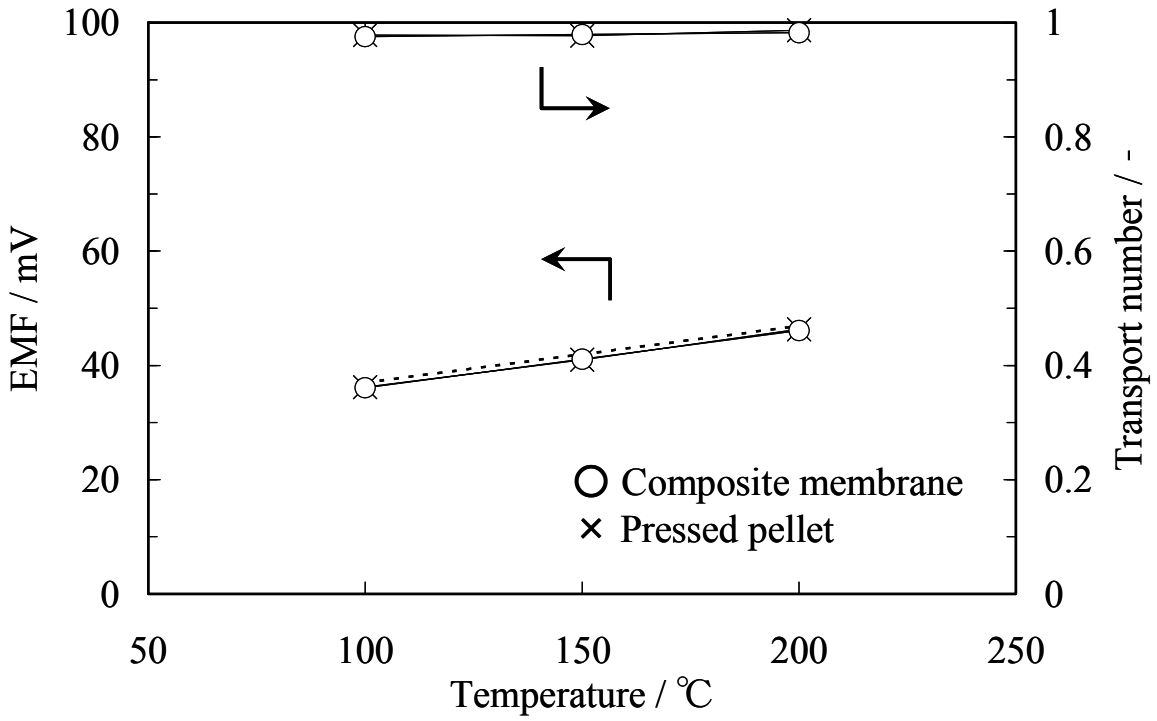

Figure 6-7. EMFs of H_2 concentration cells with $Sn_{0.9}In_{0.1}P_2O_7$ composite membrane and pellet samples, and their proton transport number as a function of temperature. Both the H_2 and H_2-Ar mixture used were unhumidified.

This method is valid, especially when the ion transport number is high because the observed EMF value is determined mainly by the Ohmic resistance of the charge carrier. The estimated proton transport numbers of the two samples were in the range of 0.96-0.98 for both the samples, indicating that the composite membrane as well as pellet are substantially pure proton conductors in H_2 atmospheres In other words, the polymer does not retard the proton transport number of $Sn_{0.9}In_{0.1}P_2O_7$ at all.

Another galvanic cell was fabricated using the $Sn_{0.9}In_{0.1}P_2O_7$ composite membrane and pellet samples with varying thickness values:

$$H_2,\ Pt/C \mid \text{electrolyte} \mid Pt/C,\ air \qquad (6\text{-}3)$$

Figure 6-8 (a) shows the influence of the electrolyte thickness on the open-circuit voltage (OCV) obtained for the two fuel cells at 200ºC. A decrease in the OCV with decreasing electrolyte thickness was observed for the pellet sample, implying that H_2 or O_2 crossover through the electrolyte increases with decreasing electrolyte thickness. In contrast, the OCVs for the composite membrane were almost independent of the electrolyte thickness. This result indicates that both H_2 and O_2 crossovers through the electrolyte are negligible, which is consistent with the SEM image shown in Fig. 6-6. However, the OCVs for the composite membranes were approximately 970 mV, which is lower than the theoretical value of 1.1 V. As reported previously in chapter 2, while the conductivity of $Sn_{0.9}In_{0.1}P_2O_7$ was almost independent of P_{O2} from 10^{-22} to 10^{-3} atm, it increased gradually with increasing P_{O2} from 10^{-3} to 1 atm. Consequently, the observed lower OCV values can be considered to be due to partial electron-hole conduction in the electrolyte, causing an internal short circuit of the fuel cell [21].

Figure 6-8 (b) shows the influence of the electrolyte thickness on the Ohmic resistance obtained for the two fuel cells at 200ºC. The Ohmic resistances of the two samples roughly linearly decreased with decreasing electrolyte thickness. In particular, the composite membrane showed linearity over the thickness range from 60 to 150 μm, assuming that the

$Sn_{0.9}In_{0.1}P_2O_7$ powders were homogeneously distributed at ~ μm- ~10 μm level in the matrixes. The Ohmic resistance values of the composite membrane samples were always higher than those of the pellet samples at the same electrolyte thickness, reflecting the difference in the proton conductivity for the two samples. However, I emphasize that the composite membrane sample showed a relatively low resistance of 0.24 Ω cm^2, while maintaining a high OCV of 986 mV, which could not be achieved for the pellet sample.

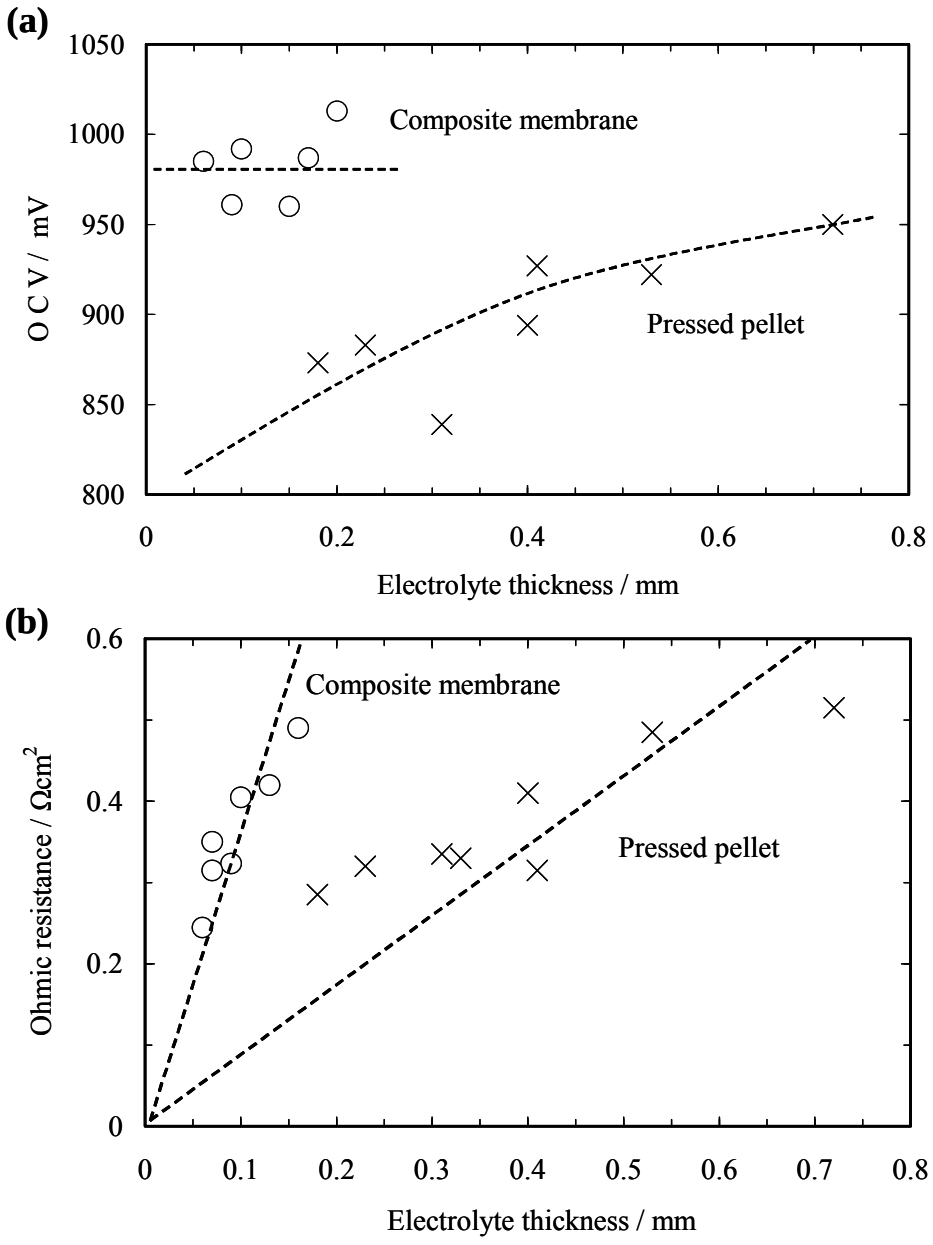

Figure 6-8. (a) OCVs and (b) Ohmic resistance of fuel cells with $Sn_{0.9}In_{0.1}P_2O_7$ composite membrane and pellet samples at 200ºC as a function of electrolyte thickness. Both H_2 and air were unhumidified.

6.3.4 Fuel cell performance

An additional objective of this study was to investigate the fuel cell performance at intermediate temperatures. Fuel cell tests were conducted using the 60 μm-thick $Sn_{0.9}In_{0.1}P_2O_7$ composite membrane as an electrolyte between 100 and 200ºC under unhumidified conditions. The current-voltage curves of the fuel cell are shown in Fig. 6-9. At all the tested temperatures, OCVs above 950 mV were obtained, and no limiting current behavior was observed at high current densities. In addition, the current-voltage slopes became lower as the operating temperature increased. The peak power density thus reached 109 mW cm^{-2} at 100ºC, 149 mW cm^{-2} at 150ºC, and 187 mW cm^{-2} at 200ºC. However, the power densities were much lower compared to those expected from the Ohmic resistances (as an example, 0.24 Ω cm^2 at 200ºC) of the electrolyte, which may be ascribed to the large polarization resistance of the fuel cell.

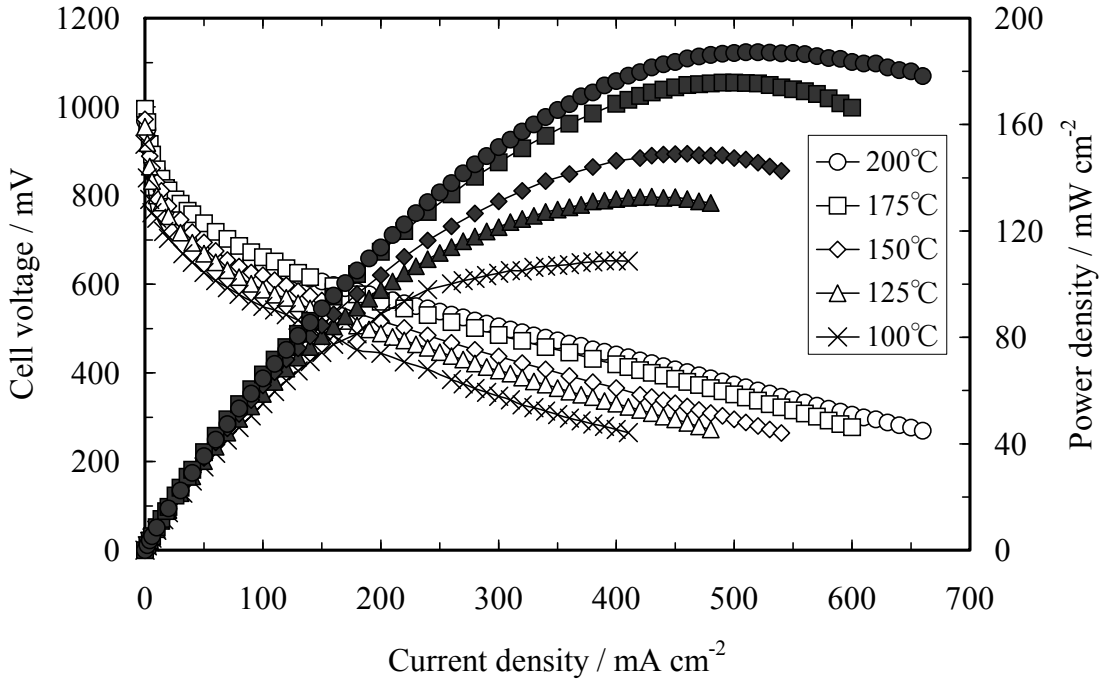

Figure 6-9. Cell voltage and power density vs. current density of fuel cells with the composite membrane between 100 and 200ºC. Unhumidified H_2 and air were supplied to the anode and cathode, respectively, at a flow rate of 30 ml min^{-1}. The electrolyte thickness was 60 μm.

In order to understand the above results, I measured the anodic and cathodic overpotentials by the current interruption method. It can be seen from Fig. 6-10 that the overpotentials were always dominated by the cathode in the temperature range of 100-200ºC; the cathodic overpotentials were estimated to account for 83-85% of the overall voltage drops during the cell discharge. On the other hand, the anodic overpotentials (as well as the IR drops, although the data is not shown in Fig. 6-10) negligibly affected the voltage drops especially at higher temperatures. Clearly, the development of a more active cathode is required to improve the fuel cell performance. Note that water formed electrochemically did not affect the subsequent cathode reaction because the discharge at high current densities gave rise to no limiting currents. It is likely that the charge-transfer reaction of oxygen reduction at the electrolyte/electrode interface proceeded at a very slow rate. Also, note that only the cathode was in physical contact with the electrolyte, probably resulting in low-density three phase boundaries (TPBs). Thus, it is necessary to optimize the electrolyte/electrode interface.

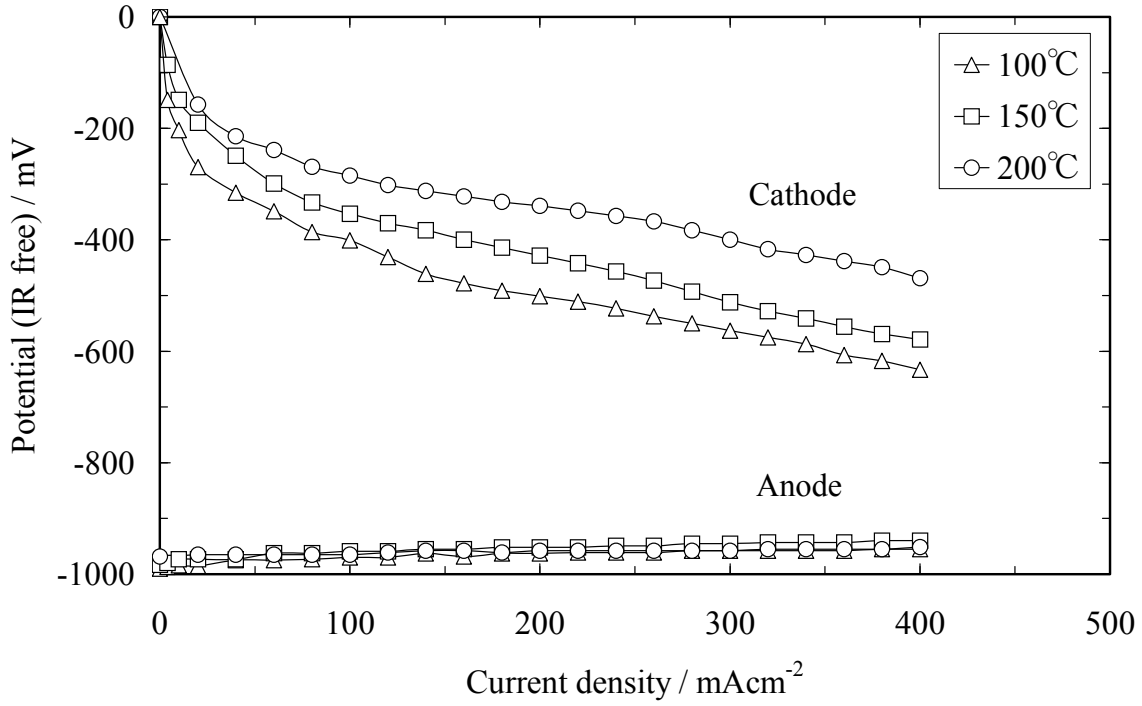

Figure 6-10. Anodic and cathodic overpotentials vs. current density of fuel cells with the composite membrane between 100 and 200ºC. The experimental conditions are the same as in Fig. 6-9.

I have previously reported that the cathodic overpotential could be reduced by applying an intermediate layer consisting of $Sn_{0.9}In_{0.1}P_2O_7$ and Pt/C powders at the electrolyte/electrode interface in the $Sn_{0.9}In_{0.1}P_2O_7$ pellet-based fuel cell (see chapter 3). An attempt was made to hot-press the intermediate layers constructed from $Sn_{0.9}In_{0.1}P_2O_7$, Pt/C, TES-Oct, and (THS)Pro-SO_3H between the electrolyte and cathode. As a result of the optimization of the weight ratio of the $Sn_{0.9}In_{0.1}P_2O_7$ electrolyte to the Pt/C catalyst, the cathodic overpotential was shown to be the most improved when $Sn_{0.9}In_{0.1}P_2O_7$: Pt/C = 20 : 1. A comparison of the

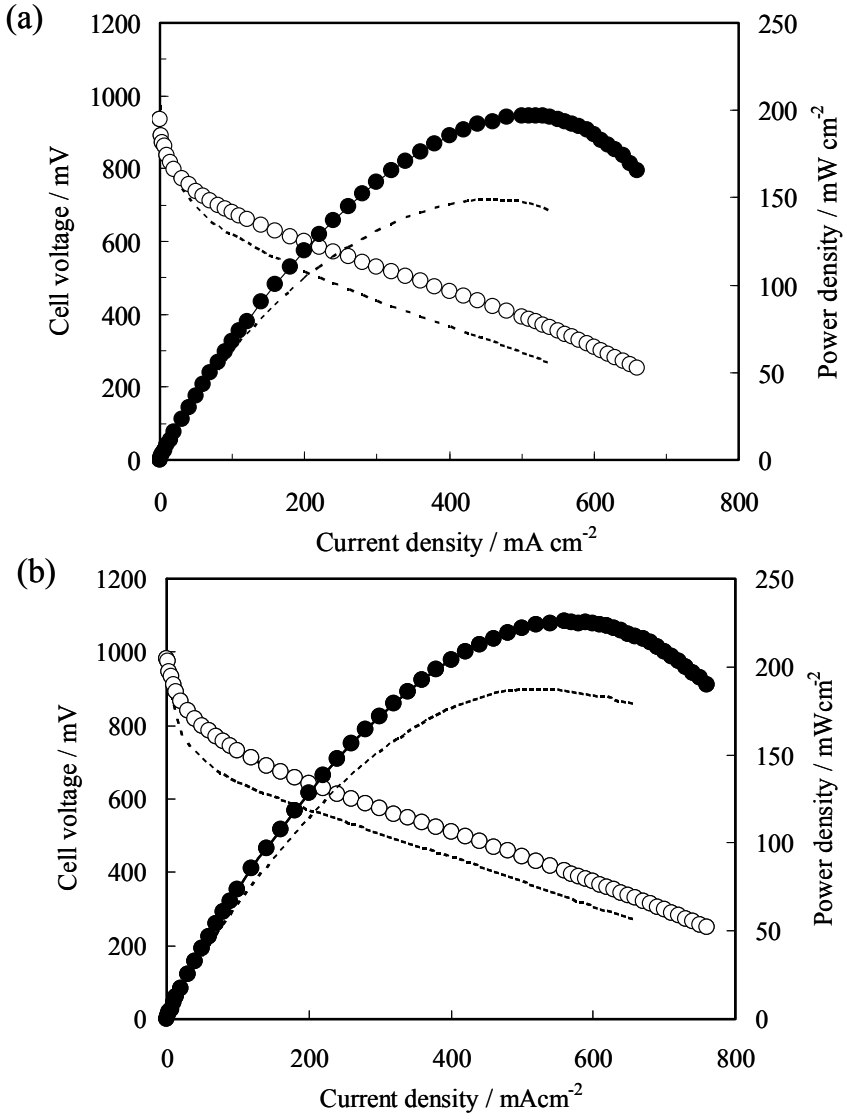

Figure 6-11. Cell voltage and power density vs. current density of improved fuel cells with the composite membrane at (a) 150°C and (b) 200°C, resepectively. The dotted lines show the results for the fuel cell without any intermediate layer. The experimental conditions are the same as in Fig. 6-9.

presence or absence of the intermediate layer at 150ºC and 200ºC is shown in Fig. 6-11, wherein the other experimental conditions were the same as those for the data in Fig. 6-10. The voltage drops were reduced by using the intermediate layer, so that the peak power densities increased from 149 to 197 mW cm^{-2} at 150ºC and from 187 to 226 mW cm^{-2} at 200ºC, respectively. One can consider that such performance gains are due to an increase in the area of the three-phase boundary for the cathode reaction. Indeed, the total polarization resistance decreased by 1.3 Ω cm^2 at 150ºC by applying the intermediate layer. These results suggest that the fuel cell performance can be further enhanced by improving the microstructure, catalytic activity, and proton conductivity of the intermediate layer. Furthermore, a membrane electrode assembly (MEA) fabrication technique offered the potential for enhancing the fuel cell performance.

6.4 Summary

Organic/inorganic hybrid composite membranes based on $Sn_{0.9}In_{0.1}P_2O_7$ were investigated for intermediate-temperature fuel cells. 1,8-bis(triethoxysilyl)octane and 3-(trihydroxysilyl)-1-propane- sulfonic acid were chosen as polymer precursors. The composite membrane prepared at a $Sn_{0.9}In_{0.1}P_2O_7$ content of 90 wt.% showed a proton conductivity of 0.04 S cm^{-1} at 175ºC in an unhumidified atmosphere. The membrane was also found to be flexible. $Sn_{0.9}In_{0.1}P_2O_7$ powders were relatively homogeneously packed in the matrix, with no pores were visible. The proton transport numbers of the composite membrane estimated by the EMF technique were 0.96-0.98 between 100 and 200ºC. A fuel cell with the composite membrane maintained the OCV at an almost constant value of 970 mV regardless of the electrolyte thickness and also showed a decreasing Ohmic resistance with decreasing electrolyte thickness. The resulting peak power density reached 109 mW cm^{-2} at 100ºC, 149 mW cm^{-2} at 150ºC, and 187 mW cm^{-2} at 200ºC. These cell performance were also improved by applying

the intermediate layers constructed from $Sn_{0.9}In_{0.1}P_2O_7$, Pt/C, TES-Oct, and (THS)Pro-SO_3H between the electrolyte and cathode; the peak power density increased to 197 mW cm^{-2} at 150ºC and to 226 mW cm^{-2} at 200ºC.

6.5 References

[1] T. Kenjo, Y. Ogawa, *Solid State Ionics*, **76**, 29 (1995).

[2] S. M. Haile, D. A. Boysen, C. R. I. Chisholm, R. B. Merle, *Nature*, **410**, 910 (2001).

[3] T. Matsui, S. Takeshita, Y. Iriyama, T. Abe, M. Inaba, Z. Ogumi, *Electrochem Commun.*, **6**, 180 (2004).

[4] D. A. Boysen, T. Uda, C. R. I. Chisholm, S. M. Haile, *Science*, **303**, 68 (2004).

[5] W. Wieczorek, G. Zukowska, R. Borkowska, S. H. Chung, S. Greenbaum, *Electrochim. Acta*, **46**, 1427 (2001).

[6] A. Matsuda, T. Kanzaki, K. Tadanaga, M. Tatsumisago, T. Minami, *Solid State Ionics*, **154-155**, 687 (2002).

[7] J. S. Wainright, M. H. Litt, and R. F. Savinell, High-temperature membranes, in W. Vielstich, A. Lamm and H. Gasteiger, Editors, *Handbook of Fuel Cells—Fundamentals, Technology, Applications*, Wiley (2003).

[8] M. Nagao, T. Yoshii, T. Hibino, M. Sano, and A. Tomita, *Electrochem. Solid-State Lett.*, **9**, J1 (2006).

[9] M. Nagao, Y. Namekata, T. Hibino, M. Sano, and A. Tomita, *Electrochem. Solid-State Lett.*, **9**, H48 (2006).

[10] A. Okada and A. Usuki, *Mater. Sci. Eng. C*, **3**, 109 (1995).

[11] P. Staiti, M. Minutoli, and S. Hocevar, *J. Power Sources*, **90**, 231 (2000)

[12] G. Alberti, M. Casciola, and R. Palombari, *J. Membr. Sci.*, **172**, 233 (2000).

[13] B. Bonnet, D.J. Jones, J. Rozière, L. Tchicaya, G. Alberti, M. Casciola, L. Massinelli, B. Bauer, A. Ieraio, and E. Ramunni, *J. New Mater. Electrochem. Syst.*, **3**, 87 (2000).

[14] J. D. Kim and I. Honma, *Electrochim. Acta.*, **48**, 3633 (2003).

[15] D. R. Vernon, F. Meng, S. F. Dec, D.L. Williamson, J. A. Turner, and A. M. Herring, *J. Power Sources*, **139**, 141 (2005).

[16] M. Nagai and Y. Chiba, *Solid State Ionics,* **76**, 2991 (2005).

[17] J. D. Kim, T. Mori, and I. Honma, *J. Electrochem. Soc.*, **153**, A508 (2006).

[18] H. Nakajima, S. Nomura, T. Sugimoto, S. Nishikawa, and I. Honma, *J. Electrochem. Soc.*, **149**, A953 (2002).

[19] O. Nishikawa, T. Sugimoto, S. Nomura, K. Doyama, K. Miyatake, H. Uchida, and M. Watanabe, *Electrochim. Acta*, **50**, 667 (2004).

[20] P. K. Gover, N. D. Withers, S. Allen, R. L. Withers, S. O. Evans, *J. Solid State Chem.*,

166, 42 (2002).
[21] S. Hamakawa, T. Hibino, and H. Iwahara, *J. Electrochem. Soc.*, **141**, 1720 (1994).

7 Conclusions and Outlook

7.1 Conclusions

The aim of this study was to demonstrate the feasibility of intermediate-temperature fuel cells using $Sn_{0.9}In_{0.1}P_2O_7$ as an electrolyte and to prove desirable attributes in the intermediate-temperature fuel cells over present PEMFCs.

$Sn_{0.9}In_{0.1}P_2O_7$, which is an anhydrous proton conductor, showed high proton conductivities above 10^{-1} S cm^{-1} at intermediate temperatures between 125 and 300ºC under unhumidified conditions, where a conductivity value of 1.95 x 10^{-1} S cm^{-1} was achieved at 250ºC (Chapter 2). This material had proton transport numbers of ~ 1 and exhibited a large H/D isotope effect on conductivity, indicating that the charge carriers of $Sn_{0.9}In_{0.1}P_2O_7$ were not H_3O^+ ions, but protons which migrated between the lattice oxide ions according to a hopping mechanism.

Performance of a H_2/air fuel cell using $Sn_{0.9}In_{0.1}P_2O_7$ and Pt/C as electrolyte and electrodes, respectively, was evaluated in the temperature range of 150-300ºC under unhumidified conditions (Chapter 3). The cathodic overpotentials were much larger than the anodic overpotentials over the whole temperature range. The intermediate layer consisting of $Sn_{0.9}In_{0.1}P_2O_7$ and Pt/C catalysts was applied to the interface between the electrolyte and electrode, which significantly reduced the cathode polarization. As a result, the fuel cell yielded the peak power densities of 152 mW cm^{-2} and 264 mW cm^{-2} at 250ºC using the electrolytes of 1.00 and 0.35 mm thickness, respectively. More importantly, the fuel cells showed excellent CO tolerance and good thermal stability under unhumidified conditions. The cell performance and polarization resistances were clearly not influenced by the presence of 10% CO at 250ºC. In the stability test, the cell voltage (700 mV) with a constant current density, maintained at a constant value for 60 h in the presence of 10% CO at 250ºC.

The Pt-free catalysts were investigated at intermediate temperatures between 150 and 300ºC (Chapter 4). As the Pt-free catalysts, the Mo_2C-ZrO_2/C showed high anode performance toward the hydrogen oxidation and the ZrO_2/C showed high cathode performance for the ORR, respectively. The addition of ZrO_2 to the catalyst allowed the Mo_2C to become highly dispersed on the carbon support, so that the catalytic activity could be improved to the level of the Pt catalyst. A fuel cell using the Mo_2C-ZrO_2/C as an anode, yielded a peak power density of 67 mW cm^{-2} at 250ºC, which was close to the peak power density of 84 mW cm^{-2} obtained using a fuel cell with the Pt/C anode (electrolyte thickness: 1.0 mm). The catalytic activity of ZrO_2 for the ORR was considerably influenced by the ZrO_2 content on a carbon support and the heat-treatment for the ZrO_2/C, wherein the 20 wt.% ZrO_2/C that was heat-treated at 650ºC exhibited the best performance. Performance of a Pt-free fuel cell using the Mo_2C-ZrO_2/C and ZrO_2/C as the anode and cathodes, respectively, was strongly dependent on the operating temperature. The peak power density reached 29 mW cm^{-2} at 300ºC, but was significantly decreased to 6 mW cm^{-2} at 150ºC. Its relatively high performance was achieved by operating the Pt-free fuel cell at intermediate temperatures above 200ºC.

Direct DME fuel cells (DDMEFCs) and direct hydrocarbon fuel cells were investigated using $Sn_{0.9}In_{0.1}P_2O_7$ as electrolyte at intermediate temperatures between 150 and 300ºC (Chapter 5). It was found in these fuel cells that DME and hydrocarbons were electrochemically converted into CO_2 along with their direct oxidation. The anodic overpotentials of the Pt/C anode for the anode reaction of DME could be improved by the addition of Ru to Pt, wherein the added Ru played a role in activating the reforming reaction of DME. In DDMEFCs with the PtRu/C anode (electrolyte thickness: 1.0 mm), the peak power density ranged from 31 mW cm^{-2} at 200ºC to 78 mW cm^{-2} at 300ºC, which are about twice those obtained with the Pt/C anode. Direct hydrocarbon fuel cells with the Pt/C anode achieved higher cell performances with higher hydrocarbons, while the fuel cells with butane,

propane, and ethane exhibited comparable performances. The peak power densities were 23 mW cm^{-2} for methane, 35 mW cm^{-2} for ethane, 36 mW cm^{-2} for propane, and 38 mW cm^{-2} for butane at 300ºC, while these performances were enhanced with increasing Pt loadings in the Pt/C anodes. On the other hand, a direct propane fuel cell with the Mo_2C-ZrO_2/C anode yielded the peak power density of 37 mW cm^{-2} at 300ºC, which is comparable to that obtained with the Pt/C anode.

Organic/inorganic hybrid composite membranes based on $Sn_{0.9}In_{0.1}P_2O_7$ were investigated for intermediate-temperature fuel cells (Chapter 6). 1,8-bis(triethoxysilyl)octane and 3-(trihydroxysilyl) -1-propane-sulfonic acid were chosen as polymer precursors. The composite membrane prepared at a $Sn_{0.9}In_{0.1}P_2O_7$ content of 90 wt.% showed a proton conductivity of 0.04 S cm^{-1} at 175ºC in an unhumidified atmosphere and was also found to be flexible. $Sn_{0.9}In_{0.1}P_2O_7$ powders were relatively homogeneously packed in the matrix, with no pores were visible. A fuel cell with the composite membrane maintained the OCV at an almost constant value of 970 mV regardless of the electrolyte thickness and also showed a decreasing Ohmic resistance with decreasing electrolyte thickness (from 150 to 60 μm). The resulting peak power density reached 109 mW cm^{-2} at 100ºC, 149 mW cm^{-2} at 150ºC, and 187 mW cm^{-2} at 200ºC. These cell performance were also improved by applying the intermediate layers constructed from $Sn_{0.9}In_{0.1}P_2O_7$, Pt/C, TES-Oct, and (THS)Pro-SO_3H between the electrolyte and cathode; the peak power density increased to 197 mW cm^{-2} at 150ºC and to 226 mW cm^{-2} at 200ºC.

7.2 Outlook

A key to solve crucial problems in the present PEMFCs for its widespread commercialization is high temperature operation of PEMFCs above 100ºC. Therefore, considerable efforts have recently been devoted to the development of PEMFCs that operate

above 100ºC in unhumidified conditions. In this study, I have demonstrated the operation of intermediate-temperature fuel cells using a proton-conducting $Sn_{0.9}In_{0.1}P_2O_7$ electrolyte in unhumidified conditions in the temperature range from 100 to 300ºC. It was found that the intermediate-temperature fuel cells have considerable advantages over the present PEMFCs as follows. The cell operation without any humidification and with high CO tolerance of anode catalysts can eliminate the need for an external humidifier and a CO removal unit (water-gas-shift and CO preferential oxidation reactors), which will provide significant simplicity and low costs for fuel cell systems. Furthermore, the use of Pt free electrodes and direct use of alternative fuels to replace pure hydrogen, and the combination use of them would bring out the reduced materials cost of fuel cells and considerably simpler and more economic fuel cell systems.

Until the introduction of the intermediate-temperature fuel cells into commercialization, there is still much work related to materials and technical developments. In the present development stage, high performance of the fuel cells with cost-effective materials would be achieved by the combination of a Pt based cathode with low Pt loading and a Pt free anode. In this study, the Mo_2C-ZrO_2/C anode yielded high anode performance which was comparable to that obtained with the Pt/C anode. Although ZrO_2/C was applied for the Pt free cathode, its catalytic activity for ORR was still not enough to meet the criteria for an alternative material. Therefore, the cathode design for higher cathode performance with lower Pt loadings is a crucial requirement for the high performance fuel cells with cost-effective materials. It is believed that an incorporation of proton conductors near to Pt catalysts on a carbon support in a cathode is effective for such a cathode design. For example, the metal oxide such as SnO_2 can be impregnated on a carbon support in such a precipitation method as described in chapter 4 and then, through the process of a treatment of H_3PO_4 and a heat-treatment, a carbon supported SnP_2O_7 can be achieved. In this manner, the proton conductor, SnP_2O_7, with its high dispersion and small particle sizes can be located in near neighbor position with respect

to Pt particles, i.e., Pt-SnP_2O_7/C. Such a cathode design would offer the high active cathode via effectively increasing the area of the three-phase boundary (TPB) for promotion of the cathode reaction. On the other hand, in the long run, the stability problem of a carbon support may be considered, especially for a cathode, because the electrode is susceptible to corrosive conditions including low pH on an acid media, high temperature, high cathode potential, and oxidation atmospheres. Because even low rates of carbon corrosion may impact fuel cell performance over the long term, the replacement of a carbon support will be henceforth required. One of the acceptable materials is a silicon carbide (SiC), because it is preferred for corrosion and thermal resistance and electrical conductivity. However, it is important to fabricate SiC particles with a high surface area for its application into the support material

The other important works are an improvement of composite membranes and a membrane electrode assembly (MEA) fabrication, which would further enhance the present fuel cell performance. For practical application of the electrolyte material, the organic/inorganic composite membranes were fabricated. 1,8-bis(triethoxysilyl)octane and 3-(trihydroxysilyl)-1-propane-sulfonic acid were used as an organic binder material in the composite membrane. In order to improve the chemical and thermal stabilities and mechanical properties for the composite membrane, applications of different organic materials into the composite membrane are proposed. In particular, polybenzimidazole (PBI) is expected as such an organic binder due to its good thermal and chemical stabilities. It has also been reported that PBI itself shows a proton conductivity of 2×10^{-4} S cm^{-1} at room temperature. As revealed in this study (chapter 6), the binder was required to simultaneously function as a mediator of proton transfer between the $Sn_{0.9}In_{0.1}P_2O_7$ particles, which suggests that the use of PBI is also effective to maintain the high proton conductivity of the composite membrane. With the composite membrane, furthermore fundamental investigations on the fuel cells related properties affecting their performance and stability would be required. More importantly, a membrane electrode assembly (MEA) adapted into the intermediate-temperature fuel cells

should be explored to enhance their performance. For the MEA, it is focused on the novel ionomer in the electrode and the material compatibility between membrane and electrodes. Furthermore, a fuel cell stack assembly in the intermediate-temperature fuel cells will be made with some modifications of component materials in the intended purpose such as stationary power generations and automobiles.

Acknowledgements

I really thank Prof. Dr. Takashi Hibino (Graduate School of Environmental Studies, Nagoya University) for giving me a great chance to perform the interesting subject and to extend my knowledge in the field of '*Electrochemistry and Fuel cells'* and for supporting his earnest guidance, sincere encouragement and excellent research environments during the doctoral course at Nagoya University. Furthermore, he gave me the opportunity to present my work to an international audience at many conferences.

I would like to thank Prof. Dr. Mitsuru SANO (Graduate School of Environmental Studies, Nagoya University) and Prof. Dr. Masazumi OKIDO (Graduate School of Engineering, Nagoya University) for reviewing this thesis, and his valuable comments. Special thanks to Prof. OKIDO, who was my advisor in master's course, for his sincere encouragement and concerns.

I would deeply like to thank faculties in Dept. of Material Science and Engineering, Korea Maritime University including Prof. Dr. Kyeongman MOON, and Prof. Dr. Myeonghoon LEE (Dept. of Marine System Engineering, Korea Maritime University), who the first introduced me the academic world of '*Materials and Electrochemistry*' and has greatly encouraged me over a long time from the undergraduate to the doctoral course.

I would sincerely like to thank Assistant Prof. Masahiro NAGAO (Graduate School of Environmental Studies, Nagoya University), Atsuko TOMITA (AIST), and Masaya YANO (Toyota Motor) for their kind advices on the study and their collaboration in Hibino Lab. Thanks also to Kazuyo KOBAYASHI (Hibino Lab., Nagoya University) for the help in official works and her many kindnesses in Hibino Lab.

Also, I would like to express my heartfelt appreciation and thanks to graduate students in Hibino Lab. in Nagoya University; Mr. Shinya TERANISHI, Mr. Kohsuke OKAMOTO, Mr.

Junya NAKAJIMA, Mr. Yosuke NAMEKATA, Mr. Norikazu KAJIYAMA, Mr. Akihito TSUGE, Mr. Kenichi ITO, and Mr. Toshihiko HARADA as well as former graduate students; Mr. Hidetaka SHIBATA (Murata Manufacturing), Mr. Toshio KAMIYA (Aishin AW), and Mr. Takeshi YOSHII (Denso). We have spent much time for the studies in Hibino Lab. and helped each other on some matters. Especially, I must thank my co-workers; Mr. SHIBATA, Mr. KAMIYA (Aishin AW), Mr. KAJIYAMA, Mr. ITO, and Mr. HARADA in this thesis.

Special thanks go to Prof. Dr. Tsutomu MIZUNO (Graduate School of Engineering, Nagoya University) for taking care of my study during *Nagoya University Program for Academic Exchange* (NUPACE) for 1 year and his continuous encouragement. Thanks also to DR. Shigeo ARAI (EcoTopia Science Institute, Nagoya University) for the help with TEM measurement for this thesis.

I want to express my thanks to Prof. Dr. Yoichi SAKAI (Dept. of Chemistry, Daido Institute of Technology), who gave me an opportunity to lecture on '*basic chemistry*' at University and continuously encouraged me in the doctoral course. Thanks also to Prof. Dr. Makoto TAKAHASHI (Dept. of Applied Chemistry, Chubu University) and Prof. Dr. Miho HUJITA (Graduate School of Natural Sciences, Nagoya City University) for their sincere advice and concerns.

Special thanks go to Dr. Yongsoo JEONG (KIMS) and Dr. Sungmo MOON (KIMS) for giving me the opportunity to present at KIMS and devoting continuous concern and encouragement on my researches.

I would also like to thank my seniors graduated from Nagoya University; Associate Prof. Dr. Seongjong KIM (Mokpo National Maritime University), Dr. Kyounghwang LEE (RIST), Hyunho MA (Samsung Heavy Industries), Dr. Hanjin RYU (POSCO), and Dr. Woosik LEE (Toyoda Gosei) for their advices on the research as well as the life in Japan. Thanks also to my seniors at Nagoya University as well as Mikuni Nagoya Church; Dr. Hyunchang SHIN, Dr. Youngwoo KIM (EcoTopia Science Institute, Nagoya University) and Dr. Jaesoo LIM

(KIGAM), for their advices and praying for my study and life in Japan. Special thanks also to my senior in the field of '*fuel cells*', Dr. Jedeok KIM (NIMS) for his valuable advices on the study in Japan. Thanks also to my friends, Mr. Junghae CHOI (Graduate School of Environmental Studies, Nagoya University), Mr. Yongsup YUN (Graduate School of Engineering, Nagoya University), and Mr. Sunhyung LEE (Graduate School of Engineering, Nagoya University). We have done great effort to get Ph. D. in Nagoya University with helping and relying on each other.

I want to express my thanks to all members of Mikuni Nagoya Church, especially Pastor Jongha LEE. Special thanks also to Spiritual supporters in Korea, Pastor Deokjung KIM (Juchanyang Church) and Prof. Dr. Inho KIM (Tongmyong University), for their praying and encouragement.

Finally, my heartfelt thanks must go to my wife, Jihye HWANG, for her constant encouragements and supports during last 12 years and also to my two sons, Yegang HEO and Yesung HEO. I give my sincere gratitude to my parents, Muryang HEO and Ilsoon LEE, for supporting me throughout the past years.

Curriculum Vitae

Personal HEO, pilwon

Date and place of birth: January 06th, 1977, in Busan, Korea
Sexuality and Marital status: married male
Nationality: Korea

Education

April 2005 - March 2008	Doctor of Engineering, Department of Environmental Engineering and Architecture, Graduate School of Environmental Studies, Nagoya University (in Japan)
April 2003 - March 2005	Master of Engineering, Department of Materials Science and Engineering, Graduate School of Engineering, Nagoya University (in Japan)
April 2002 - March 2003	Research student, Department of Materials Science and Engineering, Graduate School of Engineering, Nagoya University (in Japan)
March 1995 - February 2002	Bachelor of Engineering, Department of Materials Engineering, School of Engineering, Korea Maritime University (in Korea) (* April 1996 – April 1998: military service in Korea)
March 1992 - February 1995	High school student, Natural Science, Geumseong High School (in Korea)

Publications (in scientific journals)

[1] **P. Heo**[a], K. Hagiwara[c], R. Ichino[c], M. Okido[c], "Electrodeposition and thermoelectric characterization of Bi_2Te_3", *Journal of The Electrochemical Society*, **153**, C213-C217 (2006). **[SCI]**

[2] **P. Heo**[a], H. Shibata[a], M. Nagao[a], T. Hibino[a], M. Sano[a], "Performance of an Intermediate-Temperature Fuel Cells Using a Proton-Conducting $Sn_{0.9}In_{0.1}P_2O_7$ Electrolyte", *Journal of The Electrochemical Society*, **153**, A897-A901 (2006). **[SCI]**

[3] **P. Heo**[a], R. Ichino[c], M. Okido[c], "ZnTe electrodeposition from organic solvents", *Electrochimica Acta*, **51**, 6325-6330 (2006). **[SCI]**

[4] **P. Heo**[a], M. Nagao[a], M. Sano[a], T. Hibino[a], "A High Performance Pt-Free Anode for Intermediate-Temperature Fuel Cells", *ECS Transaction*, **3**, 453-458 (2006).

[5] **P. Heo**[a], M. Nagao[a], M. Sano[a], T. Hibino[a], "A High Performance Mo_2C-ZrO_2 Anode Catalyst for Intermediate-Temperature Fuel Cells", *Journal of The Electrochemical Society*, **154**, B53-B56 (2007). **[SCI]**

[6] **P. Heo**[a], M. Nagao[a], T. Kamiya[a], M. Sano[a], A. Tomita[b], T. Hibino[a], "$Sn_{0.9}In_{0.1}P_2O_7$ – Based Organic / Inorganic Composition membranes: Application to Intermediate-Temperature Fuel Cells", *Journal of The Electrochemical Society*, **154**, B63-B67 (2007). **[SCI]**

[7] **P. Heo**[a], A. Tomita[b], T. Hibino[a], "An Intermediate-Temperature Fuel Cell Using a Proton-Conducting $Sn_{0.9}In_{0.1}P_2O_7$ Electrolyte", *Transactions of the Materials Research Society of Japan*, **32**, 951-954 (2007).

[8] **P. Heo**[a], M. Nagao[a], M. Sano[a], T. Hibino[a], "Direct Dimetyl Ether Fuel Cells at Intermediate Temperatures", *Journal of The Electrochemical Society*, **155**, B92-B95 (2008). **[SCI]**

[9] **P. Heo**[a], H. Shibata[a], M. Nagao[a], T. Hibino[a], "Pt-Free Intermediate-Temperature Fuel Cells", S*olid State Ionics*, in press (2008). **[SCI]**

[10] **P. Heo**[a], N. Kajiyama[a], K. Kobayashi[a], M. Nagao[a], M. Sano[a], T. Hibino[a], "Proton Conduction in $Sn_{0.95}Al_{0.05}P_2O_7$-PBI-PTFE Composite Membrane", ***Electrochemical and Solid-State Letters***, **11**, B91-B95 (2008). **[SCI]**

[11] M. Nagao[a], A. Takeuchi[a], **P. Heo**[a], T. Hibino[a], M. Sano[a], A. Tomita[b], "A Proton-Conducting In^{3+}-doped SnP_2O_7 Electrolyte for Intermediate-Temperature Fuel Cells", *Electrochemical and Solid-State Letters*, **9**, A105-A109 (2006). **[SCI]**

[12] M. Nagao[a], T. Kamiya[a], **P. Heo**[a], A. Tomita[b], T. Hibino[a], M. Sano[a], "Proton Conduction in In^{3+}-doped SnP_2O_7 at Intermediate Temperatures", *Journal of The Electrochemical Society*, **153**, A1604-A1609 (2006). **[SCI]**

[13] M. Nagao[a], **P. Heo**[a], T. Kamiya[a], A. Tomita[b], T. Hibino[a], M. Sano[a], "Proton Conduction in In^{3+}-doped SnP_2O_7 with Various P/(Sn+In) Ratios", *ECS Transaction*, **2**, 43-49 (2007).

[SCI] : Science Citation Index

Affiliation
[a]Graduate School of Environmental Studies, Nagoya University, Nagoya 464-8601, Japan
[b]National Institute of Advanced Industrial Science and Technology, Nagoya 463-8560, Japan
[c]Graduate School of Engineering, Nagoya University, Nagoya 464-8603, Japan

Conference presentations

1. International Conferences

[1] **P. Heo**[a], R. Ichino[c], M. Okido[c], "Electrodeposition of Bi_2Te_3 Thin Films", Frontiers of Surface and Interface Science and Engineering (FSISE) 2004, Guangzhou, China (May, 14-16, 2004)

[2] **P. Heo**[a], R. Ichino[c], M. Okido[c], "'Electrodeposition of Bi_2Te_3 Thin Films", 206th Meeting of The Electrochemical Society, Honolulu, USA (October, 3-8, 2004)

[3] **P. Heo**[a], R. Ichino[c], M. Okido[c], "Electrodeposition of Bi_2Te_3 Thin Films and its Thermoelectric Characterization", Fifth International Symposium on Biomimetic Materials Processing (BMMP-5), Nagoya, Japan (January, 26-28, 2005)

[4] **P. Heo**[a], R. Ichino[c], M. Okido[c], "Electrodeposition of Bi_2Te_3 Thin Films and its Thermoelectric Characterization", 207th Meeting of The Electrochemical Society, Quebec, Canada (May, 15-20, 2005)

[5] **P. Heo**[a], T. Hibino[a], M. Nagao[a], A. Takeuchi[a], M. Sano[a], D. Hirabayashi[a], A. Tomita[b], "Proton-conducting In^{3+}-doped SnP_2O_7 for intermediate-temperature fuel cells", International Symposium on EcoTopia Science 2005 (ISET05), Nagoya, Japan (August, 8-9, 2005)

[6] **P. Heo**[a], T. Hibino[a], M. Nagao[a], A. Takeuchi[a], M. Sano[a], D. Hirabayashi[a], A. Tomita[b], "Proton-conducting In^{3+}-doped SnP_2O_7 electrolyte for intermediate-temperature fuel cells", 56 th Annual Meeting of the International Society of Electrochemistry, Busan, Korea (September, 25-30, 2005)

[7] M. Nagao[a], **P. Heo**[a], A. Takeuchi[a], T. Hibino[a], M. Sano[a], "An Intermediate-Temperature Fuel Cell with Proton Conductor Based on SnP_2O_7", 208th Meeting of The Electrochemical Society, Los Angeles, USA (October, 16-21, 2005)

[8] M. Nagao[a], T. Kamiya[a], **P. Heo**[a], T. Hibino[a], M. Sano[a], A. Tomita[b], "Proton-conducting In^{3+}-doped Tin Phosphates with Various P/(Sn+In) Ratios, 209th Meeting of The Electrochemical Society, Denver, USA (May, 7-12, 2006)

[9] **P. Heo**[a], M. Nagao[a], H. Shibata[a], M. Sano[a], T. Hibino[a], "A High Performance Pt-free Anode for Intermediate-Temperature Fuel Cells", 210th Meeting of The Electrochemical Society, Cancun, Mexico (October, 29-November, 3,2006)

[10] M. Nagao[a], **P. Heo**[a], T. Hibino[a], M. Sano[a], A. Tomita[b], "Intermediate-Temperature Fuel Cells Using In^{3+}-doped SnP_2O_7 Electrolyte", 2006 Fuel Cell Seminar, Honolulu, USA (November, 13-17, 2006)

[11] **P. Heo**[a], H. Shibata[a], T. Hibino[a], "Pt-Free Intermediate-Temperature Fuel Cells", 16 th International Conference on Solid State Ionics, Shanghai, China (July, 1-6, 2007)

[12] **P. Heo**[a], T. Harada[a], M. Nagao[a], T. Hibino[a], "Intermediate-Temperature Fuel Cells Using a Proton-Conducting $Sn_{0.9}In_{0.1}P_2O_7$ Electrolyte", 46 th Symposium on basic science of ceramics, Nagoya, Japan (January, 10-11, 2008)

Affiliation

[a]Graduate School of Environmental Studies, Nagoya University, Nagoya 464-8601, Japan
[b]National Institute of Advanced Industrial Science and Technology, Nagoya 463-8560, Japan
[c]Graduate School of Engineering, Nagoya University, Nagoya 464-8603, Japan

2. Conferences in Japan

[1] **許 弼 源** [a], 水谷彰宏 [c], 市野良一 [c], 興戸正純 [c], "Bi_2Te_3 熱電半導体膜の水溶液電析", 第 109 回表面技術協会, 東京都立大学（2004 年 3 月 15 日～17 日）

[2] **許弼源** [a], 市野良一 [c], 興戸正純 [c], “Bi_2Te_3熱電半導体膜の水溶液電析とその特性評価”, 第 71 回電気化学会, 慶應義塾大学（2004 年 3 月 24 日～26 日）

[3] **許弼源** [a], 市野良一 [c], 興戸正純 [c], “Bi_2Te_3熱電半導体膜の水溶液電析とその特性評価”, 第 35 回中部化学関係学協会支部連合秋季大会, 名古屋大学（2004 年 9 月 17 日～18 日）

[4] 竹内明彦 [a], 長尾征洋 [a], **許弼源** [a], 佐野充 [a], 日比野高士 [a], 冨田衷子 [b], “SnP_2O_7のプロトン導電性とその中温域における燃料電池の特性評価”, 第 72 回電気化学会, 熊本大学（2005 年 4 月 1 日～3 日）

[5] 竹内明彦 [a], 長尾征洋 [a], **許弼源** [a], 日比野高士 [a], 佐野充 [a], 冨田衷子 [b], “In ドープ SnP_2O_7を電解質とする中温作動型燃料電池:アノード電極からの Pt フリー化”, 2005 年電気化学秋季大会, 千葉大学（2005 年 9 月 8 日～9 日）

[6] 神谷利男 [a], 長尾征洋 [a], **許弼源** [a], 日比野高士 [a], 佐野充 [a], 冨田衷子 [b], “In ドープ SnP_2O_7のプロトン導電メカニズム”, 第 46 回電池討論会, 名古屋国際会議場（2005 年 11 月 16 日～18 日）

[7] 長尾征洋 [a], 神谷利男 [a], **許弼源** [a], 日比野高士 [a], 佐野充 [a], 冨田衷子 [b], “In ドープ SnP_2O_7のプロトン導電性 : In ドープ量と P_2O_7 量の影響”, 第 31 回固体イオニクス討論会, 朱鷺メッセ新潟コンベンションセンター（2005 年 11 月 28 日～30 日）

[8] 柴田英高 [a], 長尾征洋 [a], **許弼源** [a], 日比野高士 [a], 佐野充 [a], 冨田衷子 [b], “In ドープ SnP_2O_7を電解質に用いた中温作動型燃料電池のカソード特性”, 第 73 回電気化学会, 首都大学東京（2006 年 4 月 1 日～3 日）

[9] 神谷利男 [a], 長尾征洋 [a], **許弼源** [a], 日比野高士 [a], 佐野充 [a], 冨田衷子 [b], “P_2O_7 量の In ドープ SnP_2O_7の導電性への影響”, 第 73 回電気化学会, 首都大学東京（2006 年 4 月 1 日～3 日）

[10] 柴田英高 [a], **許弼源** [a], 長尾征洋 [a], 日比野高士 [a], 佐野充 [a], 冨田衷子 [b], “中温燃料電池における Pt 代替触媒の開発”, 2006 年電気化学秋季大会, 同志社大学（2006 年 9 月 14 日～15 日）

[11] 神谷利男 [a], 長尾征洋 [a], **許弼源** [a], 日比野高士 [a], 佐野充 [a], 冨田衷子 [b], “In ドープ SnP_2O_7を用いた有機／無機コンポジット膜の作製と燃料電池特性評価”, 2006 年電気化学秋季大会, 同志社大学（2006 年 9 月 14 日～15 日）

[12] 柴田英高[a], **許弼源**[a], 長尾征洋[a], 日比野高士[a], 佐野充[a], 冨田衷子[b], “中温燃料電池における Pt 代替触媒の開発”, 第 98 回触媒討論会, 富山大学（2006 年 9 月 26 日～29 日）

[13] 神谷利男[a], 長尾征洋[a], **許弼源**[a], 日比野高士[a], 佐野充[a], 冨田衷子[b], “In ドープ SnP_2O_7 を含む有機／無機コンポジット膜のプロトン導電性と燃料電池特性”, 第 32 回固体イオニクス討論会, 九州大学（2006 年 11 月 27 日～29 日）

[14] **許弼源**[a], 日比野高士[a], 冨田衷子[b], “中温作動燃料電池用プロトン導電性 $Sn_{0.9}In_{0.1}P_2O_7$ 固体電解質”, 第 17 回日本 MRS 学術シンポジウム, 日本大学（2006 年 12 月 8 日～10 日）

[15] **許弼源**[a], 長尾征洋[a], 日比野高士[a], “ジメチルエーテルを直接燃料として使用した中温作動燃料電池”, 第 74 回電気化学会, 東京理科大学（2007 年 3 月 29 日～31 日）

[16] 梶山理一[a], 長尾征洋[a], **許弼源**[a], 小林和代[a], 佐野充[a], 日比野高士[a], “Al^{3+} ドープ SnP_2O_7 を含む有機・無機ハイブリッド膜の作製と特性評価”, 2007 年電気化学秋季大会, 東京工業大学（2007 年 9 月 19 日～20 日）

[17] 梶山理一[a], **許弼源**[a], 小林和代[a], 長尾征洋[a], 日比野高士[a], “Al^{3+} ドープ SnP_2O_7 複合体における有機バインダーのプロトン導電性への影響”, 第 33 回固体イオニクス討論会, 名古屋国際会議場（2007 年 12 月 6 日～8 日）

[18] **許弼源**[a], 梶山理一[a], 小林和代[a], 冨田衷子[b], 長尾征洋[a], 日比野高士, “$Sn_{0.95}Al_{0.05}P_xO_y$-PBI 複合膜のプロトン導電性と燃料電池特性”, 第 75 回電気化学会, 山梨大学（2008 年 3 月 29 日～31 日）

[19] 伊藤健一[a], **許弼源**[a], 佐野充[a], 日比野高士[a], “炭化水素を直接燃料として使用した中温作動燃料電池の開発”, 第 75 回電気化学会, 山梨大学（2008 年 3 月 29 日～31 日）

[20] 原田敏彦[a], **許弼源**[a], 佐野充[a], 日比野高士[a], “中温作動燃料電池における新規高活性カソードの作製と MEA 化”, 第 75 回電気化学会, 山梨大学（2008 年 3 月 29 日～31 日）

[21] 長尾征洋[a], **許弼源**[a], 伊藤健一[a], 藤原慶祐[a], 日比野高士[a], “中温作動燃料電

池の燃料多様性に関する研究” ，第 75 回電気化学会，山梨大学（2008 年 3 月 29 日～31 日）

所属
[a]名古屋大学大学院環境学研究科，日本，名古屋市
[b]産業技術総合研究所，日本，名古屋市
[c]名古屋大学大学院工学研究科，日本，名古屋市

Award

[1] Award for Encouragement of Research of Materials Science, “Intermediate-Temperature Fuel Cell Using a Proton-Conducting $Sn_{0.9}In_{0.1}P_2O_7$ Electrolyte” donated by the Materials Research Society of Japan (MRS-J), January 2007.

[2] Award for Excellent Presentation in World Young Ceramist Meeting 2008, “Intermediate-Temperature Fuel Cells Using a Proton-Conducting $Sn_{0.9}In_{0.1}P_2O_7$ Electrolyte” donated by the Ceramic Society of Japan, February 2008.

[3] Award for Poster Presentation in 75th Meeting of The Electrochemical Society of Japan, “Study on Fuel flexibility for Intermediate-Temperature Fuel Cells” donated by the Electrochemical Society of Japan, March 2008.

Patent

[1] Title of Invention: “Hybrid Electrolyte Membrane and its Production Method”,
Country: Japan, Application No.: 2007-331774, Application Date: December, 25, 2007

[2] Title of Invention: “Electrode Catalyst and its Production Method”,
Country: Japan, Application No.: 2007-331786, Application Date: December, 25, 2007